ELUCIDATING ANAEROBIC HEME DEGRADATION IN PATHOGENIC E. COLI

by

LIJU GEORGE MATHEW

(Under the Direction of William N. Lanzilotta)

ABSTRACT

Iron is an essential nutrient required by pathogens to survive and proliferate in the host environment. Host heme represents one viable iron source for bacterial pathogens, which have evolved diverse heme degradation pathways to acquire iron, in both aerobic and anaerobic environments. ChuW catalyzes anaerobic heme degradation in *Escherichia coli* O157:H7, converting the porphyrin substrate into the linear tetrapyrrole product termed anaerobilin and liberating iron. Although ChuW is an established anaerobic heme degrader, further mechanistic investigation is required, and the role of adjacent heme utilization proteins in the degradation process require further investigation. Here, we provide evidence for a heme-iron independent porphyrin ring-opening mechanism, as well provide evidence for other *E. coli* heme utilization proteins acting as heme and anaerobilin chaperones during catalysis.

INDEX WORDS: Anaerobic, heme, Radical SAM, iron-sulfur cluster, bacterial pathogen

ELUCIDATING ANAEROBIC HEME DEGRADATION IN PATHOGENIC E. COLI

by

LIJU GEORGE MATHEW

B.S., University of Georgia, 2017

A Dissertation Submitted to the Graduate Faculty of The University of Georgia in Partial Fulfillment of the Requirements for the Degree

DOCTOR OF PHILOSOPHY

ATHENS, GEORGIA

2022

ELUCIDATING ANAEROBIC HEME DEGRADATION IN PATHOGENIC E. COLI

by

LIJU GEORGE MATHEW

Major Professor:	William Lanzilotta
Committee:	Michael Adams
	Jorge Escalante
	Amy Medlock
	Zachary Wood

Electronic Version Approved:

Ron Walcott
Vice Provost for Graduate Education and Dean of the Graduate School
The University of Georgia
August 2022

ACKNOWLEDGEMENTS

I am extremely grateful to my advisor, William Lanzilotta, for his continued guidance and mentorship over the course of my PhD training, as well as providing training through the entire process. I want to thank each of my committee members, Michael Adams, Jorge Escalante, Amy Medlock, and Zachary Wood, for providing their insight and advice on my projects. Specifically, thank you to the Adams Lab, who helped immensely with troubleshooting anaerobic protein purification and characterization, and were always available to discuss science and brainstorm new ideas. Thank you to Jorge for providing new perspectives on scientific questions from the perspective of a microbiologist. Thank you to Zac, for making time to discuss protein crystallization and best practices for communicating science effectively.

The collaborative environment cultivated by the BCMB department directly contributed to my ability to thrive; I am thankful to the faculty and staff here who made that possible.

Finally, I want to thank my friends and family for their prolonged support throughout the course of my studies, and reminding me that there is a world outside of science. The sacrifices made by my parents to come to a strange new country so that we could have a better life directly led me to this moment.

You are all the reasons for my success.

TABLE OF CONTENTS

Page

CHAPTER 1

INTRODUCTION AND LITERATURE REVIEW

1.1 Motivation

Iron is an essential nutrient necessary for bacterial pathogen survival and virulence.[1,2] Pathogenic bacteria have adapted multiple strategies for iron acquisition. In the host environment, 95% of iron is stored as heme, sequestered primarily in hemoglobin, therefore pathogen exploitation of this source is a viable avenue towards successful infection.[3] Many pathogens possess multiple pathways for heme uptake, the deletion of which results in decreased infectivity.[4,5] Following bacterial heme uptake, the iron must be liberated by destruction of the heme porphyrin ring, alternatively, the heme may be incorporated as a cofactor in other bacterial proteins. Bacterial heme degradation can be divided into two major classes, based on whether the process is aerobic or anaerobic, the latter process only discovered more recently.[6]

In the absence of oxygen, Nature harnesses radical chemistry as the catalyst for porphyrin ring opening. The recent discovery of anerobic heme degradation in enterohemorrhagic *Escherichia coli* (EHEC) provides insight into bacterial survival in difficult host environments, such as the anoxic environment of the distal intestine. The *E. coli* heme utilization (Chu) operon contains heme utilization genes which are regulated by the ferric uptake regulator (fur); these genes are therefore upregulated under scarce iron conditions.[7] Within the *E. coli* heme utilization (Chu) operon, ChuW catalyzes the heme ring-opening reaction through a radical-mediated mechanism. As a member of the

Radical S-adenosyl-l-methionine (SAM) superfamily, ChuW belongs to an enzyme group performing essential physiological tasks in all domains of life.[8] Most radical SAM enzymes initiate catalysis through the reductive cleavage of SAM to produce L-methionine and a 5'-deoxyadenosine radical (5'-dAdo), and all these enzymes contain a [4Fe-4S] cluster responsible for the reductive cleavage. This radical-mediated mechanism in ChuW is distinct from O_2-dependent bacterial heme degradation systems.[6]

The recent discovery of ChuW as an anaerobic heme degrading enzyme has prompted further mechanistic studies. Although ChuW is a Radical SAM enzyme, the exact nature of the radical-mediated ring opening is not well understood. Further exploration of this system could prove useful in the development of novel antibacterial therapeutics targeting enteric pathogens, and may also be useful in developing synthetic biology systems that utilize radical chemistry. Here, we use a combination of biochemical and biophysical approaches to understand the intricacies of anaerobic heme degradation more carefully.

1.2 Background

1.2.1 Bacterial Heme Utilization

Most bacterial pathogens employ similar principles during heme uptake. Various pathogens have heme-responsive transcriptional regulators which facilitate heme sensing as a host tissue detection method.[1] Pathogen-mediated erythrocyte lysis, also known as hemolysis, facilitates the release of heme binding proteins into surrounding bacteria-inhabited tissues.[9] Damaged heme proteins, or free heme now available to bacteria, have several potential routes for uptake and degradation, varying based on the pathogen in question, and the host environment. The following section will detail heme

utilization strategies, highlighting the diversity of degradation mechanisms seen in bacteria.

Host Heme Sources

Certain bacterial pathogens, such as *Escherichia coli* and *Staphylococcus aureus* secrete hemolytic toxins. Secretion, Gb3 receptor binding and erythrocyte pore formation cause heme protein release into surrounding tissues.[9] Hemoglobin represents the major protein available following hemolysis, but other high affinity heme binding proteins, such as haptoglobin and hemopexin, can also be targeted for heme acquisition.[10,11] Bacteria may either secrete heme-binding proteins, or hemophores, to bind heme or damaged hemoglobin, or express heme-binding proteins at the cell surface as receptors.[12]

Following heme binding at an outer membrane receptor, Gram negative pathogens facilitate active transport into the periplasm using a TonB-dependent mechanism. TonB, along with exbB and exbD form a complex at the inner membrane and are necessary for transducing proton motive force to the outer membrane.[13] Upon entering the periplasm, heme is bound by a periplasmic heme binding protein, which transports it to the inner membrane. At the inner membrane, an ATP binding cassette will then transport heme into the cytosol.[14]

Gram positive pathogens such as *Staphylococcus aureus* lack the TonB system found in Gram negative bacteria, but rather utilize cell wall-associated heme-binding proteins to facilitate transport.[15] Isd-like proteins found in *Staphylococcus aureus* and *Bacillus anthracis* utilize near transporter (NEAT) domains, which consist of a β-sandwich fold and contain a hydrophobic heme-binding pocket.[16] These proteins may bind free heme, damaged hemoglobin, or hemopexin; following heme extraction from damaged

host hemoproteins, heme is transferred to a cell wall-anchored protein.[17] From here, heme is shuttled to an ABC transporter complex at the membrane for delivery into the cytosol.[18]

Heme Degradation Strategies

Following heme transport into the cytosol, the metal-bound porphyrin complex will either be degraded enzymatically or incorporated into bacterial hemoproteins as a cofactor. If degraded, the linear tetrapyrrole formed varies depending on the bacterial pathogen in question, and its environment. *Corynebacterium diphtheriae, Neisseria meningitidis, and Pseudomonas aeruginosa* produce various biliverdin isoforms. *Mycobacterium tuberculosis* and *Staphylococcus aureus* produce mycobilin and staphylobilin, respectively. Under aerobic conditions, all heme degradation pathways activate molecular oxygen via the heme-iron, opening the porphyrin ring and freeing iron from the macrocycle.[19] Key structural distinctions between each heme degradation product are highlighted in Figure 1.1.

The canonical heme degradation pathway refers to the pathway found in eukaryotes and is also found in certain Gram-positive and Gram-negative pathogens. Heme degradation in these systems produces α-biliverdin IX, aptly named as the ring is broken at the α-meso carbon bridge. Additionally, one equivalent of CO is produced with each turnover, corresponding to the oxidation and release of the meso bridging carbon. Classical heme oxygenase assays are coupled with biliverdin reductase in a UV-Vis cuvette, tracking the formation of bilirubin at 468nm, as it is more stable in solution than biliverdin.[20] Alternatively, the disappearance of heme may also be monitored by following the rate of decay of Soret and Q band features in the UV-Vis spectra.

Previous structural characterization of human Heme Oxygenase 1 (hHO-1) revealed a helical fold, with a heme binding pocket juxtaposed between two helices.[21] The proximal helix provides a histidine ligand to the heme iron, whereas a conserved Asp-Leu-Ser-Gly-Gly motif provides flexibility in the distal helix region. Additionally, the targeted α-meso carbon of heme is positioned in a hydrophobic region of this binding pocket, orienting it for hydroxylation. Finally, K18 forms a salt bridge with one of the heme propionate moieties at the protein surface. The combination of a polar, flexible distal helix and the α-meso carbon positioning deep in the active site are believed to facilitate selectivity for the α-meso carbon in the heme degradation reaction.

Subsequent work sought to characterize the enzymatic activity and structure of the distantly related heme oxygenase in *Neisseria meningitidis (Nm)* and *Corynebacterium diphtheriae (Cd).*[22] Despite sharing less than 25% sequence identity with hHO-1, UV-Vis spectroscopy and HPLC analysis demonstrated that the *Nm hemO* and *Cd hmuO* gene products yield α-biliverdin.[23] Both canonical heme degrading enzymes share a similar overall fold, both containing a flexible distal helix and heme iron coordination by a proximal histidine residue.[24] Key differences arise in the heme binding pocket size; bacterial HO-1 exhibits an over fivefold decrease in solvent-accessible volume (7.5 $Å^3$) when compared against its mammalian homologues (59.7 $Å^3$). hHO-1 additionally contains conserved residues involved in forming ionic bonds with the heme propionate groups, such as K18; the absence of these interactions in bacterial homologues alters substrate specificity.

Related bacterial pathogens possess genes with high sequence identity to HemO in *Neisseria meningitidis.* The *Pseudomonas aeruginosa* HO, annotated previously as PigA, shares 37% sequence identity with HemO, yet biochemical characterization

demonstrated that it produces the β and δ isoforms of biliverdin.[25] The shift in the targeted meso bridging carbon by the enzyme was attributed to an in-plane rotation of the heme substrate in the active site by ~100°, placing the δ-meso carbon in the hydrophobic pocket. *Pa* HO does not possess an equivalent surface lysine residue to K18 found in hHO-1. Rather, K132 is a unique lysine residue which forms a salt bridge with the heme propionate on the opposite of the active site, thereby stabilizing the buried δ-meso carbon conformation.[26] HPLC quantification of *Pa* HO reaction products revealed the formation of 70% δ biliverdin and 30% β biliverdin. Compared to its mammalian counterparts and the *Nm* HO homologue, key residues involved in positioning the substrate via hydrogen bonding are missing in the active site, a structural property that may facilitate heme rotation. This hypothesis was further corroborated by mutation of an arginine residue to aspartate in rat HO; the resulting enzyme variant was active but produced β and δ biliverdin isoforms in addition to the established α biliverdin.[27]

IsdG-like Alternate Heme Oxygenases

Staphylococcus aureus and related bacteria possess genes encoding enzymes that are structurally distinct from the HO enzymes found in mammalian systems and Gram-negative pathogens.[28] The Iron-regulated surface determinant (Isd) system contains genes for heme uptake and utilization, including two cytosolic heme oxygenases, IsdG and IsdI, which share 64% sequence identity.[29] These enzymes produce linear tetrapyrroles (staphylobilins in *Staphylococcus aureus* and mycobilins in *Mycobacterium tuberculosis),* which closely resemble the β and Δ biliverdin isoforms produced by *Pa* HO, the key distinction being the addition of a ketone to the bridging carbon opposite the

carbon targeted for breaking the porphyrin ring open.[30] Product quantification by HPLC indicates a roughly 1:1 formation of either the β or Δ staphylobilin isoform.

The IsdG and IsdI proteins belong to the ferredoxin fold superfamily, where the dimer interface forms a β barrel, in stark contrast to the primarily helical, monomeric structure found in other HOs. Bound heme exhibits “ruffling” in the active site, a distortion of the planar porphyrin ring. This 2 Å out of plane distortion positions the heme iron closer to an axially coordinated histidine residue, the imidazole moiety of this residue is aligned with the heme β-Δ bridge axis. The positioning of histidine in line with the substrate could explain the lack of stereospecificity for ring breakage at either position when observing IsdG products.

The heme degrading enzyme in *Mycobacterium tuberculosis,* MhuD, shares 45% identity with staphylococcal IsdG and belongs to the same ferredoxin fold superfamily, yet this enzyme produces a different heme degradation product.[31] MhuD structural characterization revealed an active site that accommodates two heme molecules in the binding pocket, although only one heme is axially coordinated by a histidine residue. Unlike the monoheme ruffled conformation of IsdG, the diheme form of MhuD lacks porphyrin ring distortion, where both hemes are parallel, stacked at van der Waals distance.[32] Both diheme and monoheme forms of MhuD are enzymatically active,[33] producing the unique product termed mycobilin. The mycobilin product exists in either an “a” or “b” isoform, designated based on whether ketone addition occurs at either the β or Δ carbon position. Ring opening is targeted to the α-meso carbon, where a ketone and an aldehyde are formed. Previous work by the Ikeda-Saito group demonstrated that MhuD mediated heme degradation does not produce CO, unlike all other aerobic heme

degradation mechanisms.[31] The coupled assay used heme-bound myoglobin as a probe for CO release, by taking advantage of spectral shifts in myoglobin upon coordinating CO.[34]

ChuS-like Proteins and Reported Heme Degradation Activity

Yersiniae were initially shown to utilize heme as a sole iron source in the early 1970s during cell growth assays; genes implicated in heme utilization were later cloned into *Escherichia coli* K12 in the 1990s.[35,36] HemS, a 42 kD cytosolic protein, was among these genes from *Yersinia entercolitica* that was necessary for heme utilization when grown in the absence of iron and proposed to act as a heme chaperone. Later structural and biochemical characterization of ChuS, a homologue with 80% identity to HemS in *Escherichia coli* O157:H7, identified ChuS as a novel heme degrading enzyme.[37] The beta sheet-dominated structure contains 18 antiparallel beta strands forming a saddle motif; closer observation shows a structural duplication, and the N and C-terminal halves of ChuS align to 2.1 Å RMSD (Root Mean Square Deviation). Initial UV-Vis assays using ascorbate as a reducing partner showed some evidence for ChuS-dependent heme degradation. Yet catalase addition, to account for nonenzymatic peroxide-based heme degradation, abolished the observed heme degradation activity in subsequent studies.[38] The heme bound ChuS structure reveals heme is stabilized in the binding pocket by a hydrophobic cleft and is axially coordinated by a conserved histidine residue.[39]

Further *in vivo* work conducted with PhuS, a ChuS homologue found in *Pseudomonas aeruginosa,* presented evidence for a role in trafficking heme to the *Pa* HO.[40] Binding studies conducted by the Wilks Group demonstrated that *holo* PhuS binds *Pa* HO at a 1:1 stoichiometry, shown using Surface Plasmon Resonance and Isothermal

Titration Calorimetry. Further sedimentation velocity studies and limited proteolysis data presented evidence for conformational changes to PhuS upon binding HO.[41] PhuS shares 41% sequence identity with ChuS; structural analysis revealed *apo* enzyme conformations that are incredibly similar (0.16 Å RMSD when comparing ChuS to PhuS structures); structural similarities and heme binding modes are highlighted in Figure 1.2.[38] Comparing the heme binding pockets in the two proteins reveals a similar hydrophobic binding pocket, as well as water coordinating the heme iron on the distal side of the pocket. Together, structural, and biophysical data alongside the knockout studies performed in *Pseudomonas aeruginosa* provide compelling evidence that ChuS-like proteins act as heme chaperones, rather than as heme oxygenases *in vivo.*

HutZ-like Proteins

The Heme utilization system (Hut) in *Vibrio cholerae* is yet another Fur-regulated system that contains genes pertaining to heme uptake and utilization.[42] Under conditions where *V. cholerae* must utilize heme as its sole iron source, HutZ was shown to be necessary and sufficient for heme utilization.[43] HutZ complementation into HO knockout strains of both *Corynebacterium diphtheriae* and *Corynebacterium ulcerans* restores heme utilization capabilities as well. HutZ purification and heme reconstitution reveals a strongly bound, hexacoordinate heme species, although no heme degradation activity was observed. Hence, it was concluded by the Payne group that HutZ may act as a heme chaperone in this system but is not a heme oxygenase.

Later work by the Uchida group demonstrated *V. cholerae* HutZ heme degradation activity in the presence of asorbate as a reducing partner and catalase; in light of a HutZ structure, the discrepancies between the two groups' findings is understood. The HutZ structure

(Accession ID- 3TGV) revealed a dimer in the asymmetric unit and included intersubunit hydrogen bonds near the heme binding pocket. Specifically, D132 is within hydrogen bonding distance of H170 in the adjoining subunit, the latter acting as the axial ligand to heme. It was predicted this interaction would promote imidazolate characteristics in the axial heme ligand, a common feature of heme peroxidases.[44] Mutation of either the histidine or aspartate was detrimental to both heme binding and degradation activity. The catalytic significance of the intersubunit hydrogen bond was further underscored by an increase in activity as pH decreases.[45] After a one hour turnover assay, HutZ fully degraded one equivalent of heme at pH 6.0, whereas the same assay at pH 8.0 produced tenfold less product. The previous HutZ assays conducted by the Payne group were performed at pH 7.5. Distantly related Heme utilization genes (Hug) are operons found in *Campylobacter jejuni* and *Helicobacter pylori,* and share 24% and 21% identity with *V. cholerae* HutZ, respectively.[43] *C. jejuni* HugZ efficiently catalyzes heme degradation using ascorbate as a reductant, and in the presence of catalase.[46] *H. pylori* demonstrated heme oxygenase activity when provided with either cytochrome P450 reductase or ascorbate as a reductant.[47] Both HugZ homologues are very similar in sequence and produce the δ-biliverdin isoform as product.

Although distantly related, the exact causes for activity differences between HutZ and HugZ proteins remained unclear until structural data became available. Belonging to a larger split-barrel fold protein family, this fold is commonly seen among FMN binding proteins, but not previously seen in heme-binding proteins. The *holo* HugZ structure was solved by introducing azide to the crystallization solution; the resulting structure reveals azide bound to the distal side of the heme iron in the binding pocket.[48] A conserved

arginine residue forms sidechain interactions with an ordered water molecule, which in turn hydrogen bonds to azide. Histidine then provides the sixth iron ligand on the proximal side of the heme. Subsequent mutagenesis and enzyme assays demonstrated that arginine is essential to activity, whereas histidine is not.

Vc HutZ possesses both the arginine and histidine ligands, but the crystal structure points to a proline residue in the C-terminal region that may be responsible for significant structural deviations.[49] Given the role of the CTD in heme binding, alterations here may explain the differences in activity between HutZ, which can efficiently degrade heme at pH 6.0, and HugZ, which efficiently degrades heme at physiological pH. A summary of heme oxygenase enzyme structural diversity can be viewed in Figure 1.3.

Degradation of C-type Heme

All previous cases mentioned pertain to free, b-type heme degradation; recent work elucidates a pathway for c-type heme degradation.[50] C-type hemes are covalently linked as cofactors in hemoproteins via two thioether bonds and are ubiquitous in processes such as cellular respiration and photosynthesis.[51,52] HugZ from *Paracoccus denitrificans* lacks heme degrading activity when provided with heme b, but when incubated with heme c, ascorbate and catalase, a peptide-linked δ-biliverdin and CO are formed. Belonging to the same family as *H. pylori* and *C. jejuni* HugZ, the enzyme possesses the same FMN split-barrel fold with some key differences. Structural characterization and comparison of the *apo* enzyme structure with *H. pylori* and *C. jejuni* HugZ structures reveals the loss of a C-terminal loop involved in heme coordination, as well as the loss of an N-terminal domain, thus creating a larger substrate-binding pocket. This larger binding pocket likely

facilitates heme c binding in *P. denitrificans* where other HugZ homologues cannot. Enzymatic heme c degradation provides yet another viable iron source for bacterial pathogens.

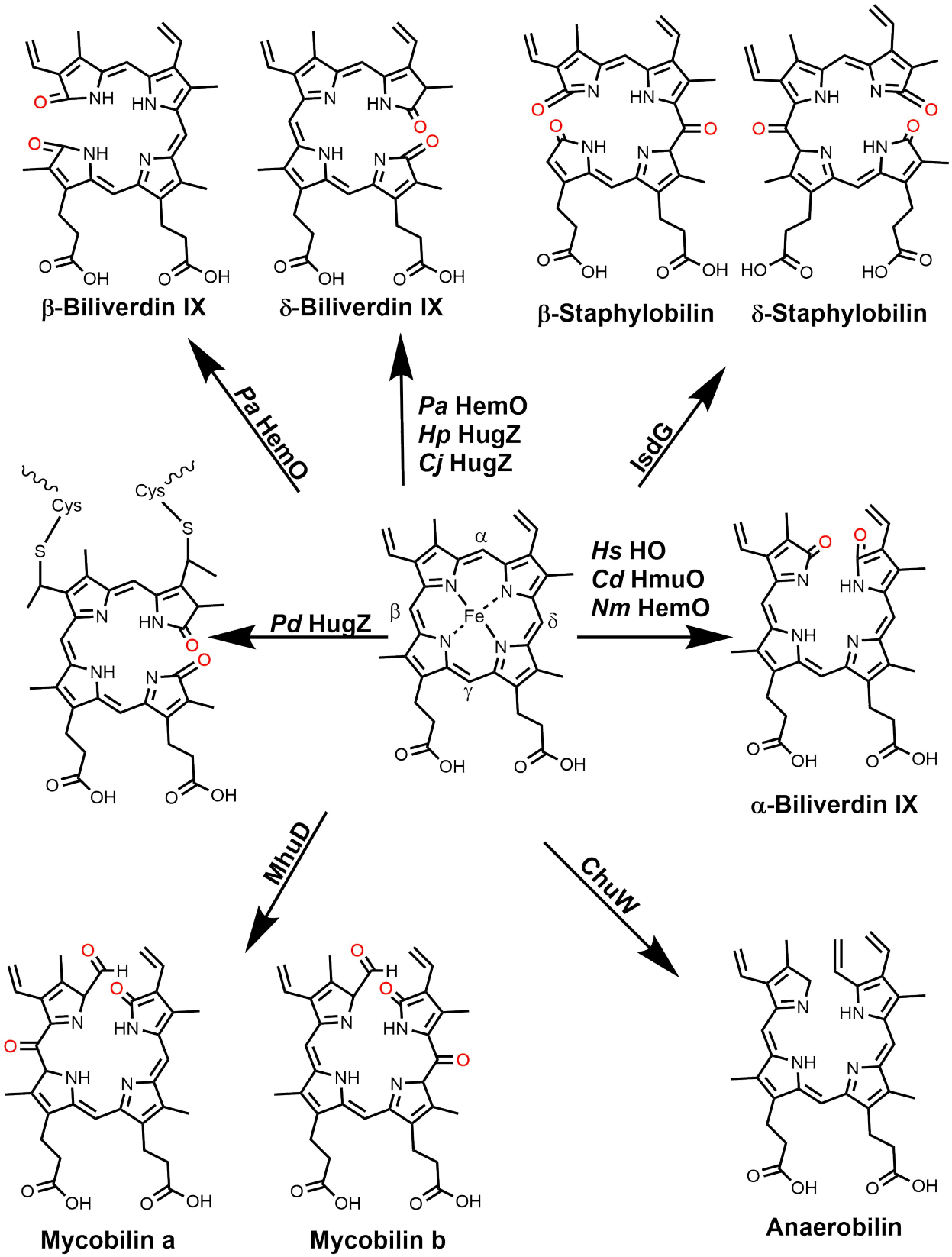

Figure 1.1. Structural Diversity of Heme Degradation Products

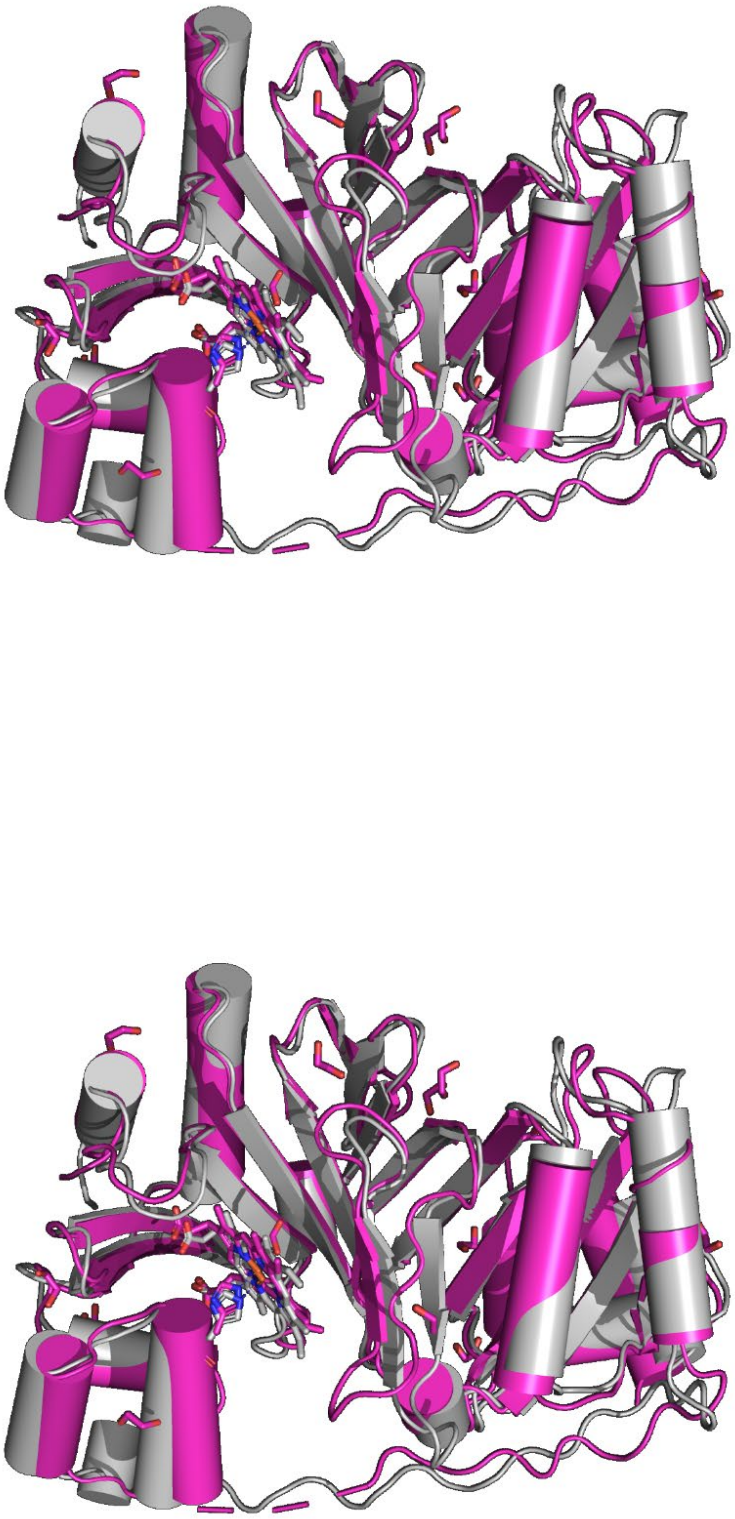

Figure 1.2. Wall eyed-stereogram of structurally aligned ChuS and PhuS. ChuS is shown in magenta, PhuS in gray. Accession IDs- ChuS:4CDP, PhuS:4MF9

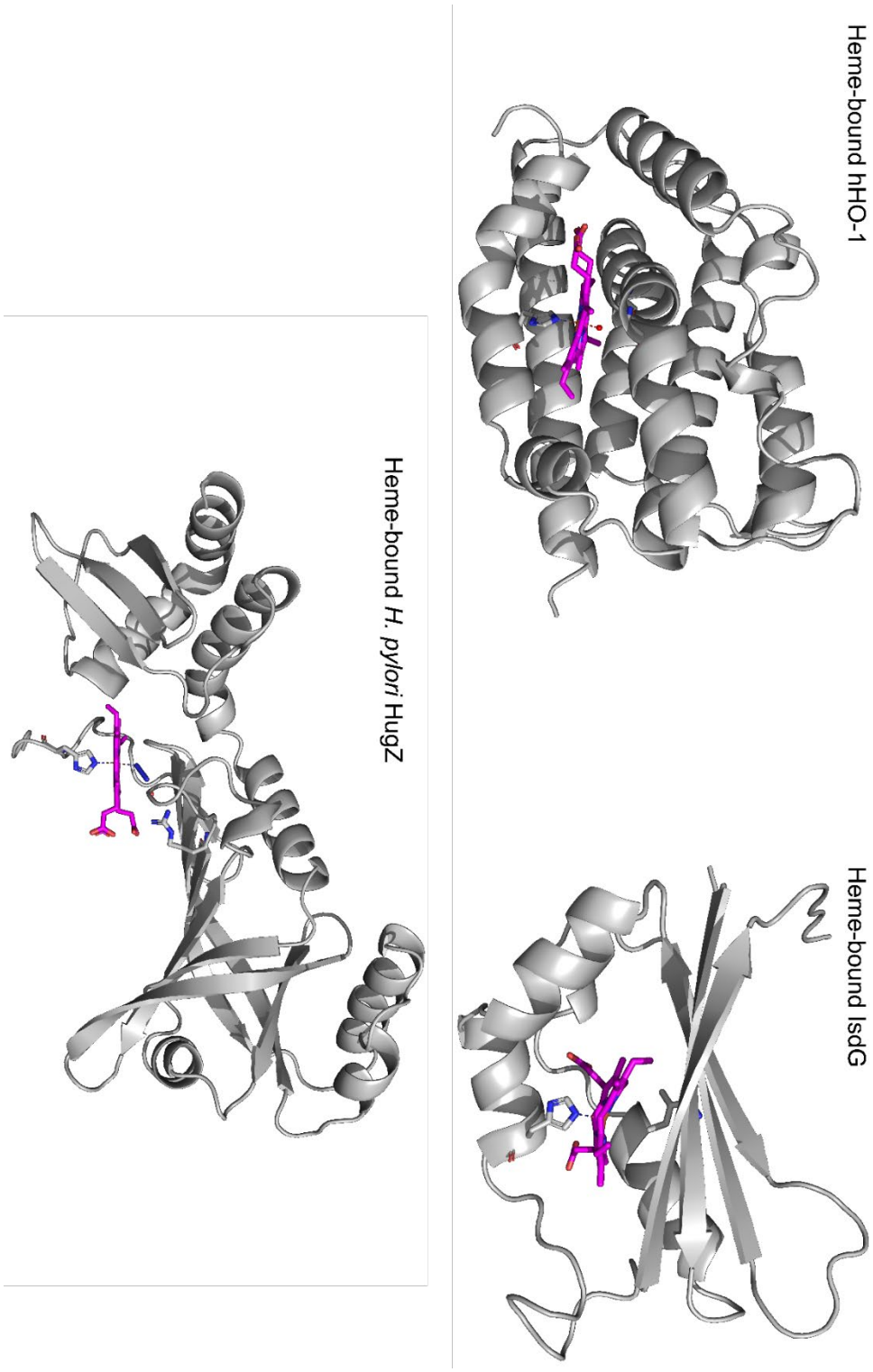

Figure 1.3. Structural Diversity of Heme Degrading Enzymes. Heme is shown in magenta. Accession IDs- hHO-1: 1QQ8, IsdG: 2ZDO, HugZ: 3GAS

1.2.2 The Radical SAM Superfamily

Radical S-Adenosyl-(L)-methionine (SAM) enzymes are found across all domains of life and catalyze a diverse array of reactions, often essential to organism fitness.[8] Though it is a ubiquitous enzyme superfamily found in all domains, the identification of unifying features across family members was not apparent until careful bioinformatic analysis was conducted in 2001.[53] The pairing of sequence analysis with previous biochemical characterization provided the necessary information required to identify over 600 family members. A number that has reached over 500,000 unique sequences today.[54,55] This section will provide a brief history of Radical SAM enzymes, highlighting common themes found across the superfamily, prior to discussing HemN-like Radical SAM enzymes in more detail, a subset of which catalyzes anaerobic heme degradation.

Shared Characteristics in the Superfamily

Initial structural characterization of early family members demonstrated that all Radical SAM enzymes i) have a [4Fe-4S] cluster binding motif at the N terminus, ii) have a SAM binding motif, and iii) possess a Triose Phoshate Isomerase (TIM) barrel fold.[8,56,57] The conserved cluster binding region consists of a CxxxCxΦC motif, where Φ represents any aromatic residue. Cysteine residues coordinate 3 out of the 4 iron atoms from the cluster, where the fourth, uncoordinated residue is referred to as the “unique iron.”[58] As is the case with aconitase, the unique iron is particularly labile, and sensitive to oxidative species.[59] The unique iron is coordinated in a bidentate fashion by the carboxy and amino termini of SAM when bound in the active site; this property is observed in many crystal structures and has been demonstrated orthogonally using spectroscopic methods.[60–62]

The [4Fe-4S] cluster is responsible for reductive cleavage of SAM to form a 5'-deoxyadenosyl radical (5'-dAdo·) and L-methionine.[63,64] To do so, the cluster must be in the +1 reduced state, which is often accomplished by using flavodoxin, an FMN-binding physiological electron donor.[65] The redox couple for the +2 to +1 redox couple is typically in the range of -450 to -550 mV based on electrochemical studies.[66] Polarography studies determined trialkylsulfonium compounds, which have a similar structure to SAM, to have a reduction potential of -1800mV, far lower than the known range of Radical SAM enzymes.[67] The large disparity between SAM and the cluster narrows slightly upon substrate binding; the cluster potential lowers to around -600mV, and the potential of SAM is estimated to increase from -1800mV to around -990mV.[68] The near 390mV remaining difference is postulated to be overcome by substrate proximity to the cluster, as well as conformational changes during turnover and the exclusion of water in the active site.

The exact mechanism by which 5'-dAdo· is formed requires further characterization, but there are two current working theories from the Broderick and Mansoorabadi groups. Spectroscopic studies identified the formation of an organometallic intermediate from an enzyme turnover sample which was freeze-quenched after 500 milliseconds.[69] The structure of this species was predicted to consist of 5'-dAdo forming a direct bond with the unique iron of the [4Fe-4S] cluster, similar to the Co-5'-dAdo bond observed in adenosylcobalamin enzymes.[70] More recent computational work employs Density Functional Theory to more carefully inspect the spectroscopic results which seem to provide evidence for Ω. These results point to a near attack conformer intermediate, rather than an intermediate where 5'-dAdo is bound to the cluster.[71] This model proposes that during catalysis, nonbonding electrons of the SAM

sulfonium ion are brought near the unique iron, facilitating reductive cleavage of the C-S bond to form 5-dAdo·. This model is in line with the original catalytic mechanism proposed by Frey.[72]

Lysine 2,3-Aminomutase: The First Characterized Radical SAM Enzyme

During the late 1960s, a growing interest in the community to understand bacteria's ability to ferment amino acids spurred investigations into *Clostridium butyricum* SB4 and lysine metabolism.[73] Early studies identified β-lysine as the first product in the lysine fermentation pathway, and lysine 2,3-aminomutase was then identified as the enzyme responsible for this reaction.[74] Several salient enzyme features emerged from biochemical analysis: the addition of pyridoxal phosphate, SAM and ferrous iron improved activity, oxygen and oxidizer exposure was detrimental to activity, and the purified enzyme had an absorbance peak at 420nm. Given the apparent oxygen sensitivity, sodium dithionite was a necessary reaction component, acting as an oxygen scavenger and a strong chemical reductant. At this time, it was not understood how SAM and iron addition improved activity, or the catalytic role of these cofactors.

Subsequent studies by Frey's group used tritiated SAM to determine its role in turnover.[75] When S-[2,8,5'-^{3}H]adenosylmethionine is used as a substrate, tritium was incorporated into the β-lysine product, whereas use of S-[2,8-^{3}H]adenosylmethionine or S-adenosyl[methyl-^{3}H]methionine did not yield tritiated product. These results implicated the 5'-deoxyadenosine portions of SAM in the hydrogen transfer reaction for lysine isomerization. This work was the first to elucidate the specific function of SAM in the reaction mechanism, and the first to draw parallels between 5'-deoxyadenosine utilization in a Radical SAM enzyme and adenosylcobalamin-dependent enzymes.

Frey's group used a combination of radiolabeling, substrate analogue assays, spectroscopy and finally, crystallography to parse out SAM's role in catalysis. The use of site-specific ^{14}C radiolabeled SAM determined the stoichiometries of produced L-methionine and 5'-deoxyadenosine to be 1:1 when L-lysine was also incubated with the enzyme.[76] Electron Paramagnetic Resonance (EPR) spectroscopy studies conducted over the reaction time course determined an organic radical forming over time, most likely a lysine-based radical, consistent with isotopic labeling.[77] Mechanistic proposals involved formation of a 5'-dAdo· species involved in hydrogen abstraction, which would thus generate the lysine radical intermediate, yet direct observation of the putative 5'-dAdo· proved challenging due to its predicted instability and short life in solution. Later studies were able to identify the 5'-dAdo· using a more stable allylic SAM analogue, containing an unsaturated C-C bond at 3'-4' position of the ribose ring.[78] Only more recently have groups been able to directly identify an unmodified form of 5'-dAdo· using more advanced cryoreduction methods.[63]

Other Early Radical SAM Enzymes: Mechanisms and Unifying Themes

At the same time Frey and colleagues were studying Lysine 2,3-aminomutase, extensive work was being conducted on Biotin Synthase (BioB), molybdenum cofactor biosynthesis enzyme (MoaA), and the oxygen-independent coproporphyrinogen III oxidase (HemN), with each enzyme catalyzing a vastly different reaction.[79–81] Observations made in each of these early enzyme investigations would reappear as trends in other Radical SAM Enzymes as more information became available.

BioB catalyzes sulfur insertion as the ultimate step in biotin biosynthesis, converting dethiobiotin into the final product.[82] In addition to the N-terminal catalytic

cluster, BioB contains a [2Fe-2S] which is now generally accepted as the sulfur source for insertion during turnover. EPR studies employing site-specifically labeled dethiobiotin demonstrate hydrogen abstraction first from C9 of dethiobiotin by 5'-dAdo·, followed by sulfur insertion. A second catalytic cycle will then generate a second 5'-dAdo· species, abstracting a hydrogen from position C6.[83] The cannibalization of an Fe-S cluster as a sulfur source for an enzymatic reaction was at the time controversial but has now been demonstrated in other Radical SAM enzymes as well.[84]

MoaA catalyzes the first step in molybdenum cofactor biosynthesis, converting 5'-GTP to a tetrahydropyranopterin termed precursor Z.[85] Initial MoaA structural characterization revealed a second C-terminal [4Fe-4S] cluster which also contained a unique iron site.[60] Mounting evidence suggests the C-terminal cluster is involved orienting the 5'-GTP substrate during turnover, observed in the structure as it coordinates the C-terminal unique iron.[86] Since the substrate bound MoaA structure was reported, more cases of auxiliary clusters coordinating substrate have been reported.[87]

HemN catalyzes the oxidative decarboxylation of Coproporphyrinogen III to form Protoporphyrinogen IX; in doing so, two propionate groups of the porphyrin substrate are converted to vinyl groups.[88] Layer and colleagues identified a second, conserved SAM binding site upon crystallizing HemN, a feature later found to be shared by Radical SAM enzymes which catalyze methyl transfer reactions.[89] The exact role of the second SAM molecule in the catalytic mechanism did not become clear until later studies utilizing Liquid Chromatography High Resolution Mass Spectrometry (LC-HRMS). Analysis and MS fragmentation of an isolated turnover sample determined it to be consistent with a SAM-porphyrin adduct. These results suggested that the second SAM molecule serves

as part of a hydrogen atom relay. Observation of this adduct also provides credence to a mechanism where the first SAM molecule, after generating 5-dAdo·, abstracts a hydrogen atom from a second SAM molecule, forming a methylene radical, that other enzymes have evolved to utilize in different ways. This second SAM molecule will abstract a hydrogen atom from the beta carbon atom of the propionate, and initiate the oxidative decarboxylation.[90]

HemN-like Enzymes

HemW in *E. coli* shares 33% identity with HemN but is unable to catalyze oxidative decarboxylation on coproporphyrinogen III *in vitro*.[91] Spectroscopic and metal analysis of purified HemW provided evidence for one [4Fe-4S] per monomer, and gel filtration of both *apo* and *holo* enzyme provide evidence for [4Fe-4S]-dependent dimerization. Given the lack of HemN activity for HemW, it was predicted that the enzyme may instead bind the heme product, rather than participate in the biosynthetic pathway. HemW demonstrated *in vivo* and *in vitro* heme binding and was thought to act as a heme chaperone.[92] SDS-PAGE analysis was followed by treatment of the HemW band with Enhanced Chemiluminescence (ECL) reagent. Heme-dependent luminol oxidation determined that HemW covalently binds heme, though the residues responsible for this covalent binding remain unclear. Using a bacterial two-hybrid system, HemW binding partners were determined to be respiratory chain proteins which require heme b. Taken together, HemW covalently binds heme and acts as a heme chaperone to respiratory chain proteins in bacteria. The distantly related HemW homologue in humans, was also determined to bind heme *in vitro*, and presented as another heme chaperone, though further evidence is necessary to determine its client proteins, and whether heme binding occurs *in vivo*.[91]

Radical SAM Methyltransferases

The first characterization of a Radical SAM enzyme catalyzing methyl transfer in 2008 involved modification of an RNA substrate.[93] Since this discovery, Radical SAM methyltransferases (RSMTs) have been implicated in the biosynthesis of a variety of natural products, antibiotics, as well as the post-translational modification of proteins, and have been grouped into four distinct classes. Members of each class can be determined by sequence similarity, and also share similar methyl transfer mechanisms. The following section will summarize mechanistic strategies employed by different RSMT (Radical SAM methyltransferases) classes.

Class A Radical SAM Methyltransferases

Often found in multidrug resistant strains of pathogenic bacteria, Cfr and RlmN catalyze the methylation of C8 and C2, respectively, on adenosine 2503 (A2503) of 23S rRNA.[94,95] In addition to acting on rRNA, RlmN also methylates adenosine 37 in *E. coli* tRNA, which improves translational fidelity.[96] The rRNA modification mechanism involves hydrogen atom abstraction from a conserved, methylated cysteine residue.[97] The generated methylene radical will then directly attack at position C2 or C8, dependent on whether RlmN or Cfr is the enzyme in question. The basis for this mechanism was a combination of LC-MS and crystallographic data; LC-MS demonstrated the methyl group was protein-derived, and a methylcysteine residue was evident from both fragmentation data as well as electron density.[98,99]

The tRNA modification mechanism is proposed to utilize the same strategy seen with rRNA. A crystal structure of RlmN crosslinked to a tRNA demonstrates that both RNA substrates have similar tertiary structures, though they share little sequence identity.

RlmN forms direct interactions with the sugar phosphate backbone, allowing it to bind and recognize the entire span of the tRNA substrate. RlmN further remodels the anticodon region of tRNA to access the adenosine 37 base for modification.[100]

Studies pertaining to Cfr homologues identify an abundance of Cfr-like genes in the gut microbiome and other pathogenic bacteria. Cfr found in *Clostridium dificil* contains an additional C-terminal domain, which binds a single iron ion in a rubredoxin-like environment. Removal of the C-terminal domain does not affect catalytic activity under substrate-limiting conditions but does cause a marked decrease in turnover when substrate is provided in excess.[101] This second iron site may act as an electron donor to the catalytic [4Fe-4S] or may interact with other redox partner proteins in the cell.

Class B Radical SAM Methyltransferases

Class B RSMTs employ a cobalamin cofactor in addition to the catalytic cluster and are primarily found in antibiotic biosynthetic pathways, acting on sp^3-hybrizied carbon centers.[102] The reaction proceeds with generation of 5'-dAdo·, that abstracts the Pro-R hydrogen from substrate. The carbon-centered substrate radical then directly attacks methylcobalamin, initiating homolytic cleavage of the Co-C bond. Methylcobalamin may then be regenerated with the introduction of a second SAM molecule in the active site to act as a methyl donor.[103–105] In certain cases, Class B RSMTs can iteratively methylate substrate targets, creating ethylated or even t-butylated forms of product.[106,107]

Recent structural characterization of TokK, a Class B RSMT involved in carbapenem biosynthesis, provides further insight into cobalamin interactions with the [4Fe-4S] cluster and substrate in the active site. The cobalamin binding domain at the N-

terminus adopts the Rossman fold and positions the -OH group of hydroxycobalamin 4.2 Å away from the target carbon on the β-lactam substrate. Cobalamin adopts the "base-off" conformation, and a non-coordinating conserved tryptophan residue abuts the axial face of the ring structure.[106] Tryptophan positioning occludes water coordination; this active site environment represents a common strategy in modulating activity in Class B RSMTs.

Class C Radical SAM Methyltransferases

Class C RSMTs share high sequence homology with HemN and have a conserved SAM2 binding site; they act primarily on sp^2-hybridized carbon centers. Given the sequence similarity to HemN, initially proposed mechanisms involve hydrogen atom abstraction from the second SAM molecule following 5'-dAdo· generation.[6,108,109] Hydrogen abstraction from the second SAM molecule generates a SAM-derived methylene radical, which directly attacks the target substrate carbon.

Among the Class C RSMTs, Radical SAM enzymes involved in antibiotic biosynthesis remain the most well characterized members. TbtI catalyzes methylation of a thiazole moiety on Thiomuracin A1, a macrocyclic thiopeptide antibiotic that targets bacterial EF-Tu.[110,111] Following hydrogen atom abstraction from SAM2, the proposed methylene radical attacks an sp^2-hybridized carbon center on the thiazole ring, forming a resonance-stabilized radical. An active site residue acts as a general base and deprotonates the thiazole β carbon to eliminate S-adenosylhomocysteine (SAH). The remaining intermediate radical is proposed to be reduced by the catalytic cluster.

NosN and NocN also produce macrocyclic thiopeptide antibiotics nosiheptide and nocathiacin, respectively.[102,109] The NosN mechanism following hydrogen abstraction

from SAM2 proceeds with methylene radical attack on C4 of the 3-methyl-2-indolic acid substrate. General base deprotonation of C4 results in SAH elimination and the formation of an exocyclic methylene radical and an aryl radical intermediate. The aryl radical intermediate is proposed to be quenched (oxidized) by the cluster, and the remaining electrophilic methylene group is attacked by a substrate carboxylate oxygen, forming a ring.[112]

Class D Radical SAM Methyltransferases

One of the most recent classes to emerge as a Radical SAM methyltransferase, Class D enzymes utilize methylenetetrahydrofolate as a methyl group donor.[113] The sole characterized member of this family, MJ0619, is found in *Methanocaldococcus janaschii* and catalyzes methyl transfer to pterin in the methanopterin biosynthetic pathway. Metabolic feeding studies with heterologously expressed MJ0619 in *E. coli revealed* formation of 7-methylpterin from cell extracts. The addition of cobalamin to growth media did not enhance product yields, but the addition of deuterated acetate led to deuterium enriched 7-methylpterin. The reported pattern of deuterium enrichment is consistent with the utilization of methylenetetrahydrofolate as the methyl donor. Unlike previous RSMT classes, MJ0619 does not have a conserved cysteine residue for methyl transfer, does not utilize cobalamin, and does not appear to have a second SAM binding site. Moreover, MJ0619 has an additional four cysteine residues at the N-terminus, potentially binding a second [4Fe-4S], but is not detrimental to product formation.

Other Radical SAM Methyltransferases

Radical SAM enzymes that catalyze methyl transfer, but do not share the previously mentioned characteristics may represent newly emerging classes of RSMTs. NifB, the Radical SAM enzyme responsible for carbide insertion into FeMoco, has been described as a “Class E” methyltransferase.[114] NifB contains two additional [4Fe-4S] clusters, flanking the regions of the structure before and after the catalytic cluster. These clusters, termed K1 and K2, act as a scaffold for generating the FeMoco cofactor necessary for nitrogenase function.[115] The proposed mechanism for carbide insertion begins with methyl transfer directly from a single SAM molecule to the K2 cluster, forming SAH and a methylated sulfide on K2. A second SAM molecule will then replace SAH, and following homolytic cleavage, 5’-dAdo· will abstract a hydrogen from the methyl group on K2. Two successive deprotonations are proposed to be catalyzed by a nearby histidine residue, followed by ligand exchange with the K1 cluster, forming the FeMoco precursor.[116]

Methanogenesis marker 10 (mmp10) catalyzes C5 methylation of an active site arginine residue in Methyl Coenzyme M Reductase (MCR). The crystal structure reveals unusual domain and cofactor architecture; the unique iron of the catalytic cluster, though typically not coordinated, here is coordinated by a conserved tyrosine residue. A cobalamin cofactor responsible for methylation is reminiscent of the cobalamin seen in Class B RSMTs but is in a C-terminal domain instead of the N-terminus, where it is normally found in Class B enzymes. The domain itself is only vaguely like the typical Rossman fold observed with cobalamin binding proteins, as it is lacking several β-strands and α-helices characteristic to the fold. An additional iron binding loop is also observed

abutting the cobalamin domain, which may play a role in electron transfer during turnover.[117]

1.2.3. ChuW and HutW: Radical SAM Enzymes and Heme Utilization

Recent work has provided evidence for an anaerobic heme utilization system in enteric bacterial pathogens; such pathogens inhabit anoxic environments in the gut.[6] The proteins responsible for degrading heme anaerobically have been identified as Class C RSMTs, and thus also share high sequence identity with HemN. The following section will describe the proteins found in these heme utilization operons, and their reported function.

ChuW/HutW

Originally annotated to be a HemN enzyme, ChuW is found in *Escherichia coli* O157:H7, and homologues can be found in other enteric pathogens.[43,118] Genes encoding ChuW homologues .are located alongside genes responsible for heme uptake and utilization and are Fur-regulated. These data, alongside evidence showing that ChuW homologues cannot rescue HemN knockout strains in *Salmonella enterica,* called into question the initial annotation.[43] Biochemical characterization of purified ChuW showed that the enzyme contained one [4Fe-4S] per monomer, that was readily reduced by titanium citrate. Sequence analysis with HemN provides evidence for conservation of the second SAM binding site in ChuW, though ChuW was unable to catalyze oxidative decarboxylation.

When incubated with SAM and a chemical reductant in the absence of a porphyrin substrate, ChuW produced 5'-dAdo and L-methionine in a process termed "abortive cleavage", often viewed as an artifact of using strong chemical reductants.[119] When incubated with SAM, heme and the physiological, flavodoxin- or ferredoxin-based

reducing system, ChuW-catalyzed heme degradation is observed by monitoring the disappearance of the heme Soret band feature at 407nm. The formation of an apparent product, termed anaerobilin, was observed as bands appeared at 445 and 795nm, an enzymatic process that could be quantified using isosbestic points from the UV-Vis turnover spectra. Anaerobilin could be further separated from the heme substrate following an acidified methanol treatment and HPLC isolation.

Product MS analysis using deuteroheme, a more soluble porphyrin substrate, identified deuteroanaerobilin, that had a mass shift consistent with the loss of iron and addition of a methyl group. The use of either ^{13}C-labeled SAM or methyl-d_3 SAM resulted in a one or two mass unit shift, respectively, consistent with the methyl group being SAM-derived. MS/MS fragmentation provided evidence for a linear tetrapyrrole product containing a methyl group added at the α-meso bridging carbon. Assays conducted in buffered D_2O yielded product with a 43% enrichment in the [A+1] peak, indicating the incorporation of a single solvent-derived deuteron in the product during turnover.

ChuW was identified as a Class C Radical SAM Methyltransferase that catalyzes anaerobic heme degradation based on this work. Bioinformatic analysis suggested high sequence identity to HemN, and biochemical characterization provided evidence for the use of two SAM molecules during turnover. The unequivocal conclusion was that the reaction liberates iron by opening the porphyrin macrocycle. However, given that the proposed mechanism was similar to all other RS enzymes and invoked a radical intermediate, what role the heme-iron plays in the reaction, as well as the role of other proteins in the same operon with ChuW, remain unclear.

ChuX

ChuX follows ChuW in the operon and homologues are annotated as heme binding proteins with low micromolar affinities for heme *in vitro.*[37,120] *E. coli* ChuX structural analysis reveals a strong secondary structural alignment of the ChuX dimer with the *E. coli* ChuS monomer (2.4 Å RMSD). The similarity in fold between he two proteins was surprising, given the incredibly low sequence identity (18%), of the ChuX monomer to either N or C-terminus of ChuS. ChuX lacks a structurally equivalent histidine residue to the proximal histidine observed in ChuS, which is responsible for heme coordination, and lacks heme degradation activity in the presence of ascorbate or a cytochrome P450 reductase reducing partner. A K_d of 2μM was determined by a UV-Vis titration of ChuX into heme solutions, although a structure of the ChuX-heme complex was unable to be solved.

HutX in *Vibrio cholerae* shares 37% sequence identity with ChuX, and their structures align well with an RMSD of 2.4 Å.[120] In addition to characterization as a heme-binding protein, HutX was proposed to act as a heme chaperone and binding partner to HutZ. Surface Plasmon Resonance (SPR) determined the K_d for *holo HutX* binding to *apo* HutZ to be 400μM, several orders of magnitude weaker than interactions between other heme chaperones and their client proteins.[121] The reason for a markedly lower affinity between HutX and HutZ compared to other systems is not well understood.

ChuY

ChuY, located adjacent to ChuX and ChuW in heme utilization operons, was first characterized in uropathogenic *Escherichia coli* strain CFT073.[122] ChuY is conserved among other pathogenic bacteria and has been annotated as an important virulence

factor. ChuY structural characterization in the absence of ligand revealed a Rossman fold with high structural similarity to human β-biliverdin reductase (RMSD 2.4 Å). ChuY bound NADPH with an affinity of 190nM based on ITC data, supporting the hypothesis that it may be using NADPH as a cofactor in reduction of an unknown substrate.[122] Given the high sequence similarity to human β-biliverdin reductase, it was predicted ChuY may reduce biliverdin or FMN. In determining ChuY's potential role in virulence, *in vitro* infectivity assays were conducted with WT and ChuY knockout strains of uropathogenic *E. coli* using HEK293 and mouse macrophage cells. In both cases, there was a decreased infectivity potential in strains lacking the ChuY gene, which was rescued when ChuY was reintroduced on a separate plasmid.

The exact reaction catalyzed by ChuY was not clearly demonstrated by Kim et al.,[122] however, this was clarified by work published one month later by LaMattina and colleagues.[123] ChuY, though unable to reduce biliverdin *in vitro,* demonstrated anaerobilin reductase activity when incubated with the isolated product formed by ChuW.[6] Enzymatic activity was tracked using UV-Vis spectroscopy to observe the decay of bands consistent with the linear tetrapyrrole product. MS and MS/MS fragmentation data provide evidence for a four-electron reduction, occurring over two catalytic cycles.

HutZ, revisited

HutZ-like enzymes, in genomes lacking the neighboring HutW and HutX genes, demonstrate heme oxygenase activity in the presence of catalase, as is the case for *H. pylori* and *C. jejuni.*[46,47] Organisms containing the full HutWXZ operon lack the associated heme oxygenase activity, as is the case for HutZ in *Vibrio cholerae.*[43] Organisms which contain HutWXZ genes typically lack a homologue to the ChuY gene seen in other

systems. Although the two proteins are quite different structurally, this finding, and the operon structure, hint at potential similar functions for ChuY and HutZ.

CHAPTER 2

NEW INSIGHT INTO THE MECHANISM OF ANAEROBIC HEME DEGRADATION[1]

[1] Liju G. Mathew, Nathaniel R. Beattie, Clayton Pritchett, and William N. Lanzilotta. *Biochemistry* **2019** *58* (46), 4641-4654. Copyright 2019, adapted with permission from American Chemical Society

Abstract

ChuW, ChuX, and ChuY are contiguous genes downstream from a single promoter that are expressed in the enteric pathogen *Escherichia coli* O157:H7 when iron is limiting. These genes, and the corresponding proteins, are part of a larger heme uptake and utilization operon that is common to several other enteric pathogens, such as *Vibrio cholerae*. The aerobic degradation of heme has been well characterized in humans and several pathogenic bacteria, including *E. coli* O157:H7, but only recently was it shown that ChuW catalyzes the anaerobic degradation of heme to release iron and produce a reactive tetrapyrrole termed “anaerobilin”. ChuY has been shown to function as an anaerobilin reductase, in a role that parallels biliverdin reductase. In this work we have employed biochemical and biophysical approaches to further interrogate the mechanism of the anaerobic degradation of heme. We demonstrate that the iron atom of the heme does not participate in the catalytic mechanism of ChuW and that *S*-adenosyl-l-methionine binding induces conformational changes that favor catalysis. In addition, we show that ChuX and ChuY have synergistic and additive effects on the turnover rate of ChuW. Finally, we have found that ChuS is an effective source of heme or protoporphyrin IX for ChuW under anaerobic conditions. These data indicate that ChuS may have dual functionality in vivo. Specifically, ChuS serves as a heme oxygenase during aerobic metabolism of heme but functions as a cytoplasmic heme storage protein under anaerobic conditions, akin to what has been shown for PhuS (45% sequence identity) from *Pseudomonas aeruginosa.*

Introduction

For decades biochemistry textbooks espoused the function of *S*-adenosyl-l-methionine (SAM) as an important methyl donor in strictly S_N2-catalyzed methyl transfer reactions. This paradigm changed significantly with the identification and characterization of the radical SAM (RS) superfamily and the utilization of SAM in the generation of a highly reactive radical intermediate.[8,124,125] Our understanding of the radical generation mechanism by RS enzymes has come a long way over the past two decades, and more recently it has been shown that reductive cleavage of SAM, by a catalytically conserved [4Fe–4S] cluster, involves an organometallic intermediate.[69,126,127]The latter discovery brings the field full circle considering early investigations that compared RS enzymes to what was known about the mechanism of B_{12}-dependent enzymes. Following these initial investigations, extensive work has demonstrated that RS enzymes exert an astonishing amount of control in “tuning” the initial radical as well as guiding multiple radical intermediates during catalysis[128–130] allowing these enzymes to do far more than simply catalyze the anaerobic equivalent of essential oxygen-dependent reactions.

Paradoxically, it has also been discovered that a subclass of RS enzymes utilizes SAM as a methyl donor in addition to using SAM for radical generation.[89] Currently four distinct classes of RS methyltransferases (RSMTs) have been identified.[89,102,131,132] Each RSMT class utilizes a distinct cofactor/cosubstrate repertoire to facilitate notably different methyl transfer reactions. In general, RSMTs are involved in the methylation of inert carbon or phosphorus centers, hence the requirement for a radical intermediate. The mechanism of class A RSMTs, in the methylation of RNA bases, has been understood for some time and involves two strictly conserved cysteine residues to facilitate the methylation of sp^2-

hybridized carbon centers.[99,100,133,134] The class B RSMTs require a cobalamin cofactor to facilitate the methylation reaction and include enzymes such as CysS,[107] Fom3,[135,136] GenK,[137] PoyC,[138] Sven0516,[139] and ThnK.[140] Class B RSMTs are more diverse, catalyzing the methylation of phosphonate phosphorus atoms as well as sp^2- and sp^3-hybridized carbon centers. Class C, or "HemN-like", RSMTs complete the methylation of sp^2-hybridized carbon centers without using cysteine residues.[109,141–144] The vast majority of class C RSMTs are involved in the biosynthesis of natural products, with one notable exception.[6] Finally, the class D RSMTs use methylenetetrahydrofolate as a methyl donor[113] and function in methanopterin biosynthesis. Of all the classes, the class C and D RSMTs are currently the least understood.

In this work, we address several unanswered questions regarding the mechanism of ChuW, a class C RSMT that was recently identified in the anaerobic degradation of heme by the enterohemorrhagic serotype *Escherichia coli* O157:H7.[6] In fact, ChuW, ChuX, and ChuY are all expressed as part of a previously identified heme uptake and utilization operon (Figure 2.1).[145] The expression of ChuW, ChuX, and ChuY is under the control of the *fur* promoter, and ChuW has been shown to catalyze the oxygen-independent opening of iron-protoporphyrin IX (heme).[6] The physiological role of this gene cluster is the liberation of iron during colonization and infection of the intestine.[145] However, unlike the canonical heme oxygenase reaction, ChuW utilizes an oxidative carbon radical to initiate and ultimately catalyze the opening of the porphyrin macrocycle. On the basis of observations with other RSMTs, we now propose that the metal ion does not participate in the mechanism of ring opening (Figure 2.1). Like the product of aerobic heme degradation (biliverdin), the product of anaerobic heme degradation, termed

“anaerobilin”, is a hydrophobic tetrapyrrole with potentially toxic properties. Hence, in a role analogous to biliverdin reductase, it has been shown that ChuY catalyzes the NADPH-dependent reduction of anaerobilin.[123] The parallels to heme oxygenase and biliverdin reductase function are striking and suggest that accumulation of anaerobilin may be toxic to the pathogen. Consistent with this hypothesis, deletion of ChuY from the enterohemorrhagic *E. coli* CFT073 has been shown to result in a decrease in infectivity of the pathogen.[122] These data clearly indicate that ChuW and ChuY must function synergistically in vivo during anaerobic heme degradation by the pathogen and raise new questions about the function of ChuX, a protein expressed from the same operon from a gene (*chuX*) located between the *chuW* and *chuY* genes (Figure 2.1). Turnover of ChuW in D_2O results in the incorporation of a single, nonexchangeable, deuterium atom. Therefore, our preferred mechanism involves transient formation of a hydride and, depending on which C–C bond is broken, formation of one of potentially two anaerobilin isomers. For simplicity only one product isomer of anaerobilin is shown in Figure 2.1.

Several additional questions regarding anaerobic heme degradation arise when other observations are considered. For example, cytoplasmic storage of external heme acquired by the pathogen is an open question. The *chuX* gene is located between *chuW* and *chuY*, and all three proteins are expressed at the same time. Previous work has reported that heme binds to ChuX with an affinity of 1.99 μM.[37] However, the same investigators have also shown that another cytosolic protein, ChuS, has a significant affinity (~1 μM under anaerobic conditions) for heme and can catalyze a peroxide-dependent heme degradation reaction in the presence of ascorbic acid and molecular oxygen.[146] More importantly, knockouts of the *chuS* homologue in *Shigella dysenteriae*,

shuS, showed an impaired ability to utilize heme as an iron source at low heme (<15.0 μM) levels with higher heme levels (>40.0 μM) being lethal to the knockout strain.[147] This is consistent with observations in other enteric pathogens that, without a “heme buffer”, high cytosolic heme levels become toxic to the cell. These data provide evidence that in the absence of molecular oxygen ShuS, and by homology ChuS, has an important role in heme storage in addition to the proposed role in heme degradation when molecular oxygen is present.[148] Specifically in the absence of molecular oxygen, a condition consistent with the colonization of the distal intestine, we propose that ChuS may function as a heme binding protein. This is consistent with the report that under anaerobic conditions ChuS binds heme (K_d = 1.0 μM) with greater affinity than ChuX.[148] Under anaerobic conditions heme-loaded ChuS would be capable of storing heme as well as delivering heme to ChuW for degradation. Moreover, given the location and expression profile of ChuX, we hypothesize that this protein may function in a protein–protein complex with ChuW and ChuY during anaerobic heme degradation. Notably, a metal binding site has been identified in at least one other ChuX homologue (PDB ID 3FM2).

In this work we address several of these unanswered questions and hypotheses presented above, including whether the metal ion is required for opening the porphyrin ring. The data reported herein provides information about the biophysical properties of ChuW and sheds significant new light on the anaerobic heme degradation mechanism, including the identification of a catalytic residue. In addition, this investigation examines the roles of ChuS, ChuX, and their interactions with ChuW during anaerobic heme degradation. Evidence is presented that supports a new model wherein all four proteins work together in the anaerobic catabolism of heme.

Materials and Methods

Expression, Purification, and Reconstitution

ChuW was expressed in *E. coli* BL21 DE3 using a commercially available pET expression plasmid exhibiting kanamycin resistance with an isopropyl β-D-1-thiogalactopyranoside (IPTG)-inducible promoter and a 6x his-tag. ChuW was coexpressed with the pDB1282 plasmid (ampicillin resistant) containing the *isc* operon during cell growth at low temperature. Briefly, a 20 mL starter culture was added to 2 L of M9 minimal media (4 L culture flasks) containing 0.02% casamino acids and grown at 37 °C, with shaking at 200 rpm. At an OD of 0.3, arabinose was added to 0.2% (wt/vol). At an OD_{600} of 0.6, IPTG was added to a final concentration of 200 μM, and cultures were incubated at 17 °C with shaking at 180 rpm for 17 h. Cells were harvested by centrifugation (10 000 × *g*) and stored at −80 °C until further use. The cells were resuspended in degassed buffer (50 mM Tris buffer at pH 8.0 with 250 mM KCl, and 10% (v/v) glycerol containing DNase, Lysozyme, and PMSF) in an anaerobic glovebox, which was then sealed; the samples were then brought out of the glovebox to further degas with argon while being stirred. The solubilized cells were then lysed anaerobically by equilibrating a closed-system French press with anaerobic buffer while maintaining a stream of argon in the drawing and collection flasks. The lysate was centrifuged at 60 000 × *g* for 1.5 h. The supernatant was collected, and ChuW was purified anaerobically by a gravity flow cobalt column equilibrated with buffer. The column was then washed with three column volumes of buffer containing 0 and 10 mM imidazole. ChuW was eluted in buffer containing 250 mM imidazole, and fractions were analyzed by SDS/PAGE. The protein was then diluted to 1 mg/mL for reconstitution. Briefly, the protein was diluted in 50 mM Tris, pH 8.0, 250 mM

KCl, 10% glycerol, and 5 mM DTT. After incubation for 5 min, 100 mM ferric chloride was added to 4 equiv of protein concentration while swirling. After a 30 min incubation, 15 µL of 100 mM sodium sulfide was added every 10 min until reaching 1 equiv (eq) of the iron added. The mixture was capped and incubated in the glovebox for 12 h. The precipitate was removed by centrifugation, and the supernatant was run over a DEAE Sepharose anion exchange column by gravity flow in the glovebox. The column was washed with 20 mM Tris, pH 8.1, and 10% glycerol (buffer A), and the protein was eluted using a stepwise gradient of 1 M KCl in buffer A. Protein fractions were pooled, concentrated anaerobically, and stored in liquid nitrogen until further use.

Iron Analysis

Iron quantification of purified ChuW was performed using a colorimetric assay. Iron standards were prepared in acid-washed glassware at a concentration of 0.5 mM ferrous ammonium sulfate heptahydrate and diluted to various concentrations between 0.012 and 0.2 mM to a final volume of 250 µL with identical buffers (20 mM Tris, pH 8.0, 300 mM KCl, and 10% glycerol). After acid precipitation and heat incubation at 80 °C, 750 µL of dH_2O was added, and then precipitates were pelleted by centrifugation; 750 µL of each solution was transferred to a new microcentrifuge tube, where 50 µL of 10% hydroxylamine and 250 µL 0.1% bathophenanthroline were added with vortexing between additions. Samples were incubated at room temperature for 1 h and measured at 535 nm following the incubation period. ChuW samples were prepared in the same manner with triplicate measurements per concentration tested, whereas independent experiments were performed in triplicate as well. The same protocol was used to detect the total amount of iron available to the chelator in the ChuW assay before and after turnover. Any

protein-bound iron is released during the acid hydrolysis and is subject to chelation by bathophenanthroline, whereas heme-, deuteroheme-, or mesoheme-bound iron is not.

UV–Vis Activity Assays

All UV–visible spectra were recorded on an HP 8453 diode array spectrophotometer running on OlisWorks using a Peltier temperature controller set to 25 °C and a stir speed of 1200 rpm. Typical enzyme assays were conducted anaerobically with degassed buffer containing 5% DMSO; 1 μM ChuW; 5 μM 3 *E. coli* Flavodoxin (flv); 2 μM *E. coli* NADP:Flavodoxin oxidoreductase (flx); 250 μM NADPH; and 20 μM of heme, protoporphyrin IX, deuteroheme, or deuteroporphyrin IX. Reactions were initiated by the addition of SAM to a final concentration of 250 μM. Spectra were taken from 350 to 900 nm every 10 s for 30 min. Previously published extinction coefficients for DAB and anaerobilin were used to determine ChuW activity.[6] When determining the effect ChuX and ChuY had on ChuW activity, varying concentrations of the respective proteins were added to the assay mix prior to SAM addition. All data were fit and processed in either PRISM or Igor.

LC-MS Activity Assays

All LC-MS data was collected using an Orbitrap Q-TOF coupled to an Agilent 1500 HPLC system. For a standard 2 mL reaction mixture, titanium(III) citrate was added to a final concentration of 2 mM in 50 mM Tris buffer, pH 8.0 that also contained 150 mM KCl. ChuW and SAM were then added to a final concentration of 50 and 2 mM, respectively. The reaction mixture was then incubated for 5 min prior to the addition of porphyrin substrate. Heme, protoporphyrin IX, deuteroheme, or deuteroporphyrin IX was added to

a final concentration of 250 μM. Reaction mixtures were covered and left in the dark overnight, with stirring. Following overnight incubation, the mixture was taken and added to DMSO, in a ratio of 2:1 DMSO to reaction buffer. The mixture was then spun down at 14 800 × *g* for 2 min to pellet precipitated protein. The supernatant was directly injected into an 88 μL injection loop prior to loading onto the column. An SAS-Hypersil C1 analytical column (150 × 4.6 mm) from Thermo-Fisher was used for product separation. Separation was carried out using 100% methanol (solvent A) and 5 mM ammonium acetate pH 4.6 (solvent B) at a flow rate of 1.0 mL/min. Elution: start, 40% solvent A, 60% solvent B; 10 min, 73% solvent A, 27% solvent B; 20 min, 90% solvent A, 10% solvent B; 25 min, 95% solvent A, 5% solvent B. Total runtime was 30 min for each sample.

EPR Spectroscopy

Samples for electron paramagnetic (EPR) spectroscopy were prepared in an anerobic chamber where the oxygen concentration was maintained below 1 PPM at all times. EPR was used primarily as a “fingerprint” for the electronic environment of the [4Fe–4S] (formally 1+) cluster and to monitor SAM-dependent changes in the spectrum. Unless otherwise stated in the figure legend, all EPR spectra were recorded at 12 K with a microwave power of 0.1 mW and microwave frequency of 9.352 GHz, a modulation amplitude of 4.0 G, and modulation frequency of 100 kHz. Sodium dithionite was also included to a final concentration of 2 mM, in all the buffers used for EPR experiments. Samples were prepared in the anaerobic chamber, sealed, and then flash frozen in liquid nitrogen.

ChuX Alignment and Docking Studies

Alignment of the backbone α-carbon atoms for the ChuX protein from *E. coli* O157:H7 (PDB 2OVI, green), *A. variabilis* (PDB ID 3FM2, light blue), and *V. cholerae* HutX (PDB ID 5EXV, purple) was performed using PYMOL. ChuX from *E. coli* O157:H7 was used as the reference structure, and the maximum root-mean-square deviation (RMSD) that was obtained for any alignment described herein was 1.2 Å. This corresponded to the RMSD obtained when the model of HutX from *V. cholerae* was aligned with the ChuX model from *E. coli* O157:H7. In order to identify potential binding modes for anaerobilin binding to ChuX, we employed Autodock VINA[149] using an energy-minimized model for anaerobilin generated with eLBOW.[150]

Sedimentation Velocity Analysis

ChuX was dialyzed into 50 mM Tris buffer (pH 8) and 250 mM KCl for 24 h at 4 °C. The dialyzed protein was quantified on an Agilent 8453 spectrophotometer using an ε_{280} of 14 105 M^{-1} cm^{-1} as determined by ProtParam.[151] The protein sample was diluted with the dialysis buffer to a final concentration of 0.72 mg/mL (4 μM) and loaded into cells with 12 mm double-sector Epon centerpieces. The loaded cells were equilibrated in the rotor for 1 h at 20 °C, and sedimentation velocity data were collected at 50 000 rpm at 20 °C in an Optima XLA analytical ultracentrifuge. Data were recorded at 280 nm in radial step sizes of 0.003 cm. SEDNTERP[152] was used to calculate the partial specific volume of ChuX (0.736638 mL/g) as well as the density (1.0114 g/mL) and viscosity coefficient (0.0101367) of the buffer. SEDFIT[153] was used to analyze the raw sedimentation data. Data were modeled as a continuous sedimentation coefficient distribution ($c(s)$) by fitting the baseline, meniscus, frictional coefficient, and systematic time-invariant and radial-

invariant noise. The fit data for the experiment had a root-mean-square deviations of (rmsd) < 0.005 AU. The predicted sedimentation coefficient (*s*) values were calculated from the highest-resolution atomic coordinates of ChuX (PDB ID 6U9J) using HYDROPRO20.[154]

ChuX and ChuY Expression and Purification

ChuX and ChuY were grown and purified under the same conditions. Each protein was expressed in *E. coli* BL21 DE3 cells using an IPTG-inducible expression plasmid with kanamycin resistance. LB media (1 L) was inoculated with a 20 mL starter culture, then grown at 37 °C with shaking at 200 rpm. At an OD_{600} of 0.6, IPTG was added to a final concentration of 1 mM; cultures were then grown overnight at 17 °C. Cells were harvested by centrifugation before freezing and storage at −80 °C until further use. Frozen cell pellets were solubilized in buffer containing 50 mM Tris pH 8.0 250 mM KCl 10% glycerol with 0.05 mM PMSF, 0.05 mg/mL lysozyme, and 50 μg/mL DNase. Cells were lysed aerobically with a French pressure cell, and the lysate was centrifuged at 100 000*g* for 1.5 h. The supernatant was applied to TALON resin and washed with 2 column volumes of water and 8 column volumes of buffer. After the column was washed with 10 mM imidazole in buffer, protein was eluted with buffer containing 250 mM imidazole. Protein was analyzed by SDS-PAGE analysis and absorption at 280 nm prior to freezing at −80 °C for further use.

ChuS Expression, Purification, and Heme Reconstitution

ChuS expression and growth was the same as ChuX and ChuY procedures. Upon harvesting and freezing cells expressing ChuS, cells were solubilized anaerobically in 50

mM Tris pH 8.0 250 mM KCl 10% glycerol containing PMSF, DNase, and lysozyme. Cells continued to solubilize and degas under argon prior to anaerobic cell lysis as described above when purifying ChuW. Lysate was centrifuged at 100 000 × *g* for 1.5 h, then supernatant was loaded onto pre-equilibrated TALON resin. The column was washed with several column volumes of 10 mM imidazole prior to elution with 250 mM imidazole. Following elution, fractions containing ChuS were analyzed using SDS-PAGE then washed with buffer to remove imidazole prior to diluting to 5 mg/mL in buffer. Heme or PPIX stock solutions prepared in DMSO were added in 250 µL aliquots every 10 min with stirring to 5 equiv ChuS concentration. ChuS:Heme or ChuS:PPIX mixtures were concentrated to at least 1 mM prior to running over a pre-equilibrated (50 mM TRIS, 250 mM KCl, pH 8.0) Sephadex G-25 column to remove excess porphyrins. ChuS concentration was determined using absorption at 280 nm, and heme was determined to be 1:1 by using the previously published ChuS extinction coefficient ε_{410} = 159 $mM^{-1} \cdot cm^{-1}$.

Site-Directed Mutagenesis of ChuW

Acidic amino acids that were predicted to be in the active site of ChuW and not in the conserved TIM barrel fold near the catalytic [4Fe–4S] cluster or cluster ligands were identified by structural modeling using PHYRE.[124] The predicted model and additional input from the conserved residues identified in a ClustalW sequence alignment of ChuW with HemN (PDB ID 1OLT) were used. Each mutation was engineered using Quickchange site-directed mutagenesis. In brief, complementary mutagenic oligonucleotide primers were designed to contain the desired mutation flanked by a 15–20 base pair extension on each end homologous to the parent plasmid. Each PCR

reaction contained a total volume of 50 µL with 4 µM of each primer, 200 µM of each dNTP, and 10 µg of parent DNA, in ThermoPol reaction buffer (20 mM Tris–HCl (pH 8.8), 10 mM KCl, 10 mM $(NH_4)_2SO_4$, 2 mM $MgSO_4$, 0.1% Triton X-100). After preheating each condition at 95 °C for 5 min, 1.0 µL of $Vent_R$ DNA Polymerase (New England Biolabs; #M0254S) was added to each tube, and the PCR reactions were allowed to proceed (annealing: 55–58 °C, 1 min; extension: 68–72 °C, 20 min; denaturing: 95 °C, 1 min; 18 complete cycles). Following the PCR reaction, 1.0 µL of DpnI (New England Biolabs; #R0176S) was added to each tube and allowed to react at 37 °C for 6 h. The suspensions were then transformed into competent BL21 DE3 *E. coli*, and identification of plasmids with the desired mutations was performed by subsequent isolation, PCR, and sequencing of plasmid DNA from candidate colonies.

Results

Proposed Reaction Mechanism for ChuW

RS enzymes share a common mechanism for generation of the initial catalytic radical and have been shown to elicit an astonishing amount of control over radical intermediates during the course of their catalytic mechanisms.[109,130,155] Therefore, although the physiological role of ChuW is to liberate iron from heme, we hypothesized that the iron atom does not participate in the catalytic mechanism of ChuW. This new proposal is outlined in Figure 2.1. Like other class C RSMTs we have presented evidence that ChuW utilizes two SAM molecules during a single turnover.[6] Moreover, the vast majority of RS enzymes utilize a catalytic [4Fe–4S] cluster to generate a 5′-deoxyadenosyl radical (5′-dAdo·); therefore, the reaction mechanism shown in Figure 2.1 begins after the initial 5′-dAdo· has abstracted a hydrogen atom from a second SAM molecule, leading to the

formation of a transient methylene radical (Figure 2.1, I to II). Methylene radical addition to the conjugated ring system at the *meso*-carbon atom would proceed rapidly, leading to a covalent SAM-porphyrin adduct (Figure 2.1, intermediate II). Synthetic substrates that incorporate radical "traps" have proven extremely useful in previous work,[156] and an attempt to capture this adduct is underway using modified porphyrins. However, it should be noted that a similar adduct has been captured for the class C RSMT NosN.[112] Breaking carbon–carbon bonds for sp^2-hybridized carbon atoms is thermodynamically difficult and, consistent with previous observations,[6] protonation (Figure 2.1, intermediate III) to yield sp^3-hybridization at both carbon atoms will lower the thermodynamic barrier, facilitating the β-scission reaction (Figure 2.1, III to IV). At least one additional electron is required to complete the reaction scheme and produce the proposed tetrapyrrole structure that is consistent with the available mass spectroscopy data.[6,123] Initially, our hypothesis was that the iron atom of heme could facilitate additional electron transfer steps or even serve as the source of one electron because under physiological conditions the heme would most likely be in the ferrous state. However, given the catalytic precedent that has been set by several other RS enzymes it is also possible that the mechanism of ring opening is independent of any metal ion.

The Metal Ion Is Not Necessary for ChuW Catalysis

To address the potential role of the metal ion in the mechanism described above, the metal-free forms of both heme and deuteroheme, specifically protoporphyrin IX (PPIX) and deuteroporphyrin IX, were acquired and tested as substrates in the anaerobic degradation assay (Figure 2.2). All the porphyrin molecules (metalated as well as metal-free) investigated were acceptable substrates for ChuW. The metal-free porphyrins have

notably different absorption spectra in the 450–600 nm range due to the lack of metal-porphyrin bonds, but the longer wavelength absorption feature of the linear tetrapyrrole product remains unchanged (795 nm for anaerobilin and 780 nm for deuteroanaerobilin). A significant challenge with these assays is the fact that the substrates are essentially insoluble in aqueous solutions, especially PPIX.

We address the solubility issue below by using the protein ChuS, also expressed when iron concentrations are low from a neighboring operon, as a “porphyrin carrier” for both heme and PPIX. Regardless, the absorption changes that we observe during the time course of the assay are consistent with production of a similar product despite the type of substrate. In order to further address this, we also performed liquid column chromatography with mass spectroscopy (LC-MS) analysis on the turnover samples. As can be seen in Figure 2.3, when the turnover samples are analyzed by LC-MS, the extracted ion chromatograms and ion *m*/*z* data are the same whether the metalated or nonmetalated substrate is used.

Evidence for SAM-Dependent Conformational Changes in ChuW

HemN-like class C RSMTs require the binding of two SAM molecules,[157] in addition to the metabolic substrate that is being methylated and/or chemically modified. For ChuW, we have proposed that SAM binding induces conformational changes required for the proper orientation of heme and may involve changes in the coordination environment of the heme iron. Building on this hypothesis, a reasonable prediction would be that conformational changes associated with SAM binding increase the affinity for heme and/or may be required for efficient turnover. In addition, considering the damage uncontrolled radicals can cause, it would make sense to have a mechanism that prevents

5′-dAdo· generation in ChuW until both SAM and heme are bound. This proposal is not unique as it has long been recognized that enzymes can exist in multiple kinetic conformations;[158] however, no evidence has been presented that addresses if this is occurring for ChuW. To investigate this further, we measured the rate of anaerobilin production after ChuW was preincubated with heme (Figure 2.4, top panel) or SAM (Figure 2.4, bottom panel). Progress curves tracking the production of anaerobilin can be monitored by following the appearance of the distinct anaerobilin absorption feature at 795 nm. The progress curves in Figure 2.4 reveal a significant hysteretic lag when ChuW is preincubated with heme, indicative of a slow transition from a less active to a more active conformation. The hysteretic lag, defined as the time taken for the enzyme to reach a steady-state velocity, can be determined by fitting the progress curves to the equation derived by Frieden:[158] $P(t) = v_{ss}t - \tau(v_{ss} - v_i)(1 - e^{-t/\tau})$(1)*P* represents product concentration at time *t.* τ is equal to 1/k_{obs}, where k_{obs} is the apparent rate constant when transitioning from the initial velocity (v_i) to the steady-state velocity (v_{ss}). When preincubated with heme, ChuW exhibited a lag (calculated using lag = eτ) of 1228 s. When preincubated with SAM, the lag time decreased markedly to 69 s. Additionally, SAM preincubation caused a red shift in the heme Soret band to 416 nm and increased intensity (Figure 2.4, asterisks), indicative of a heme-bound state existing immediately before turnover. This provides evidence for a SAM-dependent transition from a less active to more active conformational state and is the first evidence of a distinct heme-bound intermediate that precedes catalysis.

Identification of a Catalytic Residue in ChuW

Consistent with the available data, the proposed mechanism for ChuW requires that a single nonexchangeable hydrogen atom, from water, is incorporated into anaerobilin.[6] Most likely, the proton transfer event is facilitated by an amino acid with solvent access, as shown in Figure 2.1. In order to address this, a homology model of ChuW was constructed using the online software PHYRE2.[159] This model was structurally overlaid with the current HemN model (PDB ID 1OLT) containing two bound SAM molecules (Figure S1). Acidic amino acids that were predicted to be within 5–10 Å of the methyl group on the SAM molecule, not coordinating the [4Fe–4S] cluster, were targeted for mutagenesis. This included residues D18, D23, D215, D244, and E443. Alanine and the corresponding neutral mutations (asparagine or glutamine) were made at each position for a total of 10 ChuW variants. All variants, including the D215N ChuW, exhibited enzymatic activity except for the D215A variant. Therefore, characterization of the D215A ChuW variant was pursued. The D215A variant may not fold correctly resulting in the loss or incomplete incorporation of the catalytic [4Fe–4S] cluster. Hence, we investigated if the purified enzyme maintained structural stability and, in particular, whether the [4Fe–4S] cluster was intact. The EPR spectra of wild-type ChuW and the D215A variant are shown in Figure 2.5. Iron analysis of the purified enzymes indicated 3.7 and 3.5 iron atoms per peptide for the wild-type and D215A variant, respectively. Moreover, both enzymes exhibit an axial EPR spectrum that is consistent with the presence of the [4Fe–4S] cluster (Figure 2.5A) containing a single unpaired electron in an asymmetric environment. The addition of SAM is known to perturb that electronic environment because of coordination of a SAM molecule to the unique iron atom of the catalytic cluster.[160] As can be seen in

Figure 2.5B, significant changes in the EPR spectrum are observed for both the wild-type ChuW and the D215A variant upon the addition of SAM. While the g-values suggest that the D215A variant may contain multiple species, a cluster similar to the active enzyme clearly exists and is still capable of coordinating a SAM molecule. This indicates that D215A variant still contains a [4Fe–4S] cluster that is capable of binding the first SAM molecule. Therefore, the lack of activity must be due to subsequent steps in the reaction cycle, suggesting that D215 may have a catalytic role.

An Alternative Function for ChuX

The genes *chuW*, *chuX*, and *chuY* are found within the same operon and expressed behind the same promoter. Logic would therefore suggest that the corresponding proteins function together as part of a protein–protein complex. Similar to what has been proposed for ChuX, evidence has been presented that HutX, a homologue of ChuX in *V. cholerae*, may serve as a heme binding protein.[120] However, on the basis of computational modeling and structural analysis of several “X” proteins, we now propose an alternative function for ChuX. We have isolated and crystallized ChuX and, similar to what has been previously reported for both HutX and ChuX,[37,120] we observe a dimeric and tetrameric arrangement in our own ChuX crystals (Table S1, PDB ID 6U9J). However, the relevant question is what is the oligomeric structure of ChuX in solution? Sedimentation velocity analysis shows that a solution of 4 μM ChuX exists primarily (81.3%) as a 2.9 S species that is consistent with the predicted values for a dimer (2.8 S) (Figure 2.6). There is also a small amount (10.8%) of a 4.5 S species that agrees with the predicted value (4.4 S) of a tetramer (Figure 2.6A–C). This is consistent with the crystal packing where the dimer interface buries substantially more surface area (Figure 2.6B) when compared to the

interface required to make the tetramer (Figure 2.6C). Specifically, a PISA analysis indicates a buried surface area of approximately 1000 Å^2 for the dimer interface (Figure 2.6A) while the other interface, required to complete the tetramer, buries approximately 500 Å^2 (Figure 2.6B,C). Moreover, the dimer interface is composed of numerous hydrophobic interactions surround by intrasubunit hydrogen bonds. These properties are hallmarks of a stable and permanent interface. In contrast, the interface that completes the tetramer consists predominantly of ionic interactions and hydrogen bonds.

Although both ChuX and HutX have been reported to bind heme with low micromolar affinities, no structural data has been obtained for either protein with heme bound. Figure 2.7 shows the structural alignment for *E. coli* O157:H7 ChuX (PDB ID 2OVI), *V. cholerae* HutX (PDB ID 5EXV), and *Anabaena variabilis* ChuX (PDB ID 3FM2). Interestingly, the *A. variabilis* ChuX structure also contained a Zn ion bound at two conserved amino acids (Figure 2.7, gray sphere). Given that the products (iron and anaerobilin) of the ChuW reaction are both potentially toxic and the ChuY deletion strain showed a substantial decrease in infectivity,[122] we propose that ChuX may have an alternative function. Specifically, we propose that ChuX works synergistically with ChuW during the opening of the porphyrin ring and release of iron atom. In this role, ChuX would act as a chaperone to transiently sequester the iron atom and/or safely transfer the anaerobilin tetrapyrrole to ChuY, the anaerobilin reductase.[123] To address this new hypothesis, we performed a docking exercise using Autodock VINA. The predicted docking mode for anaerobilin with the most favorable thermodynamic parameters is shown in Figure 2.7. Interestingly, the most favorable binding mode for anaerobilin binding to ChuX from *E. coli* O175:H7 is predicted to be proximal to the metal binding site

observed in the crystal structure of ChuX from *A. variabilis.* Only the peptide atoms were present in the model during the docking simulation. However, it is notable that several of the observed (zinc binding) and predicted (anaerobilin) interactions involve conserved amino acids. Among these are E72 and H98 (*E. coli* numbering) involved in binding the zinc ion. The anaerobilin binding mode identified by Autodock also predicts a salt bridge with R112 and a ring stacking interaction with F136; both residues appear to be conserved in the other "X" homologues. These observations provide a framework to test our hypothesis that ChuX may serve as an iron/anaerobilin chaperone during the anaerobic heme degradation reaction catalyzed by ChuW.

ChuX and ChuY Stimulate ChuW Activity Synergistically

A logical starting point to address our new hypothesis regarding ChuX function is to test whether ChuX has any effect on the turnover rate we observe for ChuW. As a positive control we can add the anaerobilin reductase ChuY to the assay because product release (due to the low solubility of anaerobilin in aqueous solution) is the rate-limiting step. This has long been established to be the case for heme oxygenase; specifically, inclusion of biliverdin reductase in a heme oxygenase assay has been shown to significantly increase the turnover rate.[161,162] Table 1 shows the changes in turnover rates when ChuY or ChuX are also included in the assay.

Table 1. Effect of ChuX and ChuY on the Rate of ChuW Heme Degradation Activity

condition	**specific activity**[a] **(nmol·min^{-1}·mg ChuW^{-1})**
ChuW alone	5.7 ± 0.3
ChuX:ChuW 4:1	16.9 ± 0.2
ChuY:ChuW 4:1	10.7 ± 0.2
ChuX:ChuY:ChuW 4:4:1	28.5 ± 0.5

[a] Specific activity determined by monitoring the degradation of heme. ε_{402} = 51.63 mM^{-1} cm^{-1}. Assay method is the same as that used in Figure 2.2, with the addition of varying concentrations of ChuX and ChuY.

The maximum effect seems to occur when the protein (ChuY or ChuX):ChuW ratios approached 4:1 (Figure S2). These results suggest that substrate release is also rate-limiting for ChuW and is in agreement with the function of ChuY as the next enzyme in the pathway (anaerobilin reductase).[122,123] Unexpectedly, including both ChuX and ChuY resulted in an additive increase in the ChuW turnover rate (Table 1). The additive increase in the turnover rate indicates a more complex and synergistic interaction may be occurring between all three proteins.

ChuS Facilitates Heme or Protoporphyrin IX Transfer to ChuW during Anaerobic Porphyrin Degradation

In addition to ChuW, ChuX, and ChuY, ChuS is also expressed from an adjacent operon under iron-limiting conditions (Figure 2.1). Although the catabolites have not been isolated in vivo, purified ChuS has been shown to catalyze the peroxide-dependent degradation of heme to nonheme iron (bound to ShuS), tripyrrole (565 nm absorption), and hematinic

acid. (58) Of considerable significance is the observation that a homologous gene cluster and protein (ShuS) is found in the pathogen *Shigella dysenteriae.* Moreover, the *S. dysenteriae* ShuS knockout was shown to be defective in utilizing heme as an iron source under aerobic growth. (40) These findings confirm that ChuS provides a viable pathway for accessing heme iron in the presence of molecular oxygen, presumably as proposed by Ouellet et al. (58) However, under anaerobic conditions, ChuS binds heme but does not degrade it. In fact, under anaerobic conditions ChuS binds heme with a high affinity and heme-loaded ChuS can be isolated with substantial yields. (39,41) We have found that heme-loaded ChuS is also quite stable and can be prepared at concentrations greater than 2.0 mM. Therefore, if heme can be transferred from ChuS to ChuW, it will be possible to use heme-loaded ChuS to increase the amount of substrate available to ChuW. The ability to use ChuS as a porphyrin source for ChuW has significant implications. In particular, this indicates ChuS can store excess heme under anaerobic conditions, protecting the cell. Moreover, increasing substrate availability to ChuW is essential to future spectroscopic investigations such as rapid freeze–quench electron paramagnetic resonance (RFQ-EPR) studies aimed at trapping and identifying the proposed radical intermediates. To this end, we have prepared heme-bound ChuS following the previously reported protocols (39,41,58) and found that it can deliver heme to ChuW in our anaerobic assay (Figure 2.8A). The spectral changes we observe in Figure 2.3 are consistent with anaerobilin formation based on the increase in absorption at 445 and 795 nm (Figure 2.8A). As expected, the reaction still required the physiological electron delivery system (*E. coli* flavodoxin and NADPH-flavodoxin/oxidoreductase) and

SAM. Moreover, none of the absorption changes resemble the previously reported tripyrrole product (42) that was observed for the aerobic heme degradation reaction.

Because ChuS could effectively deliver heme to ChuW, and protoporphyrin IX (PPIX) is also viable substrate, we tested whether PPIX-loaded ChuS could be used to provide the metal-free substrate, PPIX, to ChuW during turnover (Figure 2.8B).

This observation is significant for primarily two reasons. First, a viable attempt to capture and analyze radical intermediates will require that those intermediates are present as a substantial percentage of the total population of states in the sample. Increasing the amount of substrate available to ChuW will be an important step toward achieving this goal. In addition, PPIX does not contain a paramagnetic metal ion, thus preventing any additional spin-coupling with radical intermediates that would otherwise prevent detection and/or complicate data interpretation. As can be seen in Figure 2.8B, PPIX-loaded ChuS was also a viable way to deliver the porphyrin substrate to ChuW and resulted in turnover based on the changes seen in the UV–visible spectrum. Taken together, these data indicate that ChuS has a role in heme storage and delivery to ChuW under anaerobic conditions. The application of ChuS, as a means for increasing the availability of substrate (either heme or PPIX) to ChuW will also facilitate future spectroscopic studies aimed at dissecting the radical cleavage mechanism.

Discussion

In this work, we provide new mechanistic insight into the anaerobic heme degradation pathway in *E. coli* O157:H7 using activity assays, LC-MS analysis, biophysical approaches, and docking studies. The data presented herein demonstrate unequivocally that the heme-iron is not essential to the degradation mechanism catalyzed by ChuW.

Evidence is also presented that reveals ChuW undergoes SAM-dependent conformational changes that influence the heme binding mode and facilitate catalysis. In addition, the assays reported here demonstrate a synergistic effect on ChuW activity when other proteins from the heme utilization operon are present. Specifically, evidence presented in this work indicates that ChuS and ChuX may have multiple functions depending on the metabolic state. A new model is proposed for the anaerobic heme degradation mechanism catalyzed by ChuW and discussed in the broader context of the class C radical SAM methyltransferase superfamily. This is important as class C RSMTs have been implicated in the biosynthesis of a number of natural products with important bioreactivity, but their catalytic mechanisms remain poorly understood.[163]

Mechanism of Ring Opening

Prior to turnover, we suspect that the proper orientation of both SAM molecules has important structural/functional consequences for all HemN-like class C RSMTs. As we demonstrate here, preincubation of ChuW with SAM results in a significantly shorter lag time as well as an increase in the Soret band at 417 nm that is transiently observed (Figure 2.4, red asterisks). The logical conclusion is that the SAM-dependent conformational changes take some time but result in a heme-bound state that is more catalytically competent. In this sense, the Soret at 417 nm will allow us to probe the heme-bound intermediate further using spectroscopic techniques such as resonance Raman in the future.

In general, radical SAM enzymes have been shown to control substrate-centered radicals in order to catalyze β-scission reactions that cleave carbon–carbon and carbon–nitrogen bonds.[128] In some cases, multiple β-scission steps occur during the course of a single

turnover, as has been reported for the enzyme ThiC.[164] In the case of ChuW, primary sequence alignments as well as the mechanistic properties indicate that this enzyme belongs to the "HemN-like" or class C RSMT subfamily. In particular, two molecules of SAM are required per turnover.[6] The first SAM molecule generates the initial 5′-dAdo·, ultimately resulting in formation of methionine and 5′-deoxyadenosine, while the second molecule of SAM facilitates a methyl transfer step, resulting in production of *S*-adenosyl-l-homocysteine (SAH). Previous work with ChuW has provided evidence that the 5′-dAdo· abstracts a hydrogen atom from the second SAM molecule to form a methylene radical. Addition of this radical species to the conjugated ring system at the bridging *meso* carbon atom would result in a transient SAM-porphyrin adduct (Figure 2.1, intermediate II). Evidence for similar SAM-substrate adducts during turnover has been observed for other HemN-like class C RSMTs such as Jaw5,[165] NosN,[166] and HemN,[90] suggesting that this is a common mechanistic feature of all class C RSMTs.

The thermodynamics for breaking a C–C bond by β-scission, radical-catalyzed or otherwise, are considerably more favorable if both carbon atoms are sp^3 hybridized, and therefore, we favor a mechanism involving protonation/hydride formation. This is also consistent with the incorporation of a single nonexchangeable deuteron that we observe when ChuW turnover is perform in D_2O. The protonation event may be facilitated by an amino acid in the active site, and therefore, we investigated amino acids that could function in this role. It is tempting to conclude that D215 may be involved in the protonation event because the D215A variant is inactive. However, because the D215N variant is still active there are other possible explanations. In fact, an asparagine residue would be capable of hydrogen bonding and would also occupy the same physical space as an

aspartic acid group. Therefore, while D215 could be involved in an important hydrogen bonding network, a more attractive explanation is that D215 is involved in the orientation of the second SAM molecule within the active site of ChuW. In this case, the D215N variant is still capable of fulfilling a hydrogen bond required to orient the second SAM molecule, allowing catalysis to proceed. While SAH is already a good leaving group, it is important to note that a general base has been implicated in other class C RSMTs in order to facilitate the elimination reaction.[110,166] The porphyrin ring is essentially electron-rich and proton-deficient. In fact, if the ratio of π and lone pair electrons, relative to the total number of protons, is considered, one gets a sense of just how aromatic or electron-rich a compound is. Using this analysis, the electron:proton ratio of a single pyrrole ring is 0.1935, essentially making the pyrrole group more aromatic than benzene (electron:proton ratio of 0.167). Although we cannot eliminate the possibility that a general base facilitates the elimination of SAH, as has been proposed for NosN and TbtI,[110,166] if a similar mechanism is at work in ChuW, then one significant difference would be that SAH is lost prior to C–C bond cleavage.

Regardless of whether the β-scission reaction catalyzed by ChuW involves formation of a hydride (Figure 2.1) or utilizes a general base, the reaction will require an additional electron to quench the radical species and complete the reaction. While this work eliminates the possibility that the heme iron provides an electron or plays a role in catalysis, it is possible that the [4Fe–4S] cluster could facilitate additional NADPH-dependent electron transfer via flavodoxin or ferredoxin. We know that heme oxygenases receive subsequent electrons necessary for heme degradation from NADPH-cytochrome P450 reductase (CPR), the physiological redox partner. For radical SAM enzymes this is

a particularly important point because the electron donor has been shown to influence the catalytic reaction.[167] Artificial electron donors such as titanium(III)citrate are preferred because other chemical reductants have led to catalytic artifacts such as the “abortive cleavage” of SAM when sodium dithionite is used as the reductant.[65]

Multiple Functions for ChuX and ChuS

ChuX (HutX in *V. cholerae*) is a small peptide that has been annotated as a heme binding protein.[37,120] Interestingly, ChuS is essentially a tandem repeat of two “ChuX-like” domains. However, structural alignment of the ChuX dimer on the published ChuS model (PDB ID 4CDP) with heme bound yields an RMSD of 4.8 Å, with no equivalent heme-ligating residues seen in ChuX. Alignment of only the heme binding domains improves the RMSD to 2.2 Å. Despite the similar affinities for heme that have been reported for ChuX and ChuS, only the heme-bound form of ChuS has been characterized structurally. While ChuS may function as a heme oxygenase in the presence of molecular oxygen, this work clearly supports a role in heme storage and transport to ChuW under anaerobic conditions. Moreover, the protein PhuS from the enteric pathogen *Pseudomonas aeruginosa* shares 45% sequence identity with ChuS and has clearly been shown to play a role in cytoplasmic heme storage.[168] Having proteins that can serve multiple functions is not uncommon and will provide the pathogen with a selective advantage. In particular, given the toxicity of heme, a role in sequestering heme under anaerobic (reducing) conditions would be beneficial. We therefore propose that ChuS, like PhuS, also has a role in heme storage under anaerobic growth conditions.

HutX from *V. cholerae*, like ChuX, has been reported to bind the hydrophobic heme molecule. In both organisms, ChuX and HutX are transcribed from the gene immediately

following ChuW and HutW, respectively. It stands to reason that the breakdown product of anaerobic heme degradation in both organisms is a hydrophobic tetrapyrrole that is chemically reactive and therefore toxic. Deletion of ChuY, the anaerobilin reductase, resulted in a phenotype that is consistent with this hypothesis.[122] In fact, the only deletions that have been shown to lead to a fitness phenotype, during growth on heme as the sole iron source, in pathogenic *E. coli* or *V. cholerae*, are deletion of ChuY or HutZ, respectively.[43,122] Moreover, the observations reported here demonstrate that both ChuX and ChuY stimulate ChuW activity individually as well as in an additive manner. This observation is consistent with ChuX playing a role in binding anaerobilin prior to ChuY (HutZ in *V. cholerae*) performing the NADPH-dependent reduction of anaerobilin. The ultimate goal of heme degradation in pathogenic bacteria is to liberate iron, yet iron's fate following turnover is a significant question that requires further investigation. Whether ChuX also facilitates the safe removal, storage, and transport of iron and anaerobilin is under further investigation, but this proposal is consistent with the organization of the genes within the heme utilization operon and the stimulation of activity that we have observed. Moreover, structural alignment of ChuX from *E. coli* O157:H7 with homologues in *V. cholerae* and *A. variabilis* identifies a potential metal binding site. Two conserved amino acids, a glutamate and histidine, coordinate a Zn ion in the *A. variabilis* structure (PDB ID 3FM2). It stands to reason that anaerobilin and iron are cytotoxic molecules. In fact, the proposed anaerobilin molecule is markedly more hydrophobic than biliverdin (product of canonical heme oxygenase), and product release has long been known to be the rate-limiting step in the heme oxygenase reaction.[161] The increased hydrophobicity may further slow product release from the ChuW active site, necessitating the use of a

transporter/chaperone like ChuX or HutX in *V. cholerae.* Whether HutW in *V. cholerae* performs a heme-degradation reaction that is similar to ChuW is currently under investigation.

Turnover of Nonmetalated Porphyrins

The observation that ChuW will utilize nonmetalated substrates, such as protoporphyrin IX and deuteroporphyrin IX, provides a means to further probe the ChuW mechanism by spectroscopic means without the complication of an additional paramagnetic center, further advancing our understanding of class C RSMTs. Although heme-iron liberation is the physiological goal of this system, we have shown that the heme-iron itself is not essential to the ring-opening reaction catalyzed by ChuW. The product features associated with anaerobilin formation at 456 and 795 nm form over time with clear isosbestic points when heme or protoporphyrin IX is incubated with reduced ChuW (Figure 2.2; compare panels A and B). The same holds true when incubating deuteroheme or deuteroporphyrin IX with reduced ChuW, forming a product consistent with deuteroanaerobilin at 439 and 780 nm (Figure 2.2; compare panels C and D). LC-MS analysis corroborates the UV–vis assay data, demonstrating the same products are formed when degrading metalated porphyrins or their nonmetalated counterparts (Figure 2.3). ChuW can degrade heme and protoporphyrin IX to anaerobilin, consistent with a product at 577 *m*/*z* that eluted at 16 min (Figure 2.3A,B). The product intensity is noticeably weaker when using protoporphyrin IX as a substrate and can be attributed to its increased insolubility in aqueous solution. ChuW was also able to degrade deuteroheme and deuteroporphyrin IX to DAB, consistent with a product at 525 *m*/*z* that eluted at 14 min (Figure 2.3C,D). The product masses observed were consistent with

previously reported work, and together the UV–vis and LC-MS data demonstrate the metal is not involved in the degradation mechanism. All of these observations support the use of the nonmetalated substrates for future spectroscopic investigations aimed at trapping and characterizing radical intermediates.

Conclusions

Radical SAM (RS) enzymes continue to be identified that expand the catalytic diversity of the superfamily and the mechanism(s) by which the peptide environment controls radical catalysis. ChuW belongs to the “HemN-like”, or class C RSMT, subfamily of RS enzymes, and although this subfamily is the least understood, our work supports some core mechanistic principles. Specifically, that HemN-like RS enzymes require two SAM molecules to function. The first SAM molecule generates the catalytic radical, presumably via the “omega species”,[169] that abstracts a hydrogen atom from the second SAM molecule to form a methylene radical. The methylene radical attacks a double bond on a nearby substrate that may undergo substantial radical rearrangements in subsequent steps.

For ChuW, the implication that additional proteins, such as ChuX or ChuS, have multiple roles or function synergistically as part of a protein–protein complex in vivo is intriguing. In particular, if enzymes in this subfamily do function as part of larger complexes then this may explain some experimental inconsistencies and the utility of the protein fold as a heme chaperone. For example, HemW is one such HemN-like protein that has been shown to be a heme chaperone but that is also still capable of SAM cleavage.[91] In this case, the precise role of SAM binding and cleavage is not clear. One possible explanation is that other proteins interact with HemW for in vivo function with heme transfer requiring

SAM cleavage. Regardless, for persistent enteric pathogens that can utilize heme as an iron source, heme and the breakdown products of heme will have certain toxic effects. The data presented in this work support a new model whereby ChuS, ChuW, ChuX, and ChuY function together to ensure the safe and efficient catabolism of heme under anaerobic conditions when iron is limiting.

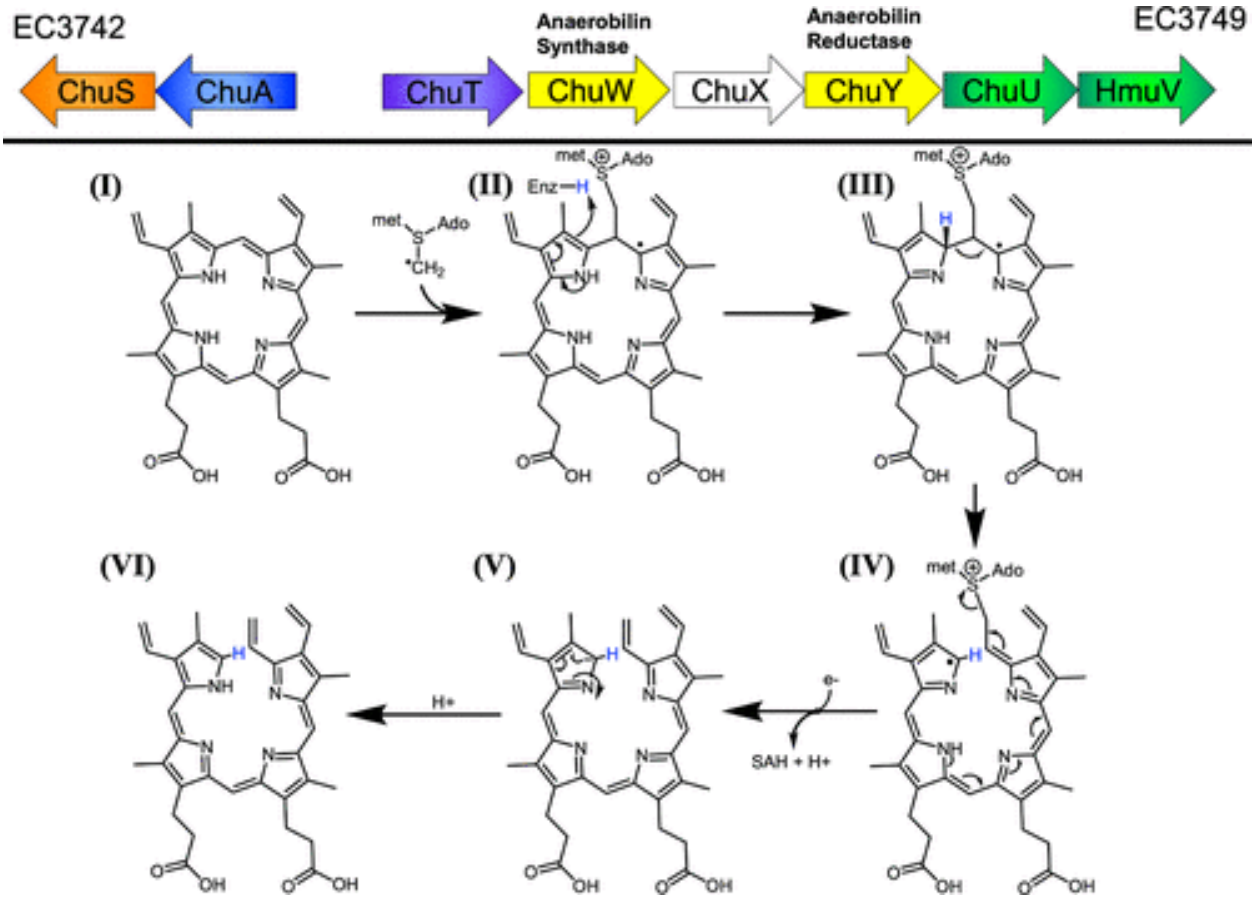

Figure 2.1. Heme utilization operon in *E. coli* O157:H7 (upper panel) and proposed metal-independent mechanism for ChuW (lower panel**)**. In the proposed mechanism, the iron atom of the physiological substrate (heme) is not required for catalysis and β-scission of the porphyrin ring occurs prior to scission of the sulfur–carbon bond. Consistent with other RS enzymes, reductive cleavage of one SAM molecule results in generation of a 5′-deoxyadenosyl radical (5′-dA·). The 5′-dA· then abstracts a hydrogen atom from a second SAM molecule to generate a methylene radical that will add to the *meso* carbon atom of the porphyrin ring (I → II). Protonation of the porphyrin ring (II → III) will facilitate a β-scission reaction (III → IV) and accounts for the incorporation of a single, nonexchangeable, proton in the anaerobilin product as has been previously observed. Further reduction, hydride formation (V), and protonation quench the radical and complete the reaction.

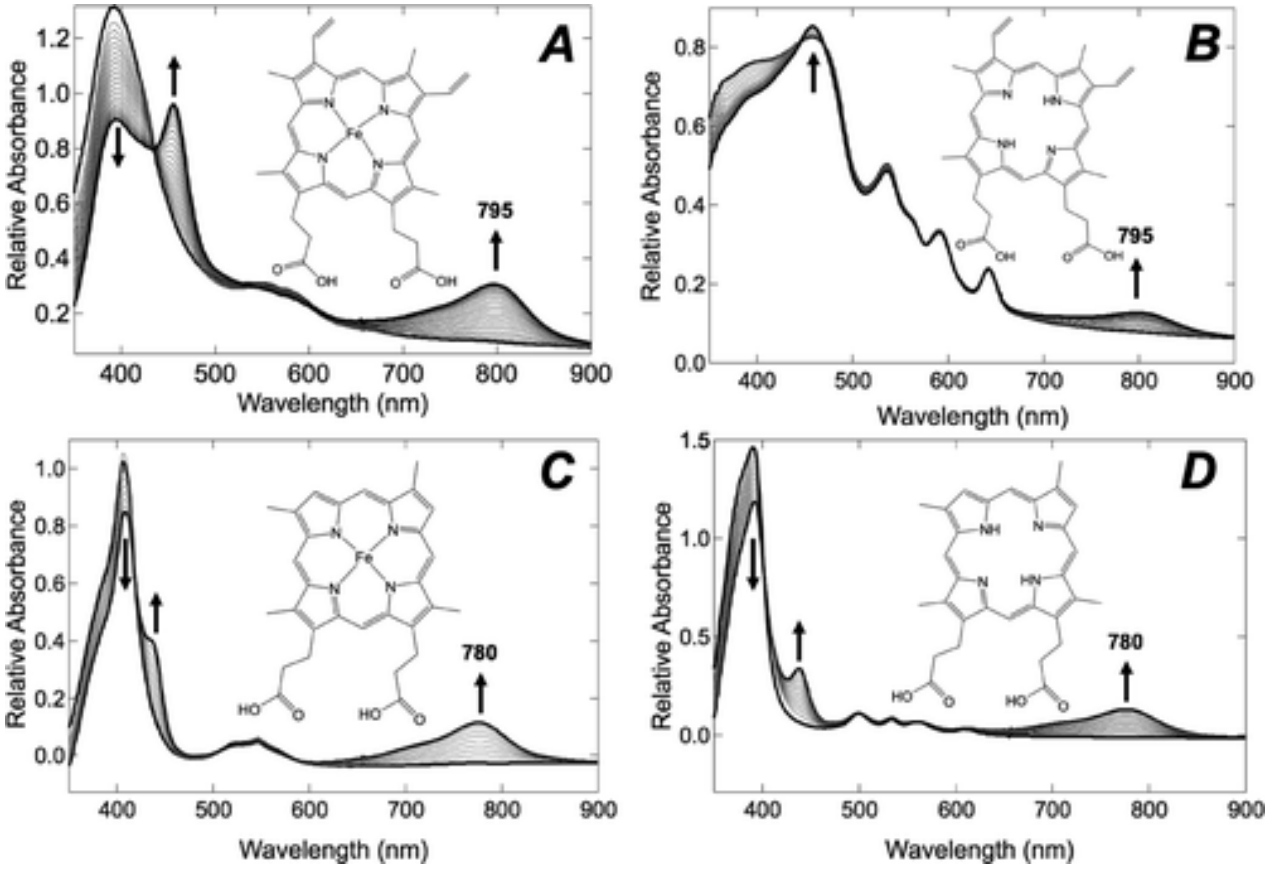

Figure 2.2. UV–visible spectra monitoring the anaerobic degradation of heme (A), protoporphyrin IX (B), deuteroheme (C), and deuteroporphyrin IX (D) catalyzed by ChuW. ChuW assays were performed as described in Materials and Methods. The structure of each substrate is shown as an inset in the respective panels, and the arrows indicate the direction of spectral changes during the assay.

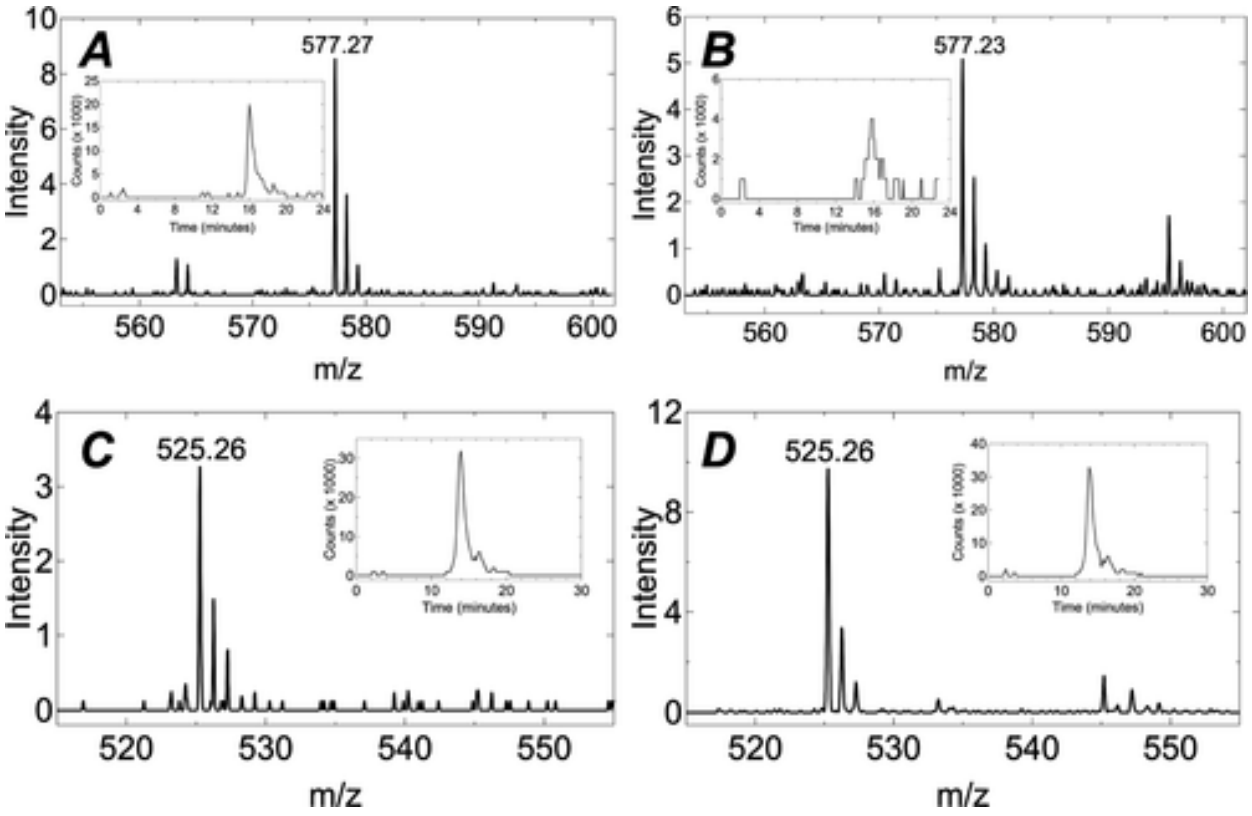

Figure 2.3. LC-MS analysis of ChuW turnover using heme (A), protoporphyrin IX (B), deuteroheme (C), or deuteroporphyrin IX (D) as the substrate. The reaction mixtures from each of the turnover assays shown in Figure 2.1 were analyzed by LC-MS as described in Materials and Methods. The extracted ion chromatogram for each product peak is shown in the panel inset.

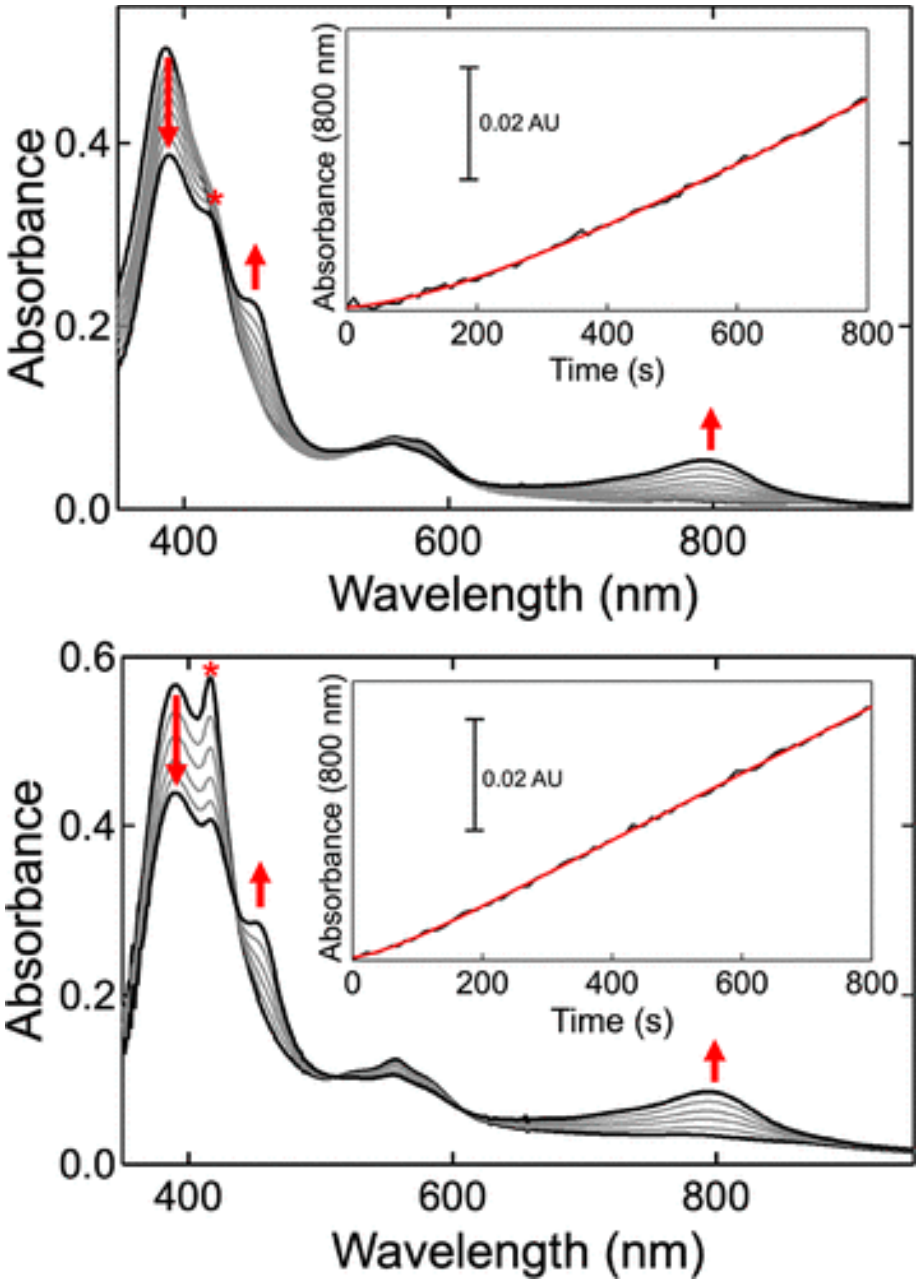

Figure 2.4. Progress curves monitoring heme turnover by ChuW without (top panel) and following (lower panel) preincubation with 1 mM SAM. Assays using 0.5 μM ChuW were performed as previously described[6] except that, in the case of the data shown in the lower panel, 1 mM SAM was preincubated with ChuW for 5 min. In both cases the rate of product formation was followed by monitoring the appearance of the absorption feature at 795 nm (inset in both panels). Frieden's equation for describing a hysteretic enzyme was used to determine the lag time in both cases (red line fit) as described in the text. The asterisks highlight an absorption band, and potential intermediate, that is considerably more intense when ChuW is preincubated with SAM, prior to initiating the reaction.

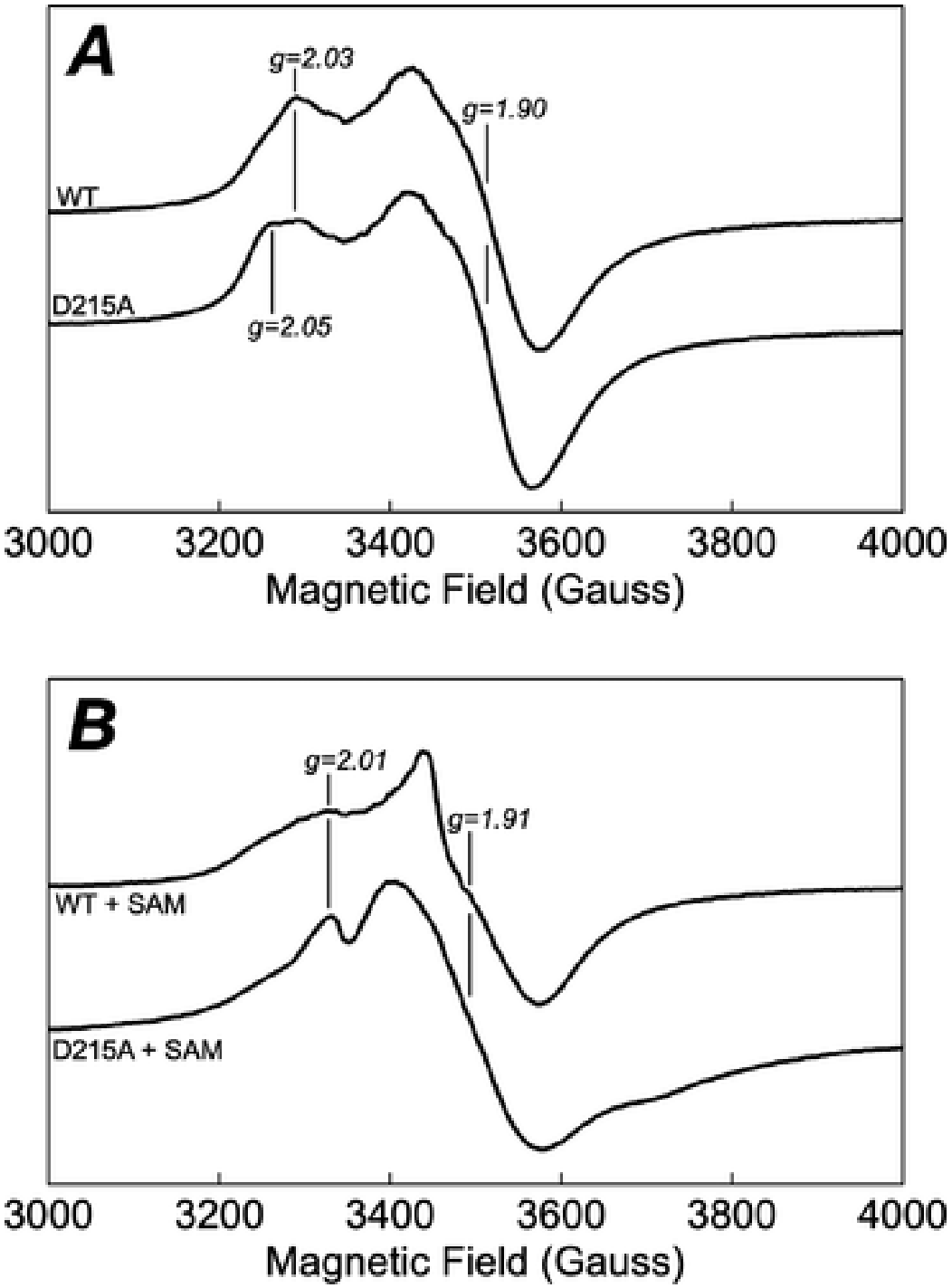

Figure 2.5. EPR spectra for the wild-type (WT) and D215A variant of ChuW in the absence (A) and presence of SAM (B). EPR spectra of 0.4 mM wild-type ChuW (WT) or the D215A variant (D215A) were recorded at 12 K in the absence (A) or presence of 1.0 mM SAM (B). Spectra were recorded at 12 K with a microwave power of 0.1 mW and microwave frequency of 9.352 GHz, a modulation amplitude of 4.0 G, and modulation frequency of 100 kHz. All spectra represent the sum of 10 scans.

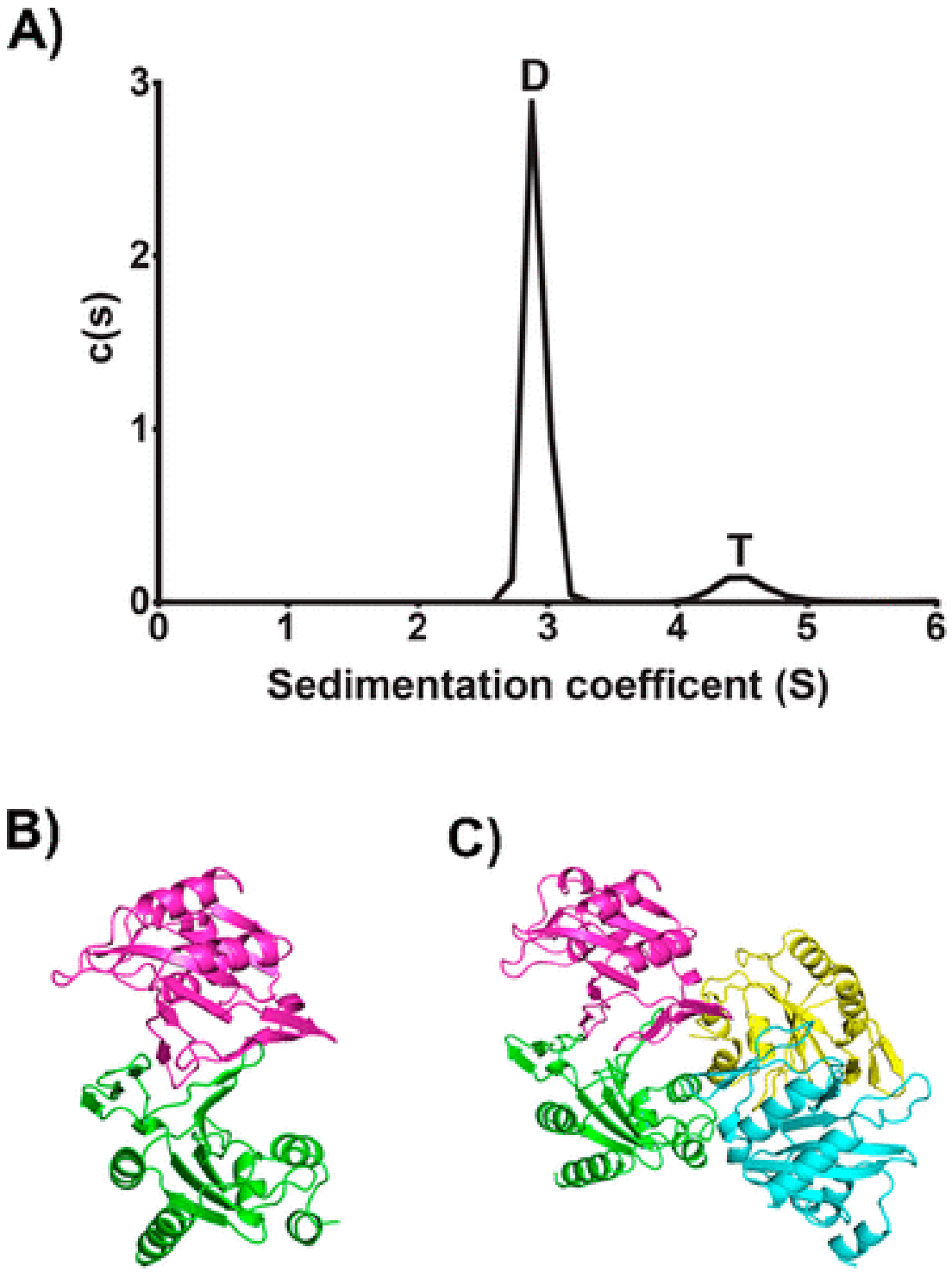

Figure 2.6. (A) Sedimentation velocity *c*(*s*) distribution of ChuX. Analysis was performed as described in Materials and Methods. ChuX was found to consist of a 2.9 S dimer (D) and 4.5 S tetramer (T). (B) ChuX dimer model colored by chain. C) ChuX tetramer model colored by chain. Both models were generated from the crystal structure (PDB ID 6U9J, Table S1).

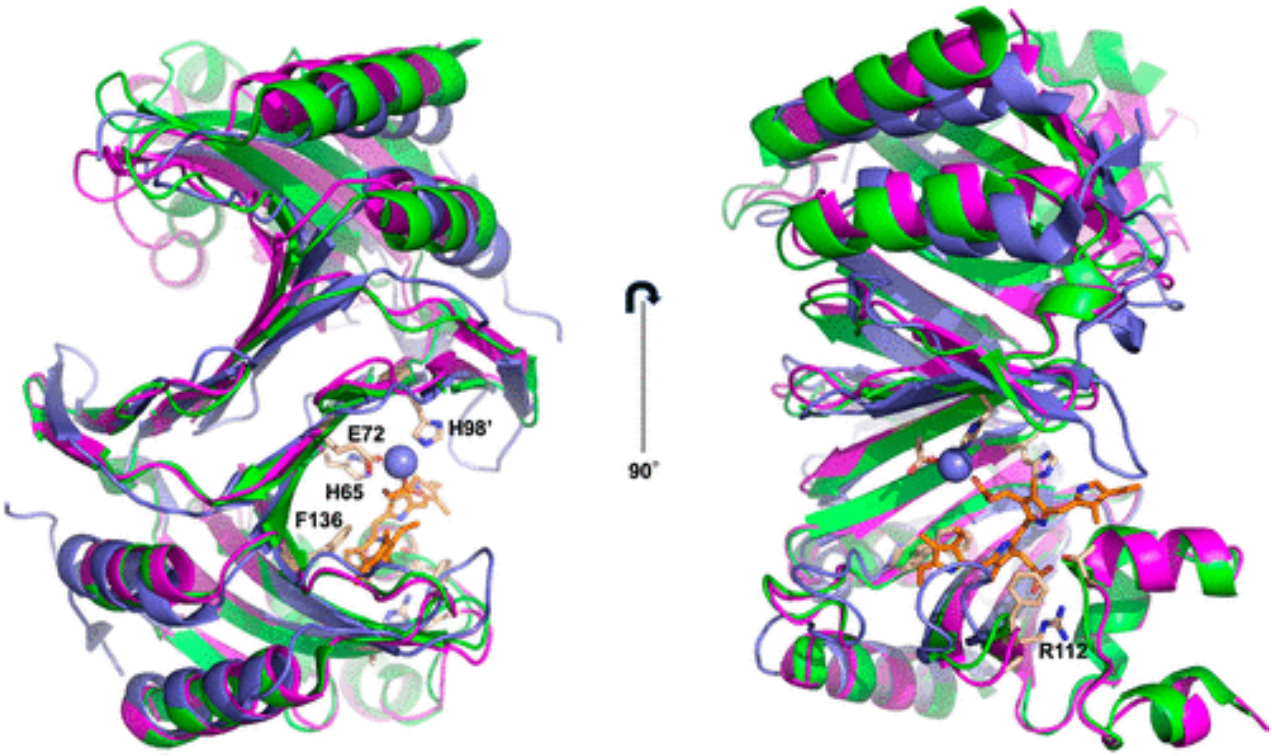

Figure 2.7. Cartoon representation showing a structural overlay for ChuX from *E. coli* O157:H7 (PDB 6U9J, green) aligned with the crystallographic models for ChuX from *A. variabilis* (PDB ID 3FM2, light blue), and *V. cholerae* HutX (PDB ID 5EXV, purple). Autodock VINA was used to predict the most favorable docking mode for the molecule anaerobilin (stick representation with orange carbon atoms) binding to ChuX from *E. coli* O157:H7 (orange stick representation). Interestingly, a zinc ion (light blue sphere) is observed in the crystallographic model for ChuX from *A. variabilis*. The zinc ion is bound by at least two conserved amino acids (E72 and H98 using *E. coli* ChuX numbering).

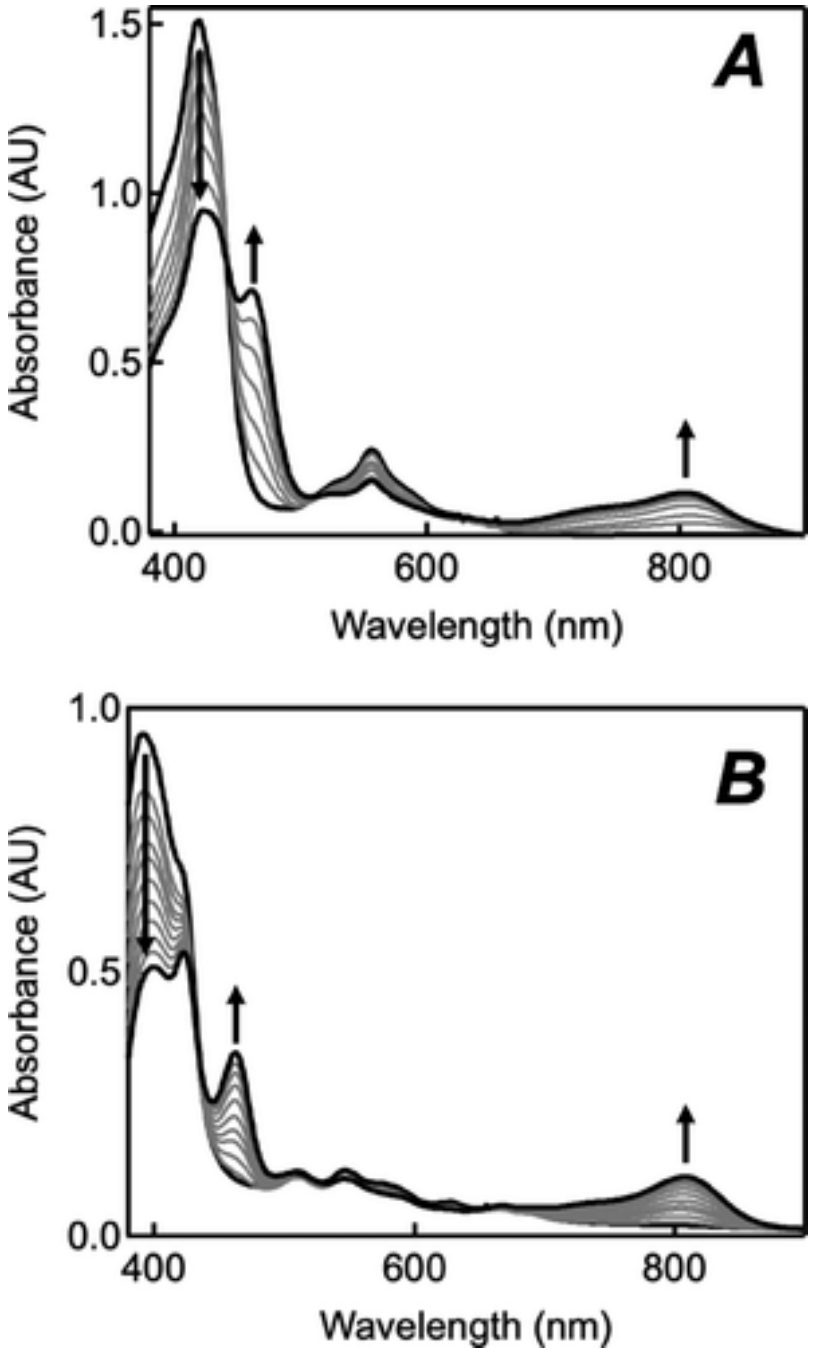

Figure 2.8. UV–visible spectra monitoring the degradation of heme (A) or protoporphyrin IX (B) catalyzed by ChuW when ChuS is utilized as the porphyrin carrier. The anaerobic degradation assay was performed as described in Materials and Methods, except that either heme- or protoporphyrin IX- loaded ChuS was utilized as the substrate (10 μM). Heme-loaded ChuS was prepared as described by Suits et al.[39] and utilized in place of free heme. Protoporphyrin IX-loaded ChuS was prepared by the same protocol. Arrows indicate the direction of spectral changes during the assay. The broad absorption band at 800 nm is indicative of the formation of anaerobilin.

CHAPTER 3

CONCLUSION

3.1. Achievement of Goals

Towards addressing the oxygen-independent heme degradation mechanism in pathogenic *E. coli,* I have identified roles for other heme utilization proteins in the heme utilization operon, identified catalytic residues which are essential to ChuW activity, as well as advanced the catalytic mechanism.[170]

ChuS, previously identified as a non-canonical bacterial heme oxygenase, was a target for investigation.[171] We have demonstrated that, under anaerobic conditions, ChuS acts as a heme source for ChuW, with the latter able to convert heme from ChuS into the tetrapyrrole product, anaerobilin. These results were consistent with the proposed role for PhuS, a homologue in *P. aeruginosa* which shares 45% sequence identity with ChuS.[40] Similar to ChuS, PhuS delivers heme to a bacterial heme degrading enzyme, heme oxygenase. In light of previous work demonstrating the lack of ChuS heme degrading activity when catalase is present, the physiological role for ChuS may be that of a heme chaperone or heme storage protein.[38]

ChuX, located in the same heme utilization operon as ChuW, was previously proposed to act as a heme chaperone, given its lack of heme degrading activity when incubated with excess ascorbate as a reducing partner.[37] *In vitro* ChuW activity assays demonstrated an increase in heme degrading activity when ChuX was present; this effect was even more pronounced when ChuW, ChuX and ChuY were all present in the assay.

These results point towards a role for ChuX as an anaerobilin chaperone between ChuW and ChuY, the latter being the established anaerobilin reductase.[123] Docking studies further support these results when anaerobilin was docked into the binding pocket of the ChuX crystal structure (PDB ID: 6U9J). The linear tetrapyrrole forms favorable interactions with conserved residues in the binding pocket, which would not be formed by heme, given its more rigid structure. Together, biochemical and docking studies point towards a role for ChuX as an anaerobilin chaperone, rather than a heme chaperone. A structure of anaerobilin-bound ChuX would further corroborate or clarify the anaerobilin binding mode in the binding pocket.

The heme iron is directly involved in heme degradation in all characterized heme oxygenases to date.[172] Yet when conducting assays with metallated and nonmetallated porphyrin substrates, ChuW yields the same product, demonstrating that the metal is not essential to the turnover mechanism. Specifically, ChuW is able to methylate the sp^2-hybridized α-meso bridging carbon center and open the porphyrin ring in the absence of substrate iron.

In lieu of a ChuW crystal structure, a PHYRE2 homology model was used to inform potential sites for mutagenesis in identifying essential active site residues.[159] Residues were selected based on predicted substrate proximity and potential for acting as a proton donor to the porphyrin substrate. From the selected residues (D18, D23, D215, D244, S295, E443) only the D215A variant was found to be inactive, whereas the charge changing mutation, D215N, was still active. Further EPR characterization demonstrated that although inactive, D215A was still able to incorporate a [4Fe-4S] cluster and bind SAM. Together, these results implicated D215 as potentially having a catalytic role.

3.2. Future Directions

Outstanding questions remaining pertain to the fate of the heme iron following substrate turnover, the definitive structure of anaerobilin, how ChuW interacts with its partner proteins and how the ChuW active site is configured differently from its related HemN-like family members.

ChuW degrades metallated and nonmetallated porphyrin substrates at approximately the same rate.[170] It is still not well understood if ChuW coordinates the heme iron while substrate is bound, or how the iron ion is then transferred from ChuW to ChuX following turnover. EPR studies combined with differentially metallated porphyrin substrates may provide an answer to this issue. Following heme turnover, an EPR signal for the heme iron atom is not observed, suggesting it may have already been released into solvent. This may be addressed by using porphyrins containing either cobalt, nickel, or copper as the metal center. By using other metals in Irving-William series, the resulting ChuW-metal coordination complexes, if formed, may be stable enough to remain trapped in the active site.[173] Trapping this state would also be conducive to determining a ChuW crystal structure.

The proposed ring-opening mechanism involves formation of a SAM adduct with the porphyrin ring following hydrogen atom abstraction from SAM2. Although this adduct has not yet been directly observed in ChuW-catalyzed reactions, other HemN-like enzymes also produce a SAM-substrate intermediate.[163,165] Such experiments where an adduct was successfully identified via LC-HRMS were validated by using methyl d_3-SAM. The resulting two mass unit shift, and the corresponding fragmentation patterns, are consistent with adduct formation. Although no masses consistent with an adduct were

observed in our MS experiments, this may suggest this intermediate may be more transient in ChuW compared to other HemN-like enzymes.

Previous attempts to isolate anaerobilin in large quantities have proven difficult due to product photooxidation when exposed to light.[123] One possible solution may be to determine the anaerobilin structure while it is bound to carrier protein, such as ChuX, or a bacterial phytochrome.[174] Such proteins diffract to high resolution when crystallized, and the proposed anaerobilin structure indicates it could be accommodated into the binding pocket. Since ChuY is already established as an anaerobilin reductase, cocrystallization of ChuY with anaerobilin, or soaking with anaerobilin may be another route to determining the structure, while also gleaning new information about the ChuY mechanism.

Alternatively, ChuY may also be incubated with ChuW in a coupled heme degradation assay to accumulate anaerorubin, the reduced tetrapyrrole product.[123] anaerorubin-bound ChuY could then be used for high throughput crystallization screening. Anaerorubin could be isolated from the enzyme reaction mixture and purified using solid phase extraction and HPLC for NMR structural characterization. Such approaches have been successful for other tetrapyrrole products formed by bacterial pathogens, such as mycobilin and staphylobilin.[30,31]

The exact nature of ChuW interactions with other heme utilization proteins remains unknown. Determining interacting residues between these partner proteins may be achieved using protein crosslinking in conjunction with mass spectrometry.[175] Further studies using SPR or ITC would be useful in determining how protein-protein interactions are influenced by the presence of heme, SAM or other substrates.

Attempts to structurally characterize ChuW are ongoing; recent structural models generated using AlphaFold show some key changes at the N- and C-termini.[176] Hydrophobic residues at the N- and C-terminus form a “tethering region” which may be involved in further stabilizing ChuW.[177] This structural feature is distinct from the N-terminal "tripwire” motif observed in the HemN structure, which is predicted to be involved in substrate binding.[56] Figure 3.1 shows hydrophobic tethering region in the context of the complete ChuW structure.

Concluding Remarks

The previous identification of ChuW as an anaerobic heme degrading enzyme marked a paradigm shift in our understanding of bacterial heme utilization under anaerobic conditions.[6] Towards a better understanding of how heme utilization proteins accomplish this in an anoxic environment, we have proposed a mechanism for ChuW-catalyzed porphyrin ring opening. This process occurs independently of the substrate heme iron, another feature that delineates its mechanism from other heme degrading enzymes, but that is consistent with emerging mechanisms for other radical SAM enzymes. ChuS and ChuX act as heme and anaerobilin chaperones, respectively. Remaining questions pertaining to the mechanism would likely focus on the catalytic residues involved in degradation, as well as the residues involved in ChuW interactions with other heme utilization proteins.

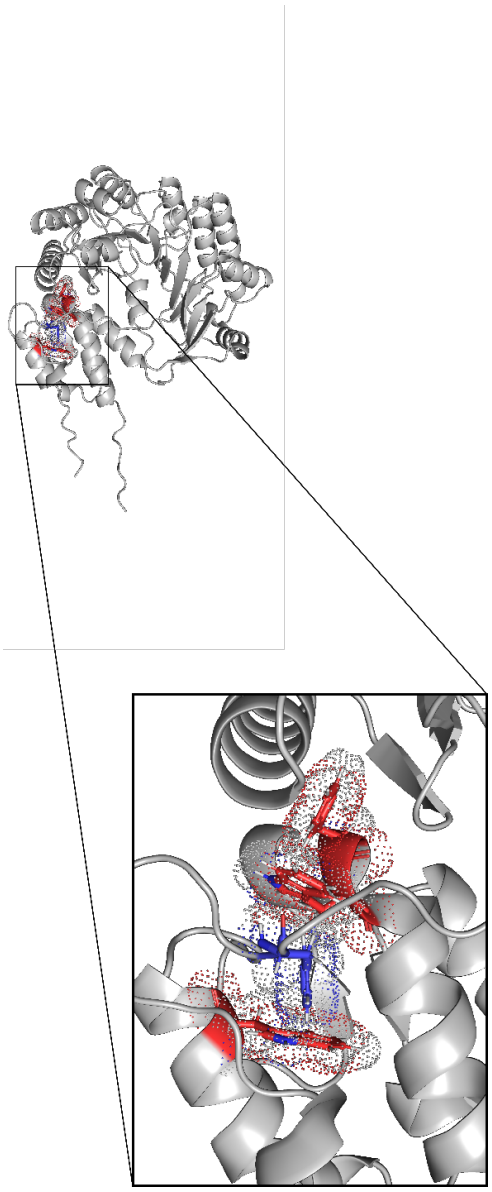

Figure 3.1. Predicted ChuW structural model generated using AlphaFold. Overall structure shown in gray, hydrophobic tether shown in inset panel. Conserved N-terminal residues shown in blue, C-terminal residues shown in red.

REFERENCES

(1) Litwin, C. M.; Calderwood, S. B. Role of Iron in Regulation of Virulence Genes. *Clin. Microbiol. Rev.* **1993**, *6* (2), 137–149. https://doi.org/10.1128/CMR.6.2.137.

(2) Neilands, J. B. Evolution of Biological Iron Binding Centers. *Struct. Bond. Vol. 11* **1972**, 145–170. https://doi.org/10.1007/BFB0002462.

(3) Hooda, J.; Shah, A.; Zhang, L. Heme, an Essential Nutrient from Dietary Proteins, Critically Impacts Diverse Physiological and Pathological Processes. *Nutr. 2014, Vol. 6, Pages 1080-1102* **2014**, *6* (3), 1080–1102. https://doi.org/10.3390/NU6031080.

(4) Torres, A. G.; Redford, P.; Welch, R. A.; Payne, S. M. TonB-Dependent Systems of Uropathogenic Escherichia Coli: Aerobactin and Heme Transport and TonB Are Required for Virulence in the Mouse. *Infect. Immun.* **2001**, *69* (10), 6179–6185. https://doi.org/10.1128/IAI.69.10.6179-6185.2001/FORMAT/EPUB.

(5) Minandri, F.; Imperi, F.; Frangipani, E.; Bonchi, C.; Visaggio, D.; Facchini, M.; Pasquali, P.; Bragonzi, A.; Visca, P. Role of Iron Uptake Systems in Pseudomonas Aeruginosa Virulence and Airway Infection.

Infect. Immun. **2016**, *84* (8), 2324–2335. https://doi.org/10.1128/IAI.00098-16/FORMAT/EPUB.

(6) LaMattina, J. W.; Nix, D. B.; Lanzilotta, W. N. Radical New Paradigm for Heme Degradation in Escherichia Coli O157:H7. *Proc. Natl. Acad. Sci.* **2016**, *113* (43), 12138–12143. https://doi.org/10.1073/pnas.1603209113.

(7) Mills, M.; Payne, S. M. Genetics and Regulation of Heme Iron Transport in Shigella Dysenteriae and Detection of an Analogous System in Escherichia Coli O157:H7. *J. Bacteriol.* **1995**, *177* (11), 3004–3009. https://doi.org/10.1128/JB.177.11.3004-3009.1995.

(8) Broderick, J. B.; Duffus, B. R.; Duschene, K. S.; Shepard, E. M. Radical S-Adenosylmethionine Enzymes. *Chemical Reviews*. 2014, pp 4229–4317. https://doi.org/10.1021/cr4004709.

(9) Chan, Y. S.; Ng, T. B. Shiga Toxins: From Structure and Mechanism to Applications. *Appl. Microbiol. Biotechnol.* **2016**, *100* (4), 1597–1610. https://doi.org/10.1007/S00253-015-7236-3/TABLES/1.

(10) Francis, R. T.; Booth, J. W.; Becker, R. R. Uptake of Iron from Hemoglobin and the Haptoglobin-Hemoglobin Complex by Hemolytic Bacteria. *Int. J. Biochem.* **1985**, *17* (7), 767–773. https://doi.org/10.1016/0020-711X(85)90262-9.

(11) Cope, L. D.; Thomas, S. E.; Hrkal, Z.; Hansen, E. J. Binding of Heme-Hemopexin Complexes by Soluble HxuA Protein Allows Utilization of This Complexed Heme ByHaemophilus Influenzae. *Infect. Immun.* **1998**, *66* (9), 4511–4516. https://doi.org/10.1128/IAI.66.9.4511-4516.1998.

(12) Skaar, E. P. The Battle for Iron between Bacterial Pathogens and Their Vertebrate Hosts. *PLOS Pathog.* **2010**, *6* (8), e1000949. https://doi.org/10.1371/JOURNAL.PPAT.1000949.

(13) Krewulak, K. D.; Vogel, H. J. TonB or Not TonB: Is That the Question? *Biochem. Cell Biol.* **2011**, *89* (2), 87–97. https://doi.org/10.1139/O10-141/ASSET/IMAGES/LARGE/O10-141F3.JPEG.

(14) Stojiljkovic, I.; Hantke, K. Transport of Haemin across the Cytoplasmic Membrane through a Haemin-Specific Periplasmic Binding-Protein-Dependent Transport System in Yersinia Enterocolitica. *Mol. Microbiol.* **1994**, *13* (4), 719–732. https://doi.org/10.1111/J.1365-2958.1994.TB00465.X.

(15) Choby, J. E.; Skaar, E. P. Heme Synthesis and Acquisition in Bacterial Pathogens. *J. Mol. Biol.* **2016**, *428* (17), 3408–3428. https://doi.org/10.1016/J.JMB.2016.03.018.

(16) Grigg, J. C.; Vermeiren, C. L.; Heinrichs, D. E.; Murphy, M. E. P.

Haem Recognition by a Staphylococcus Aureus NEAT Domain. *Mol. Microbiol.* **2007**, *63* (1), 139–149. https://doi.org/10.1111/J.1365-2958.2006.05502.X.

(17) Mazmanian, S. K.; Ton-That, H.; Su, K.; Schneewind, O. An Iron-Regulated Sortase Anchors a Class of Surface Protein during Staphylococcus Aureus Pathogenesis. *Proc. Natl. Acad. Sci. U. S. A.* **2002**, *99* (4), 2293–2298. https://doi.org/10.1073/PNAS.032523999/ASSET/51A09C80-27B6-43CB-8369-B266F2B8921F/ASSETS/GRAPHIC/PQ0325239005.JPEG.

(18) Zhu, H.; Xie, G.; Liu, M.; Olson, J. S.; Fabian, M.; Dooley, D. M.; Lei, B. Pathway for Heme Uptake from Human Methemoglobin by the Iron-Regulated Surface Determinants System of Staphylococcus Aureus. *J. Biol. Chem.* **2008**, *283* (26), 18450–18460. https://doi.org/10.1074/JBC.M801466200.

(19) Wilks, A.; Ikeda-Saito, M. Heme Utilization by Pathogenic Bacteria: Not All Pathways Lead to Biliverdin. *Acc. Chem. Res.* **2014**, *47* (8), 2291–2298. https://doi.org/10.1021/ar500028n.

(20) Tenhunen, R.; Marver, H. S.; Schmidt, R. Microsomal Heme Oxygenase CHARACTERIZATION OF THE ENZYME*. *J. Biol. Chem.*

1969, *244* (23), 6388–6394. https://doi.org/10.1016/S0021-9258(18)63477-5.

(21) Schuller, D. J.; Wilks, A.; Ortiz De Montellano, P. R.; Poulos, T. L. Crystal Structure of Human Heme Oxygenase-1. *Nat. Struct. Biol. 1999 69* **1999**, *6* (9), 860–867. https://doi.org/10.1038/12319.

(22) Schmitt, M. P. Utilization of Host Iron Sources by Corynebacterium Diphtheriae: Identification of a Gene Whose Product Is Homologous to Eukaryotic Heme Oxygenases and Is Required for Acquisition of Iron from Heme and Hemoglobin. *J. Bacteriol.* **1997**, *179* (3), 838–845. https://doi.org/10.1128/JB.179.3.838-845.1997.

(23) Zhu, W.; Wilks, A.; Stojiljkovic, I. Degradation of Heme in Gram-Negative Bacteria: The Product of the HemO Gene of Neisseriae Is a Heme Oxygenase. *J. Bacteriol.* **2000**, *182* (23), 6783–6790. https://doi.org/10.1128/JB.182.23.6783-6790.2000/ASSET/B265B52A-AA25-4561-8E2C-D825C70872CF/ASSETS/GRAPHIC/JB2300947007.JPEG.

(24) Schuller, D. J.; Zhu, W.; Stojiljkovic, I.; Wilks, A.; Poulos, T. L. Crystal Structure of Heme Oxygenase from the Gram-Negative Pathogen Neisseria Meningitidis and a Comparison with Mammalian Heme Oxygenase-1. *Biochemistry* **2001**, *40* (38), 11552–11558.

https://doi.org/10.1021/BI0110239/ASSET/IMAGES/LARGE/BI011023
9F00005.JPEG.

(25) Caignan, G. A.; Deshmukh, R.; Wilks, A.; Zeng, Y.; Huang, H. wei; Moënne-Loccoz, P.; Bunce, R. A.; Eastman, M. A.; Rivera, M. Oxidation of Heme to β- and δ-Biliverdin by Pseudomonas Aeruginosa Heme Oxygenase as a Consequence of an Unusual Seating of the Heme. *J. Am. Chem. Soc.* **2002**, *124* (50), 14879–14892. https://doi.org/10.1021/JA0274960/SUPPL_FILE/JA0274960-3_S1.PDF.

(26) Friedman, J.; Lad, L.; Li, H.; Wilks, A.; Poulos, T. L. Structural Basis for Novel δ-Regioselective Heme Oxygenation in the Opportunistic Pathogen Pseudomonas Aeruginosa. *Biochemistry* **2004**, *43* (18), 5239–5245. https://doi.org/10.1021/BI049687G/ASSET/IMAGES/LARGE/BI049687GF00007.JPEG.

(27) Yoshida, T.; Kikuchi, G.; Maines, M. D.; Faseb J. ; Lemberg, R.; Cortis-Jones, B.; Norrie, M.; Bonnett, R.; Mcdonagh, A. F.; Schuller, D. J.; Wilks, A.; et al. Participation of Carboxylate Amino Acid Side Chain in Regiospecific Oxidation of Heme by Heme Oxygenase. *J. Chem. Soc., Perkin Trans. I* **1969**, *244* (2), 8311–8312.

https://doi.org/10.1021/ja0002868.

(28) Mazmanian, S. K.; Skaar, E. P.; Gaspar, A. H.; Humayun, M.; Gornicki, P.; Jelenska, J.; Joachmiak, A.; Missiakas, D. M.; Schneewind, O. Passage of Heme-Iron across the Envelope of Staphylococcus Aureus. *Science (80-.).* **2003**, *299* (5608), 906–909. https://doi.org/10.1126/SCIENCE.1081147.

(29) Skaar, E. P.; Gaspar, A. H.; Schneewind, O. IsdG and IsdI, Heme-Degrading Enzymes in the Cytoplasm of Staphylococcus Aureus. *J. Biol. Chem.* **2004**, *279* (1), 436–443. https://doi.org/10.1074/JBC.M307952200.

(30) Reniere, M. L.; Ukpabi, G. N.; Harry, S. R.; Stec, D. F.; Krull, R.; Wright, D. W.; Bachmann, B. O.; Murphy, M. E.; Skaar, E. P. The IsdG-Family of Haem Oxygenases Degrades Haem to a Novel Chromophore. *Mol. Microbiol.* **2010**, *75* (6), 1529–1538. https://doi.org/10.1111/J.1365-2958.2010.07076.X.

(31) Ikeda-Saito, M.; Matsui, T.; Goulding, C. W.; Takahashi, S.; Nambu, S. A New Way to Degrade Heme. *J. Biol. Chem.* **2013**, *288* (14), 10101–10109. https://doi.org/10.1074/jbc.m112.448399.

(32) Chim, N.; Iniguez, A.; Nguyen, T. Q.; Goulding, C. W. Unusual Diheme Conformation of the Heme-Degrading Protein from

Mycobacterium Tuberculosis. *J. Mol. Biol.* **2010**, *395* (3), 595–608. https://doi.org/10.1016/J.JMB.2009.11.025.

(33) Snyder, S. N.; Mak, P. J. Structure-Function Characterization of the Mono- and Diheme Forms of MhuD, a Noncanonical Heme Oxygenase from Mycobacterium Tuberculosis. **2022**. https://doi.org/10.1016/j.jbc.2021.101475.

(34) Motterlini, R.; Clark, J. E.; Foresti, R.; Sarathchandra, P.; Mann, B. E.; Green, C. J. Carbon Monoxide-Releasing Molecules. *Circ. Res.* **2002**, *90* (2). https://doi.org/10.1161/HH0202.104530.

(35) Perry, R. D.; Brubaker, R. R. Accumulation of Iron by Yersiniae. *J. Bacteriol.* **1979**, *137* (3), 1290–1298. https://doi.org/10.1128/JB.137.3.1290-1298.1979.

(36) Stojiljkovic, I.; Hantke, K. Hemin Uptake System of Yersinia Enterocolitica: Similarities with Other TonB-Dependent Systems in Gram-Negative Bacteria. *EMBO J.* **1992**, *11* (12), 4359–4367. https://doi.org/10.1002/J.1460-2075.1992.TB05535.X.

(37) Pal, G. P.; Jia, Z.; Couture, M.; Lang, J.; Suits, M. D. L. Structure and Heme Binding Properties of Escherichia Coli O157:H7 ChuX. *Protein Sci.* **2009**, *18* (4), NA-NA. https://doi.org/10.1002/pro.84.

(38) Lee, M. J. Y.; Schep, D.; McLaughlin, B.; Kaufmann, M.; Jia, Z.

Structural Analysis and Identification of PhuS as a Heme-Degrading Enzyme from Pseudomonas Aeruginosa. *J. Mol. Biol.* **2014**, *426* (9), 1936–1946. https://doi.org/10.1016/J.JMB.2014.02.013.

(39) Suits, M. D. L.; Jaffer, N.; Jia, Z. Structure of the Escherichia Coli O157:H7 Heme Oxygenase ChuS in Complex with Heme and Enzymatic Inactivation by Mutation of the Heme Coordinating Residue His-193. *J. Biol. Chem.* **2006**, *281* (48), 36776–36782. https://doi.org/10.1074/JBC.M607684200.

(40) Kaur, A. P.; Lansky, I. B.; Wilks, A. The Role of the Cytoplasmic Heme-Binding Protein (PhuS) of Pseudomonas Aeruginosa in Intracellular Heme Trafficking and Iron Homeostasis. *J. Biol. Chem.* **2009**, *284* (1), 56–66. https://doi.org/10.1074/JBC.M806068200.

(41) O'neill, M. J.; Bhakta, M. N.; Fleming, K. G.; Wilks, A.; Jenkins, T. C. Induced Fit on Heme Binding to the Pseudomonas Aeruginosa Cytoplasmic Protein (PhuS) Drives Interaction with Heme Oxygenase (HemO). *Proc. Natl. Acad. Sci.* **2012**. https://doi.org/10.1073/pnas.1121549109.

(42) Henderson, D. P.; Payne, S. M. Characterization of the Vibrio Cholerae Outer Membrane Heme Transport Protein HutA: Sequence of the Gene, Regulation of Expression, and Homology to the Family of

TonB-Dependent Proteins. *J. Bacteriol.* **1994**, *176* (11), 3269–3277. https://doi.org/10.1128/JB.176.11.3269-3277.1994.

(43) Wyckoff, E. E.; Schmitt, M.; Wilks, A.; Payne, S. M. HutZ Is Required for Efficient Heme Utilization in Vibrio Cholerae. *J. Bacteriol.* **2004**, *186* (13), 4142–4151. https://doi.org/10.1128/JB.186.13.4142-4151.2004/FORMAT/EPUB.

(44) Uchida, T.; Dojun, N.; Sekine, Y.; Ishimori, K. Heme Proximal Hydrogen Bonding between His170 and Asp132 Plays an Essential Role in the Heme Degradation Reaction of HutZ from Vibrio Cholerae. *Biochemistry* **2017**, *56* (21), 2723–2734. https://doi.org/10.1021/ACS.BIOCHEM.7B00152/ASSET/IMAGES/LARGE/BI-2017-00152U_0010.JPEG.

(45) Uchida, T.; Ota, K.; Sekine, Y.; Dojun, N.; Ishimori, K. Subunit–Subunit Interactions Play a Key Role in the Heme-Degradation Reaction of HutZ from Vibrio Cholerae. *Dalt. Trans.* **2019**, *48* (12), 3973–3983. https://doi.org/10.1039/C9DT00604D.

(46) Ridley, K. A.; Rock, J. D.; Li, Y.; Ketley, J. M. Heme Utilization in Campylobacter Jejuni. *J. Bacteriol.* **2006**, *188* (22), 7862–7875. https://doi.org/10.1128/JB.00994-06/ASSET/18BB1A67-C31D-400B-8437-

E43C26FE4F84/ASSETS/GRAPHIC/ZJB0220662300006.JPEG.

(47) Guo, Y.; Guo, G.; Mao, X.; Zhang, W.; Xiao, J.; Tong, W.; Liu, T.; Xiao, B.; Liu, X.; Feng, Y.; et al. Functional Identification of HugZ, a Heme Oxygenase from Helicobacter Pylori. **2008**. https://doi.org/10.1186/1471-2180-8-226.

(48) Hu, Y.; Jiang, F.; Guo, Y.; Shen, X.; Zhang, Y.; Zhang, R.; Guo, G.; Mao, X.; Zou, Q.; Wang, D. C. Crystal Structure of HugZ, a Novel Heme Oxygenase from Helicobacter Pylori. *J. Biol. Chem.* **2011**, *286* (2), 1537–1544. https://doi.org/10.1074/JBC.M110.172007.

(49) Liu, X.; Gong, J.; Wei, T.; Wang, Z.; Du, Q.; Zhu, D.; Huang, Y.; Xu, S.; Gu, L. Crystal Structure of HutZ, a Heme Storage Protein from Vibrio Cholerae: A Structural Mismatch Observed in the Region of High Sequence Conservation. *BMC Struct. Biol.* **2012**, *12* (1), 1–10. https://doi.org/10.1186/1472-6807-12-23/TABLES/1.

(50) Li, S.; Isiorho, E. A.; Owens, V. L.; Donnan, P. H.; Odili, C. L.; Mansoorabadi, S. O. A Noncanonical Heme Oxygenase Specific for the Degradation of C-Type Heme. *J. Biol. Chem.* **2021**, *296*, 100666. https://doi.org/10.1016/j.jbc.2021.100666.

(51) Nomenclature Committee of the International Union of Biochemistry (NC-IUB). Nomenclature of Electron-Transfer Proteins.

Recommendations 1989. *J. Biol. Chem.* **1992**, *267* (1), 665–677. https://doi.org/10.1016/S0021-9258(18)48544-4.

(52) Kleingardner, J. G.; Bren, K. L. Biological Significance and Applications of Heme c Proteins and Peptides. *Acc. Chem. Res.* **2015**, *48* (7), 1845–1852. https://doi.org/10.1021/ACS.ACCOUNTS.5B00106/SUPPL_FILE/AR5B00106_SI_001.PDF.

(53) Sofia, H. J.; Chen, G.; Hetzler, B. G.; Reyes-Spindola, J. F.; Miller, N. E. Radical SAM, a Novel Protein Superfamily Linking Unresolved Steps in Familiar Biosynthetic Pathways with Radical Mechanisms: Functional Characterization Using New Analysis and Information Visualization Methods. *Nucleic Acids Res.* **2001**, *29* (5), 1097–1106. https://doi.org/10.1093/NAR/29.5.1097.

(54) Akiva, E.; Brown, S.; Almonacid, D. E.; Barber, A. E.; Custer, A. F.; Hicks, M. A.; Huang, C. C.; Lauck, F.; Mashiyama, S. T.; Meng, E. C.; et al. The Structure–Function Linkage Database. *Nucleic Acids Res.* **2014**, *42* (D1), D521–D530. https://doi.org/10.1093/NAR/GKT1130.

(55) Zallot, R.; Oberg, N.; Gerlt, J. A. The EFI Web Resource for Genomic Enzymology Tools: Leveraging Protein, Genome, and Metagenome Databases to Discover Novel Enzymes and Metabolic Pathways.

Biochemistry **2019**, *58* (41), 4169–4182. https://doi.org/10.1021/ACS.BIOCHEM.9B00735/SUPPL_FILE/BI9B00735_SI_002.PDF.

(56) Layer, G.; Grage, K.; Teschner, T.; Schünemann, V.; Breckau, D.; Masoumi, A.; Jahn, M.; Heathcote, P.; Trautwein, A. X.; Jahn, D. Radical S -Adenosylmethionine Enzyme Coproporphyrinogen III Oxidase HemN. *J. Biol. Chem.* **2005**, *280* (32), 29038–29046. https://doi.org/10.1074/jbc.m501275200.

(57) Berkovitch, F.; Nicolet, Y.; Wan, J. T.; Jarrett, J. T.; Drennan, C. L. Crystal Structure of Biotin Synthase, An. *Science (80-.).* **2004**, *303* (January), 76–79. https://doi.org/10.1126/science.1088493.

(58) Ollagnier, S.; Meier, C.; Mulliez, E.; Gaillard, J.; Schuenemann, V.; Trautwein, A.; Mattioli, T.; Lutz, M.; Fontecave, M. Assembly of 2Fe-2S and 4Fe-4S Clusters in the Anaerobic Ribonucleotide Reductase from Escherichia Coli. *J. Am. Chem. Soc.* **1999**, *121* (27), 6344–6350. https://doi.org/10.1021/JA990073M.

(59) Castro, L.; Rodriguez, M.; Radif, R. Aconitase Is Readily Inactivated by Peroxynitrite, but Not by Its Precursor, Nitric Oxide*. *J. Biol. Chem.* **1994**, *269* (47), 29409–29415. https://doi.org/10.1016/S0021-9258(18)43894-X.

(60) Hänzelmann, P.; Schindelin, H. Crystal Structure of the S-Adenosylmethionine-Dependent Enzyme MoaA and Its Implications for Molybdenum Cofactor Deficiency in Humans. *Proc. Natl. Acad. Sci. U. S. A.* **2004**, *101* (35), 12870–12875. https://doi.org/10.1073/PNAS.0404624101.

(61) Vey, J. L.; Yang, J.; Li, M.; Broderick, W. E.; Broderick, J. B.; Drennan, C. L. Structural Basis for Glycyl Radical Formation by Pyruvate Formate-Lyase Activating Enzyme. *Proc. Natl. Acad. Sci. U. S. A.* **2008**, *105* (42), 16137–16141. https://doi.org/10.1073/PNAS.0806640105.

(62) Walsby, C. J.; Ortillo, D.; Yang, J.; Nnyepi, M. R.; Broderick, W. E.; Hoffman, B. M.; Broderick, J. B. Spectroscopic Approaches to Elucidating Novel Iron-Sulfur Chemistry in the “Radical-SAM” Protein Superfamily. *Inorg. Chem.* **2005**, *44* (4), 727–741. https://doi.org/10.1021/IC0484811/ASSET/IMAGES/MEDIUM/IC0484811N00001.GIF.

(63) Yang, H.; McDaniel, E. C.; Impano, S.; Byer, A. S.; Jodts, R. J.; Yokoyama, K.; Broderick, W. E.; Broderick, J. B.; Hoffman, B. M. The Elusive 5′-Deoxyadenosyl Radical: Captured and Characterized by Electron Paramagnetic Resonance and Electron Nuclear Double

Resonance Spectroscopies. *J. Am. Chem. Soc.* **2019**, *141* (30), 12139–12146. https://doi.org/10.1021/JACS.9B05926/ASSET/IMAGES/LARGE/JA-2019-059264_0005.JPEG.

(64) Holliday, G. L.; Akiva, E.; Meng, E. C.; Brown, S. D.; Calhoun, S.; Pieper, U.; Sali, A.; Booker, S. J.; Babbitt, P. C. Atlas of the Radical SAM Superfamily: Divergent Evolution of Function Using a “Plug and Play” Domain. *Methods Enzymol.* **2018**, *606*, 1–71. https://doi.org/10.1016/BS.MIE.2018.06.004.

(65) Bruender, N. A.; Young, A. P.; Bandarian, V. Chemical and Biological Reduction of the Radical SAM Enzyme CPH 4 Synthase. *Biochemistry* **2015**, *54* (18), 2903–2910. https://doi.org/10.1021/ACS.BIOCHEM.5B00210/SUPPL_FILE/BI5B00210_SI_001.PDF.

(66) Nicolet, Y. Structure–Function Relationships of Radical SAM Enzymes. *Nat. Catal. 2020 34* **2020**, *3* (4), 337–350. https://doi.org/10.1038/s41929-020-0448-7.

(67) Colichman, E. L.; Love, D. L. Polarography of Sulfonium Salts. *J. Org. Chem.* **1953**, *18* (1), 40–46. https://doi.org/10.1021/JO01129A008/ASSET/JO01129A008.FP.PNG

_V03.

(68) Wang, S. C.; Frey, P. A. Binding Energy in the One-Electron Reductive Cleavage of S-Adenosylmethionine in Lysine 2,3-Aminomutase, a Radical SAM Enzyme. *Biochemistry* **2007**, *46* (45), 12889–12895. https://doi.org/10.1021/BI701745H/ASSET/IMAGES/LARGE/BI701745HH00001.JPEG.

(69) Byer, A. S.; Yang, H.; McDaniel, E. C.; Kathiresan, V.; Impano, S.; Pagnier, A.; Watts, H.; Denler, C.; Vagstad, A. L.; Piel, J.; et al. Paradigm Shift for Radical S-Adenosyl- l -Methionine Reactions: The Organometallic Intermediate ω Is Central to Catalysis. *J. Am. Chem. Soc.* **2018**, *140* (28), 8634–8638. https://doi.org/10.1021/JACS.8B04061/ASSET/IMAGES/LARGE/JA-2018-04061R_0006.JPEG.

(70) Frey, P. A. Lysine 2,3-Aminomutase: Is Adenosylmethionine a Poor Man's Adenosylcobalamin? *FASEB J.* **1993**, *7* (8), 662–670. https://doi.org/10.1096/FASEBJ.7.8.8500691.

(71) Donnan, P. H.; Mansoorabadi, S. O. Broken-Symmetry Density Functional Theory Analysis of the ω Intermediate in Radical S-Adenosyl- l -Methionine Enzymes: Evidence for a Near-Attack

Conformer over an Organometallic Species. *J. Am. Chem. Soc.* **2022**, *144* (8), 3381–3385. https://doi.org/10.1021/JACS.2C00678/ASSET/IMAGES/LARGE/JA2C00678_0004.JPEG.

(72) Cosper, N. J.; Booker, S. J.; Ruzicka, F.; Frey, P. A.; Scott, R. A. Direct FeS Cluster Involvement in Generation of a Radical in Lysine 2,3-Aminomutase. *Biochemistry* **2000**, *39* (51), 15668–15673. https://doi.org/10.1021/BI0022184/SUPPL_FILE/BI0022184_S.PDF.

(73) Costilow, R. N.; Rochovansky, O. M.; Barker, H. A. Isolation and Identification of β-Lysine as an Intermediate in Lysine Fermentation. *J. Biol. Chem.* **1966**, *241* (7), 1573–1580. https://doi.org/10.1016/S0021-9258(18)96751-7.

(74) Chirpich, T. P.; Zappia, ~ V; Costilow, ~ R N; And, ~; Barker, H. A. Lysine 2,3-Aminomutase. *J. Biol. Chem.* **1970**, *245* (7), 1778–1789. https://doi.org/10.1016/S0021-9258(19)77160-9.

(75) Moss, M.; Frey, P. A. The Role of S-Adenosylmethionine in the Lysine 2,3-Aminomutase Reaction*. *Commun. Val* **1987**, *262* (31), 14859–14862. https://doi.org/10.1016/S0021-9258(18)48103-3.

(76) Moss, M. L.; Frey, P. A. Activation of Lysine 2,3-Aminomutase by S-Adenosylmethionine. *J. Biol. Chem.* **1990**, *265* (30), 18112–18115.

https://doi.org/10.1016/S0021-9258(17)44724-7.

(77) Ballinger, M. D.; Reed, G. H.; Frey, P. A. An Organic Radical in the Lysine 2, 3-Aminomutase Reaction. *Biochemistry* **1992**, *31* (4), 949–953. https://doi.org/10.1021/BI00119A001/ASSET/BI00119A001.FP.PNG_V03.

(78) Magnusson, O. T.; Reed, G. H.; Frey, P. A. Characterization of an Allylic Analogue of the 5′-Deoxyadenosyl Radical: An Intermediate in the Reaction of Lysine 2,3-Aminomutase. *Biochemistry* **2001**, *40* (26), 7773–7782. https://doi.org/10.1021/BI0104569/SUPPL_FILE/BI0104569_S.PDF.

(79) Tse Sum Bui, B.; Florentin, D.; Fournier, F.; Ploux, O.; Méjean, A.; Marquet, A. Biotin Synthase Mechanism: On the Origin of Sulphur. *FEBS Lett.* **1998**, *440* (1–2), 226–230. https://doi.org/10.1016/S0014-5793(98)01464-1.

(80) Hänzelmann, P.; Hernández, H. L.; Menzel, C.; García-Serres, R.; Huynh, B. H.; Johnson, M. K.; Mendel, R. R.; Schindelin, H. Characterization of MOCS1A, an Oxygen-Sensitive Iron-Sulfur Protein Involved in Human Molybdenum Cofactor Biosynthesis. *J. Biol. Chem.* **2004**, *279* (33), 34721–34732.

https://doi.org/10.1074/JBC.M313398200.

(81) Layer, G.; Verfürth, K.; Mahlitz, E.; Jahn, D. Oxygen-Independent Coproporphyrinogen-III Oxidase HemN from Escherichia Coli*. *J. Biol. Chem.* **2002**, *277* (37), 34136–34142. https://doi.org/10.1074/JBC.M205247200.

(82) Lotierzo, M.; Tse Sum Bui, B.; Florentin, D.; Escalettes, F.; Marquet, A. Biotin Synthase Mechanism: An Overview. *Biochem. Soc. Trans.* **2005**, *33* (4), 820–823. https://doi.org/10.1042/BST0330820.

(83) Tao, L.; Stich, T. A.; Fugate, C. J.; Jarrett, J. T.; Britt, R. D. EPR-Derived Structure of a Paramagnetic Intermediate Generated by Biotin Synthase BioB. *J. Am. Chem. Soc.* **2018**, *140* (40), 12947–12963. https://doi.org/10.1021/JACS.8B07613/SUPPL_FILE/JA8B07613_SI_002.PDF.

(84) McCarthy, E. L.; Booker, S. J. Destruction and Reformation of an Iron-Sulfur Cluster during Catalysis by Lipoyl Synthase. *Science (80-.).* **2017**, *358* (6361), 373–377. https://doi.org/10.1126/SCIENCE.AAN4574/SUPPL_FILE/AAN4574_MCCARTHY_SM.PDF.

(85) Johnson, Jean L., Wuebbens, M. M.; Rajagopalan, K. V. The Structure of a Molybdopterin Precursor: Characterization of a Stable,

Oxidized Derivative. *J. Biol. Chem.* **1989**, *264* (23), 13440–13447. https://doi.org/10.1016/S0021-9258(18)80016-3.

(86) Hänzelmann, P.; Schindelin, H. Binding of 5′-GTP to the C-Terminal FeS Cluster of the Radical S-Adenosylmethionine Enzyme MoaA Provides Insights into Its Mechanism. *Proc. Natl. Acad. Sci. U. S. A.* **2006**, *103* (18), 6829–6834. https://doi.org/10.1073/PNAS.0510711103.

(87) Grell, T. A. J.; Young, A. P.; Drennan, C. L.; Bandarian, V. Biochemical and Structural Characterization of a Schiff Base in the Radical-Mediated Biosynthesis of 4-Demethylwyosine by TYW1. *J. Am. Chem. Soc.* **2018**, *140* (22), 6842–6852. https://doi.org/10.1021/JACS.8B01493/SUPPL_FILE/JA8B01493_SI_001.PDF.

(88) Tait, G. H. Coproporphyrinogenase Activity in Extracts from Rhodopseudomonas Spheroides. *Biochem. Biophys. Res. Commun.* **1969**, *37* (1), 116–122. https://doi.org/10.1016/0006-291X(69)90888-2.

(89) Bauerle, M. R.; Schwalm, E. L.; Booker, S. J. Mechanistic Diversity of Radical S-Adenosylmethionine (SAM)-Dependent Methylation. *Journal of Biological Chemistry*. 2015, pp 3995–4002.

https://doi.org/10.1074/jbc.R114.607044.

(90) Ji, X.; Mo, T.; Liu, W. A.-Q.; Ing, W.; Deng, Z.; Zhang, Q. Revisiting the Mechanism of the Anaerobic Coproporphyrinogen III Oxidase HemN. *Angew. Chemie* **2019**, *131* (19), 6301–6304. https://doi.org/10.1002/ANGE.201814708.

(91) Haskamp, V.; Karrie, S.; Mingers, T.; Barthels, S.; Alberge, F.; Magalon, A.; Müller, K.; Bill, E.; Lubitz, W.; Kleeberg, K.; et al. The Radical SAM Protein HemW Is a Heme Chaperone. *J. Biol. Chem.* **2018**, *293* (7), 2558–2572. https://doi.org/10.1074/JBC.RA117.000229/ATTACHMENT/2C3F41C3-4C07-4827-AAAF-D136F905CA6D/MMC1.DOCX.

(92) Abicht, H. K.; Martinez, J.; Layer, G.; Jahn, D.; Solioz, M. Lactococcus Lactis HemW (HemN) Is a Haem-Binding Protein with a Putative Role in Haem Trafficking. *Biochem. J.* **2012**, *442* (2), 335–343. https://doi.org/10.1042/BJ20111618.

(93) Toh, S. M.; Xiong, L.; Bae, T.; Mankin, A. S. The Methyltransferase YfgB/RlmN Is Responsible for Modification of Adenosine 2503 in 23S RRNA. *RNA* **2008**, *14* (1), 98–106. https://doi.org/10.1261/RNA.814408.

(94) Schwarz, S.; Werckenthin, C.; Kehrenberg, C. Identification of a

Plasmid-Borne Chloramphenicol-Florfenicol Resistance Gene in Staphylococcus Sciuri. *Antimicrob. Agents Chemother.* **2000**, *44* (9), 2530–2533. https://doi.org/10.1128/AAC.44.9.2530-2533.2000/ASSET/0BAD1E48-97DE-4418-A41B-8F653CBD8258/ASSETS/GRAPHIC/AC0900046002.JPEG.

(95) Schwarz, S.; Jacobsen, L.; Hansen, L. H.; Vester, B.; Kehrenberg, C. A New Mechanism for Chloramphenicol, Florfenicol and Clindamycin Resistance: Methylation of 23S Ribosomal RNA at A2503. *Mol. Microbiol.* **2005**, *57* (4), 1064–1073. https://doi.org/10.1111/J.1365-2958.2005.04754.X.

(96) Benítez-Páez, A.; Villarroya, M.; Armengod, M. E. The Escherichia Coli RlmN Methyltransferase Is a Dual-Specificity Enzyme That Modifies Both RRNA and TRNA and Controls Translational Accuracy. *RNA* **2012**, *18* (10), 1783–1795. https://doi.org/10.1261/RNA.033266.112.

(97) Kaminska, K. H.; Purta, E.; Hansen, L. H.; Bujnicki, J. M.; Vester, B.; Long, K. S. Insights into the Structure, Function and Evolution of the Radical-SAM 23S RRNA Methyltransferase Cfr That Confers Antibiotic Resistance in Bacteria. *Nucleic Acids Res.* **2010**, *38* (5), 1652–1663. https://doi.org/10.1093/NAR/GKP1142.

(98) Grove, T. L.; Benner, J. S.; Radle, M. I.; Ahlum, J. H.; Landgraf, B. J.; Krebs, C.; Booker, S. J. A Radically Different Mechanism for S-Adenosylmethionine-Dependent Methyltransferases. *Science (80-.).* **2011**, *332* (6029), 604–607. https://doi.org/10.1126/SCIENCE.1200877.

(99) Boal, A. K.; Grove, T. L.; McLaughlin, M. I.; Yennawar, N. H.; Booker, S. J.; Rosenzweig, A. C. Structural Basis for Methyl Transfer by a Radical SAM Enzyme. *Science (80-.).* **2011**, *332* (6033), 1089–1092. https://doi.org/10.1126/SCIENCE.1205358.

(100) Schwalm, E. L.; Grove, T. L.; Booker, S. J.; Boal, A. K. Crystallographic Capture of a Radical S-Adenosylmethionine Enzyme in the Act of Modifying TRNA. *Science (80-.).* **2016**, *352* (6283), 309–312. https://doi.org/10.1126/SCIENCE.AAD5367.

(101) Gumkowski, J. D.; Martinie, R. J.; Corrigan, P. S.; Pan, J.; Bauerle, M. R.; Almarei, M.; Booker, S. J.; Silakov, A.; Krebs, C.; Boal, A. K. Analysis of RNA Methylation by Phylogenetically Diverse Cfr Radical S-Adenosylmethionine Enzymes Reveals an Iron-Binding Accessory Domain in a Clostridial Enzyme. *Biochemistry* **2019**, *58* (29), 3169–3184. https://doi.org/10.1021/ACS.BIOCHEM.9B00197/ASSET/IMAGES/LA

RGE/BI-2019-00197Q_0009.JPEG.

(102) Zhang, Q.; Van Der Donk, W. A.; Liu, W. Radical-Mediated Enzymatic Methylation: A Tale of Two SAMS. *Acc. Chem. Res.* **2012**, *45* (4), 555–564. https://doi.org/10.1021/AR200202C/ASSET/IMAGES/LARGE/AR-2011-00202C_0011.JPEG.

(103) McLaughlin, M. I.; Van Der Donk, W. A. Stereospecific Radical-Mediated B12-Dependent Methyl Transfer by the Fosfomycin Biosynthesis Enzyme Fom3. *Biochemistry* **2018**, *57* (33), 4967–4971. https://doi.org/10.1021/ACS.BIOCHEM.8B00616/ASSET/IMAGES/LARGE/BI-2018-00616R_0006.JPEG.

(104) Sato, S.; Kudo, F.; Kuzuyama, T.; Hammerschmidt, F.; Eguchi, T. C-Methylation Catalyzed by Fom3, a Cobalamin-Dependent Radical S-Adenosyl- l -Methionine Enzyme in Fosfomycin Biosynthesis, Proceeds with Inversion of Configuration. *Biochemistry* **2018**, *57* (33), 4963–4966. https://doi.org/10.1021/ACS.BIOCHEM.8B00614/ASSET/IMAGES/LARGE/BI-2018-00614W_0003.JPEG.

(105) Wang, B.; Blaszczyk, A. J.; Knox, H. L.; Zhou, S.; Blaesi, E. J.; Krebs, C.; Wang, R. X.; Booker, S. J. Stereochemical and Mechanistic

Investigation of the Reaction Catalyzed by Fom3 from Streptomyces Fradiae, a Cobalamin-Dependent Radical S-Adenosylmethionine Methylase. *Biochemistry* **2018**, *57* (33), 4972–4984. https://doi.org/10.1021/ACS.BIOCHEM.8B00693/ASSET/IMAGES/LARGE/BI-2018-00693E_0013.JPEG.

(106) Knox, H. L.; Sinner, E. K.; Townsend, C. A.; Boal, A. K.; Booker, S. J. Structure of a B12-Dependent Radical SAM Enzyme in Carbapenem Biosynthesis. *Nat. 2022 6027896* **2022**, *602* (7896), 343–348. https://doi.org/10.1038/s41586-021-04392-4.

(107) Wang, Y.; Schnell, B.; Baumann, S.; Muller, R.; Begley, T. P. Biosynthesis of Branched Alkoxy Groups: Iterative Methyl Group Alkylation by a Cobalamin-Dependent Radical SAM Enzyme. *J. Am. Chem. Soc.* **2017**, *139* (5), 1742–1745. https://doi.org/10.1021/JACS.6B10901/ASSET/IMAGES/LARGE/JA-2016-109017_0008.JPEG.

(108) Zhang, Z.; Mahanta, N.; Hudson, G. A.; Mitchell, D. A.; Van Der Donk, W. A. Mechanism of a Class C Radical S-Adenosyl- l -Methionine Thiazole Methyl Transferase. *J. Am. Chem. Soc.* **2017**, *139* (51), 18623–18631. https://doi.org/10.1021/JACS.7B10203/ASSET/IMAGES/LARGE/JA-

2017-10203T_0004.JPEG.

(109) LaMattina, J. W.; Wang, B.; Badding, E. D.; Gadsby, L. K.; Grove, T. L.; Booker, S. J. NosN, a Radical S-Adenosylmethionine Methylase, Catalyzes Both C1 Transfer and Formation of the Ester Linkage of the Side-Ring System during the Biosynthesis of Nosiheptide. *J. Am. Chem. Soc.* **2017**, *139* (48), 17438–17445. https://doi.org/10.1021/JACS.7B08492/ASSET/IMAGES/JA-2017-08492D_M002.GIF.

(110) Zhang, Z.; Mahanta, N.; Hudson, G. A.; Mitchell, D. A.; Van Der Donk, W. A. Mechanism of a Class C Radical S-Adenosyl- l -Methionine Thiazole Methyl Transferase. *J. Am. Chem. Soc.* **2017**, *139* (51), 18623–18631. https://doi.org/10.1021/JACS.7B10203/ASSET/IMAGES/LARGE/JA-2017-10203T_0004.JPEG.

(111) Morris, R. P.; Leeds, J. A.; Naegeli, H. U.; Oberer, L.; Memmert, K.; Weber, E.; LaMarche, M. J.; Parker, C. N.; Burrer, N.; Esterow, S.; et al. Ribosomally Synthesized Thiopeptide Antibiotics Targeting Elongation Factor Tu. *J. Am. Chem. Soc.* **2009**, *131* (16), 5946–5955. https://doi.org/10.1021/JA900488A/SUPPL_FILE/JA900488A_SI_001.PDF.

(112) Wang, B.; Lamattina, J. W.; Marshall, S. L.; Booker, S. J. Capturing Intermediates in the Reaction Catalyzed by NosN, a Class C Radical S-Adenosylmethionine Methylase Involved in the Biosynthesis of the Nosiheptide Side-Ring System. *J. Am. Chem. Soc.* **2019**, *141* (14), 5788–5797. https://doi.org/10.1021/JACS.8B13157/SUPPL_FILE/JA8B13157_SI_001.PDF.

(113) Allen, K. D.; Xu, H.; White, R. H. Identification of a Unique Radical S-Adenosylmethionine Methylase Likely Involved in Methanopterin Biosynthesis in Methanocaldococcus Jannaschii. *J. Bacteriol.* **2014**, *196* (18), 3315–3323. https://doi.org/10.1128/JB.01903-14/FORMAT/EPUB.

(114) Hu, Y.; Ribbe, M. W. Maturation of Nitrogenase Cofactor — the Role of a Class E Radical SAM Methyltransferase NifB. *Curr. Opin. Chem. Biol.* **2016**, *31*, 188–194. https://doi.org/10.1016/J.CBPA.2016.02.016.

(115) Kang, W.; Rettberg, L. A.; Stiebritz, M. T.; Jasniewski, A. J.; Tanifuji, K.; Lee, C. C.; Ribbe, M. W.; Hu, Y. X-Ray Crystallographic Analysis of NifB with a Full Complement of Clusters: Structural Insights into the Radical SAM-Dependent Carbide Insertion During

Nitrogenase Cofactor Assembly. *Angew. Chemie - Int. Ed.* **2021**, *60* (5), 2364–2370. https://doi.org/10.1002/ANIE.202011367.

(116) Fajardo, A. S.; Legrand, P.; Payá-Tormo, L.; Martin, L.; Pellicer MartÍnez, M. T.; Echavarri-Erasun, C.; Vernède, X.; Rubio, L. M.; Nicolet, Y. Structural Insights into the Mechanism of the Radical SAM Carbide Synthase NifB, a Key Nitrogenase Cofactor Maturating Enzyme. *J. Am. Chem. Soc.* **2020**, *142* (25), 11006–11012. https://doi.org/10.1021/JACS.0C02243/ASSET/IMAGES/LARGE/JA0C02243_0004.JPEG.

(117) Fyfe, C. D.; Bernardo-García, N.; Fradale, L.; Grimaldi, S.; Guillot, A.; Brewee, C.; Chavas, L. M. G.; Legrand, P.; Benjdia, A.; Berteau, O. Crystallographic Snapshots of a B12-Dependent Radical SAM Methyltransferase. *Nat. 2022 6027896* **2022**, *602* (7896), 336–342. https://doi.org/10.1038/s41586-021-04355-9.

(118) Wyckoff, E. E.; Duncan, D.; Torres, A. G.; Mills, M.; Payne, S. M. Structure of the Shigella Dysenteriae Haem Transport Locus and Its Phylogenetic Distribution in Enteric Bacteria. *Mol. Microbiol.* **2003**, *28* (6), 1139–1152. https://doi.org/10.1046/j.1365-2958.1998.00873.x.

(119) Booker, S. J.; Cicchillo, R. M.; Grove, T. L. Self-Sacrifice in Radical S-Adenosylmethionine Proteins. *Curr. Opin. Chem. Biol.*

2007, *11* (5), 543–552. https://doi.org/10.1016/J.CBPA.2007.08.028.

(120) Sekine, Y.; Tanzawa, T.; Tanaka, Y.; Ishimori, K.; Uchida, T. Cytoplasmic Heme-Binding Protein (HutX) from Vibrio Cholerae Is an Intracellular Heme Transport Protein for the Heme-Degrading Enzyme, HutZ. *Biochemistry* **2016**, *55* (6), 884–893. https://doi.org/10.1021/acs.biochem.5b01273.

(121) Lansky, I. B.; Lukat-Rodgers, G. S.; Block, D.; Rodgers, K. R.; Ratliff, M.; Wilks, A. The Cytoplasmic Heme-Binding Protein (PhuS) from the Heme Uptake System of Pseudomonas Aeruginosa Is an Intracellular Heme-Trafficking Protein to the δ-Regioselective Heme Oxygenase *. *J. Biol. Chem.* **2006**, *281* (19), 13652–13662. https://doi.org/10.1074/JBC.M600824200.

(122) Choi, J.; Kim, D.; Chaurasia, A. K.; Kim, H.; Kim, K. K.; Ha, S. C.; Kim, T. Structural and Functional Study of ChuY from Escherichia Coli Strain CFT073. *Biochem. Biophys. Res. Commun.* **2016**, *482* (4), 1176–1182. https://doi.org/10.1016/j.bbrc.2016.12.008.

(123) LaMattina, J. W.; Delrossi, M.; Uy, K. G.; Keul, N. D.; Nix, D. B.; Neelam, A. R.; Lanzilotta, W. N. Anaerobic Heme Degradation: ChuY Is an Anaerobilin Reductase That Exhibits Kinetic Cooperativity. *Biochemistry* **2017**, *56* (6).

https://doi.org/10.1021/acs.biochem.6b01099.

(124) Frey, P. A.; Hegeman, A. D.; Ruzicka, F. J. The Radical SAM Superfamily. *Critical Reviews in Biochemistry and Molecular Biology*. 2008, pp 63–88. https://doi.org/10.1080/10409230701829169.

(125) Buckel, W.; Golding, B. T. Radical Enzymes in Anaerobes*. *Annu. Rev. Microbiol.* **2006**, *60*, 27–49. https://doi.org/10.1146/ANNUREV.MICRO.60.080805.142216.

(126) Horitani, M.; Shisler, K.; Broderick, W. E.; Hutcheson, R. U.; Duschene, K. S.; Marts, A. R.; Hoffman, B. M.; Broderick, J. B. Radical SAM Catalysis via an Organometallic Intermediate with an Fe-[5′-C]-Deoxyadenosyl Bond. *Science (80-.).* **2016**, *352* (6287), 822–825. https://doi.org/10.1126/SCIENCE.AAF5327/SUPPL_FILE/HORITANI.SM.PDF.

(127) Broderick, W. E.; Hoffman, B. M.; Broderick, J. B. Mechanism of Radical Initiation in the Radical S-Adenosyl-L-Methionine Superfamily. *Acc. Chem. Res.* **2018**, *51* (11), 2611–2619. https://doi.org/10.1021/ACS.ACCOUNTS.8B00356/ASSET/IMAGES/LARGE/AR-2018-00356F_0009.JPEG.

(128) Mehta, A. P.; Abdelwahed, S. H.; Mahanta, N.; Fedoseyenko,

D.; Philmus, B.; Cooper, L. E.; Liu, Y.; Jhulki, I.; Ealick, S. E.; Begley, T. P. Radical S-Adenosylmethionine (SAM) Enzymes in Cofactor Biosynthesis: A Treasure Trove of Complex Organic Radical Rearrangement Reactions. *J. Biol. Chem.* **2015**, *290* (7), 3980–3986. https://doi.org/10.1074/JBC.R114.623793.

(129) Gagnon, D. M.; Stich, T. A.; Mehta, A. P.; Abdelwahed, S. H.; Begley, T. P.; Britt, R. D. An Aminoimidazole Radical Intermediate in the Anaerobic Biosynthesis of the 5,6-Dimethylbenzimidazole Ligand to Vitamin B12. *J. Am. Chem. Soc.* **2018**, *140* (40), 12798–12807. https://doi.org/10.1021/JACS.8B05686/ASSET/IMAGES/LARGE/JA-2018-056862_0003.JPEG.

(130) Wang, Y.; Schnell, B.; Müller, R.; Begley, T. P. Iterative Methylations Resulting in the Biosynthesis of the T-Butyl Group Catalyzed by a B12-Dependent Radical SAM Enzyme in Cystobactamid Biosynthesis. *Methods Enzymol.* **2018**, *606*, 199–216. https://doi.org/10.1016/BS.MIE.2018.05.018.

(131) Ding, Y.; Yu, Y.; Pan, H.; Guo, H.; Li, Y.; Liu, W. Moving Posttranslational Modifications Forward to Biosynthesize the Glycosylated Thiopeptide Nocathiacin I in Nocardia Sp. ATCC202099. *Mol. Biosyst.* **2010**, *6* (7), 1180–1185.

https://doi.org/10.1039/C005121G.

(132) Fujimori, D. G. Radical SAM-Mediated Methylation Reactions. *Curr. Opin. Chem. Biol.* **2013**, *17* (4), 597–604. https://doi.org/10.1016/J.CBPA.2013.05.032.

(133) Yan, F.; Lamarre, J. M.; Röhrich, R.; Wiesner, J.; Jomaa, H.; Markin, A. S.; Fujimori, D. G. RlmN and Cfr Are Radical SAM Enzymes Involved in Methylation of Ribosomal RNA. *J. Am. Chem. Soc.* **2010**, *132* (11), 3953–3964. https://doi.org/10.1021/JA910850Y/SUPPL_FILE/JA910850Y_SI_001.PDF.

(134) Grove, T. L.; Radle, M. I.; Krebs, C.; Booker, S. J. Cfr and RlmN Contain a Single [4Fe-4S] Cluster, Which Directs Two Distinct Reactivities for s -Adenosylmethionine: Methyl Transfer by S N2 Displacement and Radical Generation. *J. Am. Chem. Soc.* **2011**, *133* (49), 19586–19589. https://doi.org/10.1021/JA207327V/SUPPL_FILE/JA207327V_SI_001.PDF.

(135) Sato, S.; Kudo, F.; Kim, S. Y.; Kuzuyama, T.; Eguchi, T. Methylcobalamin-Dependent Radical SAM C-Methyltransferase Fom3 Recognizes Cytidylyl-2-Hydroxyethylphosphonate and Catalyzes the

Nonstereoselective C-Methylation in Fosfomycin Biosynthesis. *Biochemistry* **2017**, *56* (28), 3519–3522. https://doi.org/10.1021/ACS.BIOCHEM.7B00472/ASSET/IMAGES/LARGE/BI-2017-00472R_0003.JPEG.

(136) Allen, K. D.; Wang, S. C. Initial Characterization of Fom3 from Streptomyces Wedmorensis: The Methyltransferase in Fosfomycin Biosynthesis. *Arch. Biochem. Biophys.* **2014**, *543*, 67–73. https://doi.org/10.1016/J.ABB.2013.12.004.

(137) Kim, H. J.; Liu, Y. N.; McCarty, R. M.; Liu, H. W. Reaction Catalyzed by GenK, a Cobalamin-Dependent Radical S-Adenosyl- l -Methionine Methyltransferase in the Biosynthetic Pathway of Gentamicin, Proceeds with Retention of Configuration. *J. Am. Chem. Soc.* **2017**, *139* (45), 16084–16087. https://doi.org/10.1021/JACS.7B09890/ASSET/IMAGES/LARGE/JA-2017-09890A_0003.JPEG.

(138) Parent, A.; Guillot, A.; Benjdia, A.; Chartier, G.; Leprince, J.; Berteau, O. The B12-Radical SAM Enzyme PoyC Catalyzes Valine Cβ-Methylation during Polytheonamide Biosynthesis. *J. Am. Chem. Soc.* **2016**, *138* (48), 15515–15518. https://doi.org/10.1021/JACS.6B06697/ASSET/IMAGES/LARGE/JA-

2016-06697V_0004.JPEG.

(139) Inahashi, Y.; Zhou, S.; Bibb, M. J.; Song, L.; Al-Bassam, M. M.; Bibb, M. J.; Challis, G. L. Watasemycin Biosynthesis in Streptomyces Venezuelae: Thiazoline C-Methylation by a Type B Radical-SAM Methylase Homologue. *Chem. Sci.* **2017**, *8* (4), 2823–2831. https://doi.org/10.1039/C6SC03533G.

(140) Marous, D. R.; Lloyd, E. P.; Buller, A. R.; Moshos, K. A.; Grove, T. L.; Blaszczyk, A. J.; Booker, S. J.; Townsend, C. A. Consecutive Radical S-Adenosylmethionine Methylations Form the Ethyl Side Chain in Thienamycin Biosynthesis. *Proc. Natl. Acad. Sci. U. S. A.* **2015**, *112* (33), 10354–10358. https://doi.org/10.1073/PNAS.1508615112/SUPPL_FILE/PNAS.1508615112.SAPP.PDF.

(141) Yu, Y.; Duan, L.; Zhang, Q.; Liao, R.; Ding, Y.; Pan, H.; Wendt-Pienkowski, E.; Tang, G.; Shen, B.; Liu, W. Nosiheptide Biosynthesis Featuring a Unique Indole Side Ring Formation on the Characteristic Thiopeptide Framework. *ACS Chem. Biol.* **2009**, *4* (10), 855–864. https://doi.org/10.1021/CB900133X/SUPPL_FILE/CB900133X_SI_001.PDF.

(142) Huang, W.; Xu, H.; Li, Y.; Zhang, F.; Chen, X. Y.; He, Q. L.;

Igarashi, Y.; Tang, G. L. Characterization of Yatakemycin Gene Cluster Revealing a Radical s -Adenosylmethionine Dependent Methyltransferase and Highlighting Spirocyclopropane Biosynthesis. *J. Am. Chem. Soc.* **2012**, *134* (21), 8831–8840. https://doi.org/10.1021/JA211098R/ASSET/IMAGES/MEDIUM/JA-2011-11098R_0003.GIF.

(143) Watanabe, H.; Tokiwano, T.; Oikawa, H. Biosynthetic Study of FR-900848: Origin of the Aminodeoxynucleoside Part. *J. Antibiot. 2006 599* **2006**, *59* (9), 607–610. https://doi.org/10.1038/ja.2006.82.

(144) Hurley, L. H.; Rokem, J. S. BIOSYNTHESIS OF THE ANTITUMOR ANTIBIOTIC CC-1065 BY STREPTOMYCES ZELENSIS. *J. Antibiot. (Tokyo).* **1983**, *36* (4), 383–390. https://doi.org/10.7164/ANTIBIOTICS.36.383.

(145) Torres, A. G.; Payne, S. M. Haem Iron-Transport System in Enterohaemorrhagic Escherichia Coli O157:H7. *Mol. Microbiol.* **1997**, *23* (4), 825–833. https://doi.org/10.1046/J.1365-2958.1997.2641628.X.

(146) Suits, M. D. L.; Jaffer, N.; Jia, Z. Structure of the Escherichia Coli O157:H7 Heme Oxygenase ChuS in Complex with Heme and Enzymatic Inactivation by Mutation of the Heme Coordinating Residue

His-193. *J. Biol. Chem.* **2006**, *281* (48), 36776–36782. https://doi.org/10.1074/jbc.M607684200.

(147) Wyckoff, E. E.; Lopreato, G. F.; Tipton, K. A.; Payne, S. M. Shigella Dysenteriae ShuS Promotes Utilization of Heme as an Iron Source and Protects against Heme Toxicity. *J. Bacteriol.* **2005**, *187* (16), 5658–5664. https://doi.org/10.1128/JB.187.16.5658-5664.2005/ASSET/A686A04D-60BA-4447-909F-C133C481ADF6/ASSETS/GRAPHIC/ZJB0160549870005.JPEG.

(148) Suits, M. D. L.; Pal, G. P.; Nakatsu, K.; Matte, A.; Cygler, M.; Jia, Z. Identification of an Escherichia Coli 0157:H7 Heme Oxygenase with Tandem Functional Repeats. *Proc. Natl. Acad. Sci. U. S. A.* **2005**, *102* (47), 16955–16960. https://doi.org/10.1073/PNAS.0504289102.

(149) Trott, O.; Olson, A. J. AutoDock Vina: Improving the Speed and Accuracy of Docking with a New Scoring Function, Efficient Optimization, and Multithreading. *J. Comput. Chem.* **2010**, *31* (2), 455–461. https://doi.org/10.1002/JCC.21334.

(150) Moriarty, N. W.; Grosse-Kunstleve, R. W.; Adams, P. D. Electronic Ligand Builder and Optimization Workbench (ELBOW): A Tool for Ligand Coordinate and Restraint Generation. *urn:issn:0907-4449* **2009**, *65* (10), 1074–1080.

https://doi.org/10.1107/S0907444909029436.

(151) Gasteiger, E.; Hoogland, C.; Gattiker, A.; Duvaud, S.; Wilkins, M. R.; Appel, R. D.; Bairoch, A. Protein Identification and Analysis Tools on the ExPASy Server. *Proteomics Protoc. Handb.* **2005**, 571–607. https://doi.org/10.1385/1-59259-890-0:571.

(152) Laue, T. M., Shah, B. D., Ridgeway, T. M., and Pelletier, S. L. Computer-Aided Interpretation of Analytical Sedimentation Data for Proteins. *Anal. Ultracentrifugation Biochem. Polym. Sci.* **1992**.

(153) Schuck, P.; Gillis, R. B.; Besong, T. M. D.; Almutairi, F.; Adams, G. G.; Rowe, A. J.; Harding, S. E. SEDFIT-MSTAR: Molecular Weight and Molecular Weight Distribution Analysis of Polymers by Sedimentation Equilibrium in the Ultracentrifuge. *Analyst* **2014**, *139* (1), 79–92. https://doi.org/10.1039/c3an01507f.

(154) Ortega, A.; Amorós, D.; García De La Torre, J. Prediction of Hydrodynamic and Other Solution Properties of Rigid Proteins from Atomic- and Residue-Level Models. *Biophys. J.* **2011**, *101* (4), 892–898. https://doi.org/10.1016/J.BPJ.2011.06.046.

(155) Joshi, S.; Fedoseyenko, D.; Mahanta, N.; Manion, H.; Naseem, S.; Dairi, T.; Begley, T. P. Novel Enzymology in Futalosine-Dependent Menaquinone Biosynthesis. *Curr. Opin. Chem. Biol.* **2018**, *47*, 134–

141. https://doi.org/10.1016/J.CBPA.2018.09.015.

(156) Bhandari, D. M.; Fedoseyenko, D.; Begley, T. P. Tryptophan Lyase (NosL): A Cornucopia of 5′-Deoxyadenosyl Radical Mediated Transformations. *J. Am. Chem. Soc.* **2016**, *138* (50), 16184–16187. https://doi.org/10.1021/JACS.6B06139/ASSET/IMAGES/LARGE/JA-2016-06139R_0010.JPEG.

(157) Jin, W. B.; Wu, S.; Jian, X. H.; Yuan, H.; Tang, G. L. A Radical S-Adenosyl-L-Methionine Enzyme and a Methyltransferase Catalyze Cyclopropane Formation in Natural Product Biosynthesis. *Nat. Commun. 2018 91* **2018**, *9* (1), 1–10. https://doi.org/10.1038/s41467-018-05217-1.

(158) Frieden, C. Kinetic Aspects of Regulation of Metabolic Processes. *J. Biol. Chem.* **1970**, *245* (21), 5788–5799. https://doi.org/10.1016/0022-510X(96)00153-0.

(159) Kelley, L. A.; Mezulis, S.; Yates, C. M.; Wass, M. N.; Sternberg, M. J. E. The Phyre2 Web Portal for Protein Modeling, Prediction and Analysis. *Nat. Protoc. 2015 106* **2015**, *10* (6), 845–858. https://doi.org/10.1038/nprot.2015.053.

(160) Krebs, C.; Broderick, W. E.; Henshaw, T. F.; Broderick, J. B.; Huynh, B. H. Coordination of Adenosylmethionine to a Unique Iron

Site of the [4Fe-4S] of Pyruvate Formate-Lyase Activating Enzyme: A Mössbauer Spectroscopic Study. *J. Am. Chem. Soc.* **2002**, *124* (6), 912–913. https://doi.org/10.1021/JA017562I/ASSET/IMAGES/LARGE/JA017562IF00001.JPEG.

(161) Wilks, A.; Ortiz De Montellanos, P. R. Rat Liver Heme Oxygenase. High Level Expression of a Truncated Soluble Form and Nature of the Meso-Hydroxylating Species. *J. Biol. Chem.* **1993**, *268* (30), 22357–22362. https://doi.org/10.1016/S0021-9258(18)41536-0.

(162) Wilks, A. Heme Oxygenase: Evolution, Structure, and Mechanism. *https://home.liebertpub.com/ars* **2004**, *4* (4), 603–614. https://doi.org/10.1089/15230860260220102.

(163) Jin, W. B.; Wu, S.; Xu, Y. F.; Yuan, H.; Tang, G. L. Recent Advances in HemN-like Radical S-Adenosyl-L-Methionine Enzyme-Catalyzed Reactions. *Nat. Prod. Rep.* **2020**, *37* (1), 17–28. https://doi.org/10.1039/C9NP00032A.

(164) Chatterjee, A.; Hazra, A. B.; Abdelwahed, S.; Hilmey, D. G.; Begley, T. P. A “Radical Dance” in Thiamin Biosynthesis: Mechanistic Analysis of the Bacterial Hydroxymethylpyrimidine Phosphate Synthase. *Angew. Chemie Int. Ed.* **2010**, *49* (46), 8653–8656.

https://doi.org/10.1002/ANIE.201003419.

(165) Jin, W. B.; Wu, S.; Jian, X. H.; Yuan, H.; Tang, G. L. A Radical S-Adenosyl-L-Methionine Enzyme and a Methyltransferase Catalyze Cyclopropane Formation in Natural Product Biosynthesis. *Nat. Commun. 2018 91* **2018**, *9* (1), 1–10. https://doi.org/10.1038/s41467-018-05217-1.

(166) Wang, B.; Lamattina, J. W.; Marshall, S. L.; Booker, S. J. Capturing Intermediates in the Reaction Catalyzed by NosN, a Class C Radical S-Adenosylmethionine Methylase Involved in the Biosynthesis of the Nosiheptide Side-Ring System. *J. Am. Chem. Soc.* **2019**, *141* (14), 5788–5797. https://doi.org/10.1021/jacs.8b13157.

(167) Arcinas, A. J.; Maiocco, S. J.; Elliott, S. J.; Silakov, A.; Booker, S. J. Ferredoxins as Interchangeable Redox Components in Support of MiaB, a Radical S-Adenosylmethionine Methylthiotransferase. *Protein Sci.* **2019**, *28* (1), 267–282. https://doi.org/10.1002/PRO.3548.

(168) Deredge, D. J.; Huang, W.; Hui, C.; Matsumura, H.; Yue, Z.; Moënne-Loccoz, P.; Shen, J.; Wintrode, P. L.; Wilks, A. Ligand-Induced Allostery in the Interaction of the Pseudomonas Aeruginosa Heme Binding Protein with Heme Oxygenase. *Proc. Natl. Acad. Sci. U. S. A.* **2017**, *114* (13), 3421–3426.

https://doi.org/10.1073/PNAS.1606931114/SUPPL_FILE/PNAS.201606931SI.PDF.

(169) Byer, A. S.; Yang, H.; McDaniel, E. C.; Kathiresan, V.; Impano, S.; Pagnier, A.; Watts, H.; Denler, C.; Vagstad, A. L.; Piel, J.; et al. Paradigm Shift for Radical S-Adenosyl- l -Methionine Reactions: The Organometallic Intermediate ω Is Central to Catalysis. *J. Am. Chem. Soc.* **2018**, *140* (28), 8634–8638. https://doi.org/10.1021/jacs.8b04061.

(170) Mathew, L. G.; Beattie, N. R.; Pritchett, C.; Lanzilotta, W. N. New Insight into the Mechanism of Anaerobic Heme Degradation. *Biochemistry* **2019**. https://doi.org/10.1021/acs.biochem.9b00841.

(171) Suits, M. D. L.; Pal, G. P.; Nakatsu, K.; Matte, A.; Cygler, M.; Jia, Z. Identification of an Escherichia Coli O157:H7 Heme Oxygenase with Tandem Functional Repeats. *Proc. Natl. Acad. Sci.* **2005**, *102* (47), 16955–16960. https://doi.org/10.1073/pnas.0504289102.

(172) Wilks, A.; Ikeda-Saito, M. Heme Utilization by Pathogenic Bacteria: Not All Pathways Lead to Biliverdin. *Acc. Chem. Res.* **2014**, *47* (8), 2291–2298. https://doi.org/10.1021/ar500028n.

(173) Irving, H.; Williams, R. J. P. 637. The Stability of Transition-Metal Complexes. *J. Chem. Soc.* **1953**, *3245* (0), 3192–3210.

https://doi.org/10.1039/JR9530003192.

(174) Edlund, P.; Takala, H.; Claesson, E.; Henry, L.; Dods, R.; Lehtivuori, H.; Panman, M.; Pande, K.; White, T.; Nakane, T.; et al. The Room Temperature Crystal Structure of a Bacterial Phytochrome Determined by Serial Femtosecond Crystallography. *Sci. Reports 2016 61* **2016**, *6* (1), 1–9. https://doi.org/10.1038/srep35279.

(175) Berggård, T.; Linse, S.; James, P. Methods for the Detection and Analysis of Protein–Protein Interactions. *Proteomics* **2007**, *7* (16), 2833–2842. https://doi.org/10.1002/PMIC.200700131.

(176) Jumper, J.; Evans, R.; Pritzel, A.; Green, T.; Figurnov, M.; Ronneberger, O.; Tunyasuvunakool, K.; Bates, R.; Žídek, A.; Potapenko, A.; et al. Highly Accurate Protein Structure Prediction with AlphaFold. *Nat. 2021 5967873* **2021**, *596* (7873), 583–589. https://doi.org/10.1038/s41586-021-03819-2.

(177) Mathew, L. G.; Brimberry, M.; Lanzilotta, W. N. Class C Radical SAM Methyltransferases Involved in Anaerobic Heme Degradation. *ACS Bio Med Chem Au* **2022**, *2* (2), 120–124. https://doi.org/10.1021/ACSBIOMEDCHEMAU.1C00047.

APPENDIX

AN UNPRECEDENTED FUNCTION FOR A TUNGSTEN-CONTAINING OXIDOREDUCTASE[2]

[2]**Liju G. Mathew**, Dominik K. Haja, Clayton Pritchett, Winston McCormick, Robbie Zeineddine, Leo S. Fontenot, Mario E. Rivera, John Glushka, Michael W. W. Adams, and William N. Lanzilotta. To be submitted to the Journal of Bioinorganic Chemistry.

ABSTRACT

Pyrococcus furiosus is a hyperthermophilic marine archaeon that grows optimally near 100°C. To date, five tungstopterin-containing oxidoreductases have been characterized from this organism. Each enzyme catalyzes the reversible conversion of one or more aldehyde to the corresponding carboxylic acid but they have different specificities. The physiological functions of only two of these enzymes are known. One, termed GAPOR, is a glycolytic enzyme that oxidizes glyceraldehyde-3-phosphate, while the other, termed AOR, oxidizes multiple aldehydes generated during peptide fermentation. Two of the enzymes have known structures (AOR and FOR). Herein we focus on WOR5, the fifth tungstopterin enzyme to be discovered in *P. furiosus*. Expression of WOR5 was previously shown to be increased during cold shock (growth at 72º C) although the physiological substrate is not known. To gain insight into WOR function, we sought to determine both its structure and identify its intracellular substrate. Crystallization experiments were performed with a concentrated cytoplasmic extract of *P. furiosus* grown at 72º C and the structure of WOR5 was deduced from the crystals that were obtained. In contrast to a previous report, WOR5 is heterodimeric containing an additional polyferredoxin-like subunit with four [4Fe-4S] clusters. The active site structure of WOR5 is substantially different from AOR and FOR and the significant electron density observed adjacent to the tungsten cofactor of WOR5 was modeled as an aliphatic sulfonate. Biochemical assays and product analysis confirmed that WOR5 is an aliphatic sulfonate/phosphonate ferredoxin oxidoreductase (ASOR). A catalytic mechanism for

ASOR is proposed based on the structural information and the potential role of ASOR in the cold shock response is discussed.

INTRODUCTION

The hyperthermophile *Pyrococcus furiosus* is a strictly anaerobic microorganism that grows at an optimum temperature of 100°C using carbohydrates or peptides as carbon and energy sources. Of particular metabolic significance and importance to this work is the fact that *P. furiosus* does not contain any cytochromes and growth of the organism is strictly dependent on the presence of tungsten.[177] Genomic and biochemical analysis have identified five tungsten-containing oxidoreductase enzymes that are members of the phylogenetically-diverse WOR family.[178] Transcriptomic and biochemical data are available on all five of the WOR family enzymes in *P. furiosus*, although the physiological function for only two of these enzymes has been firmly established. Glyceraldehyde-3-phosphate (GAP) ferredoxin oxidoreductase (GAPOR) is a glycolytic enzyme and replaces the expected GAP dehydrogenase.[179] GAPOR is specific for GAP and oxidizes it to 3-phosphoglycerate (3PG) generating reduced ferredoxin. This is used by the electron bifurcating enzyme NfnI (formally known as FNOR), which is thought to be critical to maintaining the redox balance of the cell.[180] In contrast to GAPOR, aldehyde ferredoxin oxidoreductase (AOR) has a broad substrate specificity and uses both aliphatic and aromatic aldehydes that are derived from amino acids,[181] consistent with a protective role for AOR from aldehyde damage to the cell during the fermentation of amino acids.

The third member of the WOR family in *P. furiosus,* formaldehyde ferrodoxin oxidoreductase (FOR), is most active with small chain aliphatic aldehydes with one to three carbon atoms but its true substrate and function are not known.[182] The physiological functions of the other two tungstoenzymes, WOR4 and WOR5, both of which oxidize a broad range of aldehydes, also remain to be established. WOR4 has been implicated in

sulfur metabolism, as its gene expression is three-fold higher when *P. furiosus* is grown in the presence of elemental sulfur.[183] Of the *P. furiosus* WOR family members, only AOR[184] and FOR[185] have been structurally characterized.

In the case of WOR5, cell cold shock treatment was previously shown to induce an almost a five-fold increase in expression of *wor5* (PF1480) occurring for up to five hours after the temperature drops from 95 to 72° C.[186] WOR5 is the most recent enzyme to be characterized in vitro and has some novel features,[187] oxidizing many of the same aliphatic aldehydes oxidized by AOR and FOR, and also longer chain aldehydes. In particular, the ability to oxidize hexanal was an order of magnitude faster[187] by comparison to any other aldehyde tested, indicative of a potentially larger, more hydrophobic active site. Purification of WOR5 from *P. furiosus* biomass revealed a single 67 kDa band on SDS-PAGE while native PAGE revealed a 135 kDa band that the authors attributed to a homodimer.[187] This was an interesting finding, given that the WOR5 gene is in a two-gene operon. Specifically, PF1479 and PF1480 code for a polyferredoxin-like protein and WOR5, respectively. Based on the predicted cysteine content, the polyferredoxin could contain as many as four [4Fe-4S] clusters. However, it was not clear if this protein was a subunit of WOR5, as it was not detected by Hagen and coworkers,[187] or the polyferredoxin actually served as its physiological electron carrier. Polyferredoxin domains and subunits are part of a superfamily of electron transfer proteins that are commonly found in oxidoreductases[188] and provide critical electron transfer conduits for enzymes involved in central metabolic processes, including integral membrane complexes.[189] Given the small size and fact that many ferredoxins do not stain well with Coomassie, it would not be surprising if the smaller subunit was missed. Indeed, a

tungsten-containing member of the WOR family that was recently isolated from a thermophilic bacterium was shown to be a heterodimer consisting of an WOR-like subunit and a polyferredoxin-like subunit.[190] Despite the wide range of aldehyde substrates that WOR5 has been reported to oxidize *in vitro*, its physiological function, as well as that of the adjacent "polyferredoxin" encoded in the genome, remain open questions.

In this work we undertook a unique crystallization strategy in an attempt to ascertain the physiological substrate of WOR5 using cytoplasmic extracts of a strain of *P. furiosus* that we had genetically engineered to overproduce an affinity-tagged WOR5 together with its predicted polyferredoxin redox partner. The goal was to capture crystals of WOR5 that contained an intracellular metabolite. Specifically, the native WOR5 enzyme was crystallized from the cytoplasmic fraction of a concentrated cell-free extract. Anomalous scattering was observed from the resulting crystals and anomalous difference maps indicated that a sulfur-containing molecule was bound to the tungsto-bispyranopterin. In addition, the putative polyferredoxin protein encoded by the gene adjacent to that encoding WOR5 is present with the larger catalytic WOR-like subunit showing that WOR5 is heterodimeric. Chemical soaking experiments and biochemical assays were performed to further address the true substrate of WOR5. We provide evidence for a novel function for WOR5 in the metabolism of sulfonated compounds that are abundant in the marine environment inhabited by *P. furiosus.*

RESULTS

Crystallization and purification of WOR5. Initial attempts to obtain diffraction quality crystals of WOR5 using enzyme purified from *P. furiosus* biomass failed. With the

knowledge that undefined components of the cellular milieu can often stabilize enzymes, we performed an uncontrolled experiment. Specifically, a concentrated cytoplasmic extract from temperature-induced (cold-shock) wild-type *P. furiosus* cells was screened under strictly anaerobic conditions using the capillary batch method. In addition to the identification of crystallization conditions, if a metabolite from the cytoplasmic extract was captured in the active site, then we would also gain insight into enzyme function. Identification of diffraction quality crystals took 18 months using sparse matrix crystal screening of concentrated extract from wild type *P. furiosus* cells grown at 80°C. Interestingly, when concentrated cytoplasmic extract was obtained from the WOR5 overexpression strain (also grown at 80ºC), reproduction of the crystallization conditions resulted in the appearance of WOR5 crystals in less than one month. The diffraction quality of the crystals obtained from the cytoplasmic extract varied from 2.0-3.5 Å (Table 1). The crystallization conditions could also be reproduced with purified enzyme and, although optimizations of pH and precipitant were tried, no improvement in diffraction quality was observed. However, it does stand to reason that the faster growth rate of diffraction quality crystals that we observe from the concentrated cytoplasmic extract of the overexpression strain relative to the wild type strain is indicative of higher WOR5 expression levels. In fact, previous work that has taken advantage of the S-layer protein promoter to express His-tagged proteins has resulted in a three to five-fold increase in expression.[191] Consistent with these observations, on average, isolation of WOR5 from the overexpression strain resulted in 3 mg of pure WOR5 from 10 g of wet cell paste. These data also represent a substantial (~6-fold) improvement in yield by comparison to

the previously reported isolation of approximately 5 mg per 100 g of wet cell paste reported by Bevers et al.[187]

Overall structure of WOR5. In both the crude-crystallized and substrate-soaked WOR5 crystals (Table 1), the asymmetric unit of the WOR5 crystals (space group $P2_12_12$) consists of two polyferredoxin-like subunits (WOR5-S for small subunit encoded by PF1479, calculated mass of 18.8 kDa), and two WOR-like subunits (WOR5-L for large subunit encoded by PF1480, calculated mass of 64.8 kDa). Therefore, the biological form of WOR5 is a heterodimeric protein consisting of the WOR5-S subunit with four [4Fe-4S] clusters and the WOR5-L containing the active site tungsto-bispyranopterin cofactor as well as another [4Fe-4S] cluster. In addition to the genetic organization, an additional line of support for this oligomeric arrangement comes from a PISA analysis of the crystal packing. Specifically, PISA analysis led to the identification of two distinct protein-protein interfaces between the polyferredoxin subunit and WOR-like subunit. However, only one interface is consistent with a viable electron transfer pathway. This interface has a buried surface area of 2,079 $Å^2$ and is shown in Figure 1, Panel A. The relative orientation of the metal cofactors within this heterodimer are shown in Figure 1, Panel B. Electron transfer in metalloproteins is well understood,[192] specifically, electron transfer in metalloproteins is optimized when the metal cofactors are between 10-12 angstroms apart.[193] The heterodimeric complex that minimizes the distance between the [4Fe-4S] cluster in the large WOR-type subunit and the closest [4Fe-4S] cluster within the polyferredoxin subunit results in a distance of approximately 11 Å (Figure 1, Panel B). This electron transfer pathway is also consistent with the proposed ferredoxin binding site on FOR reported by Hu et al.[185] These data are in contrast to a previous report on WOR5 by Hagen et al.,[187]

in that WOR5 clearly contains a second polyferredoxin-type subunit. AOR, GAPOR, FOR and WOR4 have also been reported to be single subunit proteins and, in contrast to WOR5, the genes encoding them do not have adjacent genes encoding polyferredoxin-type proteins (subunits).

Despite the notably different substrate specificities, the catalytic domains from the structures of AOR and FOR, as well as that of WOR5, share several general features. In particular, the overall fold of the catalytic subunit is conserved, especially near the tungsto-bispyranopterin cofactor and nearby [4Fe-4S] cluster. Structural alignment of the catalytic domain of AOR and FOR with the catalytic domain of WOR5 results in an RMSD for the backbone atoms of 1.5 and 1.1 Å, respectively. However, the [4Fe-4S] cluster within the catalytic domain, immediately adjacent to the tungsto-bispyranopterin, is ligated by all cysteine residues in AOR and FOR. In contrast, the [4Fe-4S] cluster in the catalytic subunit of WOR5 has three cysteine ligands and one aspartic acid ligand (Figure 1, Panel C). Based on previous studies with simple ferredoxins,{Brereton, 1999 #2639} the aspartic acid ligation should shift the midpoint reduction potential of the [4Fe-4S] cluster slightly more positive by comparison to the fully cysteine coordinated cluster. The closest contact between the tungsten cofactor and the [4Fe-4S] cluster is similar in all three tungstoenzymes for which structures are available. Specifically, a sulfur atom from one of the cysteine ligands comes within 3.3 Å of the pterin (Figure 1, Panel C, dashed line), consistent with a role for the [4Fe-4S] cluster in electron transfer to ferredoxin or, in the case of WOR5, to the polyferredoxin-like subunit.

Identification of taurine as a substrate for WOR5. Phases were obtained from the anomalous scattering of the tungsten and iron atoms in WOR5. However, at the iron

edge (7,112 eV), sulfur atoms also have a measurable anomalous signal that begins to appear at approximately 3-5 s (Supplemental Information, Figure S1). While some care must be taken when interpreting electron density around the tungsten atom due to "ripples" caused by series termination effects,[194] it is clear that there is a significant anomalous signal near the tungsten cofactor as evidenced by comparable density around the [4Fe-4S] and the sulfur atoms of nearby methionine residues (Figure S1). The anomalous signal (Df'') for tungsten at this wavelength is over 15 electrons, while the Df'' for iron is just over 4 electrons. These data indicate the presence of an additional, unknown, anomalous peak near the tungsten ion (Figure S1, black arrow). Given that these crystals were obtained from a cytoplasmic extract, a reasonable conclusion is that this signal is coming from an atom of an unknown metabolite present in the cytoplasm of this organism. More specifically, this atom is most likely sulfur. Figure 2, Panel A, shows the F_o-F_c composite omit map contoured at 3 s for the diffraction data obtained from WOR5 crystals grown from crude extract. The best fit to the unknown density was (*S*)-1-hydroxy-1-butylsulfonate (HBS, Figure 2, Panel A). This was determined by a purely qualitative fit to the electron density with a molecule that also satisfied the anomalous signal, however, modeling the "*R"* enantiomer did result in an increase in both *R* and R_{free} by 1%. No bonding restraints from the HBS molecule to the tungsten atom were used during refinement. However, the HBS molecule satisfies the density well with one sulfonate oxygen atom coming within 2.5 Å of the tungsten ion and within 3.0 Å of the side chain of H469 and another sulfonate oxygen is within 2.7 Å of E328.

We therefore propose that the physiological substrate of WOR5 is an aliphatic sulfonate. Interestingly, there are several sulfonated compounds, typically used as

cellular osmolytes, that are produced in high concentrations (> 1 mM) by marine organisms ranging from phytoplankton to mussels and clams.[195] Among the most prevalent molecules are 2-aminoethanesulfonate, which is also known as taurine, and 2,3-dihydroxyl-propane-1-sulfonate. In addition, taurine, together with the amino acids glycine and alanine, are common in marine metazoans and can represent up to 40% of the free amino acid pool in their release products.[195] To investigate whether an aliphatic substrate such as taurine might be substrate for WOR5, crystals were allowed to soak overnight in mother liquor containing 5 mM taurine. As shown in panel B, Figure 2, distinct changes in the electron density was observed at the active site. Specifically, the electron density became smaller/shorter, consistent with a smaller molecule bound near the tungsten atom. Interestingly, while E328 and H469 are conserved in FOR and AOR, Y199, H446, and D453 are unique to WOR5. In addition to the specific differences mentioned above, the active site of WOR5 is much larger forming a 10 x 15 Å cleft that is almost 10 Å deep. The net result is an active site that is accessible to much larger substrates and considerably more solvent when compared to those of AOR and FOR (Supporting information, Figure S2) suggesting that the WOR5 reaction may be more complex than simply oxidizing an aldehyde to the carboxylic acid. The larger active site of WOR5 is also consistent with its ability to oxidize the longer chain aldehyde, hexanal, which is unique among the *P. furiosus* WOR family.[187]

Oxidation of taurine by WOR5. To address the hypothesis that WOR5 could desulfonate and oxidize aliphatic sulfonates represented by taurine, the purified enzyme was incubated with taurine and the artificial electron acceptor benzyl viologen (BV) in place of the putative natural acceptor *P. furiosus* ferredoxin. For taurine, and known

substrates such as propionaldehyde and hexanal (Table 2), BV reduction proceeded only in the presence of the substrate and WOR5 (Figure 3). Based on a least-squares fit to the Michaelis Menten equation, the specific activity for taurine oxidation was 0.49 mmoles min^{-1} mg^{-1}, confirming that WOR5 can utilize this compound as a substrate. Kinetic data for taurine and the aldehydes hexanal and propionaldehyde are summarized in Table 2. The rate of taurine oxidation is notably slower than that measured with propanal (Figure 3, Panel A; 30.6 mmoles min^{-1} mg^{-1}). However, as shown in Figure 4, taurine oxidation is not simply a one step aldehyde to acid conversion. It involves two steps, an oxidative desulfonation reaction followed by the activation of a second water molecule and oxidation of the resulting aldehyde. This activity has not been reported for any other member of the WOR family and is apparently unique to WOR5. For example, we found that purified AOR or FOR from *P. furiosus* did not catalyze the same reaction. Specifically, no reduction of BV was observed with AOR or FOR under the same reaction conditions. Moreover, in addition to taurine, other sulfonated and phosphonated compounds, included hexylsulfonate, hexylphosphonate and amniomethyl-phosphonate, exhibited rates of BV reduction ranging from 1-3 $mM \bullet min^{-1} \bullet (mg\ WOR5)^{-1}$.

NMR analysis of taurine oxidation by WOR5. We utilized NMR to confirm the proposed oxidation products of taurine by WOR5 using the physiological electron acceptor, ferredoxin, rather than the artificial carrier BV. However, this made the experiment particularly challenging because excess ferredoxin must be added to ensure efficient oxidation and accumulation of sufficient product so that it is detectable by NMR. Figure 5 shows the NMR spectra that were acquired from samples taken before and after reaction of taurine WOR5. In the absence of WOR5, taurine exhibits a doublet of triplets

at δ_H = 3.21 and 3.31 ppm. After reaction with WOR5 and ferredoxin, the taurine resonances almost completely disappear and are replaced by a singlet at δ_H = 3.54 ppm, a resonance frequency characteristic of glycine. A ^{1}H-^{13}C HSQC spectrum of the reaction product (Figure 5B) enables correlation of the δ_H = 3.54 ppm to a $\delta_{,C}$= 44.13 ppm resonance, and a ^{1}H-^{13}C HMBC spectrum (Figure 5C) allows correlation of the δ_H = 3.54 ppm to a $\delta_{,C}$= 175.2 ppm peak. That these chemical shifts arise from glycine were confirmed *a)* by comparison to the 1D ^{1}H and ^{13}C spectra obtained from a glycine standard (Supporting Information, Figure S3), and *b)*, by comparison to the chemical shifts compiled in the Biological Magnetic Resonance Database.

Negative Ion Mass spectrometry of the WOR5-treated taurine samples further demonstrated the disappearance of taurine and formation of glycine over the course of the reaction (Figure 6). Finally, we showed that taurine oxidation by WOR5 generated sulfate or sulfite. Specifically, using the barium sulfate turbidimetric assay (Supporting Information, Figure S4), the presence of sulfate was detected both before and after the WOR5 reaction but there was a marked increase in the amount of sulfate post reaction. It is not clear is this is due to sulfate, or to sulfite that has been oxidized in the presence of air. A mechanism for reaction of WOR5 with an aliphatic sulfonate involving desulfonation, liberation of sulfate and oxidation of the aldehyde, is discussed below.

DISCUSSION

This work presents the first demonstration of using crystallography to investigate the physiological substrate of an enzyme. In the case of WOR5, it was clear that an aliphatic sulfonate was captured in the active site during crystallization of the enzyme

present in a cytoplasmic extract, and this provided essential clues that lead us to the identify the enzyme's function. Specifically, we demonstrate that WOR5 is an aliphatic sulfonate ferredoxin oxidoreductase (ASOR). In addition, the structure reveals that ASOR is a heterodimeric enzyme with a WOR-like catalytic subunit and a second polyferredoxin-like subunit, as this is what crystallized from the concentrated cytoplasmic extract of *P. furiosus.* A significant clue to the physiological role of ASOR may be the observation that its expression is up-regulated as part of a "cold-shock" response of this organism, with mRNA levels increasing almost 5-fold during both short (1 to 2 h) and long (4 to 5 hr) cold (72°C) adaptation experiments.[186] This is in contrast to the other four tungsten-containing enzymes of *P. furiosus,* all of which also oxidize aldehydes of various types, as the expression of the genes encoding them were not significantly affected by a drop in temperature. Due to the role of osmolytes, in particular, sugar glycerates, sulfonates and phosphonates,[196] in the adaptation to lower growth temperatures, we propose that ASOR may be involved in the oxidation of various aliphatic sulfonates and also phosphonates, and that its true suite of physiological substrates has yet to be identified.

The proposed reaction scheme for the oxidation of aliphatic sulfonates catalyzed by ASOR is shown in Figure 4. Such molecules are abundant in the marine environment inhabited by *P. furiosus*. Indeed, taurine itself is a key organic osmolyte across all cellular life, playing an important role in stabilizing protein structure in general as well as regulating cellular content in mammalian cells.[197] To date, there is no known biological mechanism to cleave the C-S bond in aliphatic sulphonates such as taurine, despite the occurrence of this compound in several ecological niches. In fact, the enzymes that allow intestinal bacteria to access sulfate from taurine have only recently been identified.[198] A

mechanism for enzymatic cleavage of a C-S bond has never been reported, although a mechanism for reductive cleavage of a similar C-S bond has been proposed.[199] Regardless, the activity we have observed for ASOR is a significant finding that will require a multifaceted approach to identify its physiological substrate and function. The biochemistry and structural data reported here provide a foundation from which to build upon.

Overall structure and active site architecture. The enzymatic oxidation of aldehydes to carboxylic acids by pyranopterin-containing enzymes is well established.[184] Likewise, the mechanism of the pyranopterin-dependent oxidation of sulfite by sulfite oxidase has also been investigated in detail.[200,201] However, the observation that a single enzyme can catalyze both a desulfonation reaction as well as the oxidation of an aldehyde and do so using a pyranopterin-based active site is unprecedented. As anticipated, there are notable differences in the active site architecture of sulfonate-oxidizing ASOR and aldehyde-oxidizing AOR and FOR, despite structural similarity in the overall fold of the catalytic subunit. The root mean square deviation (RMSD) for the alignment of the backbone carbon atoms in the catalytic subunit of ASOR with AOR and FOR is 1.5 Å and 1.1 Å, respectively. However, when these structural alignments are compared it becomes clear that there are several regions of the AOR and FOR that are extended, resulting in a considerably smaller active site cleft (Supporting Information, Figure S2) for both of these enzymes. In general, ASOR has a substantially larger active site cleft that can accommodate longer molecules. These observations are consistent with the report that ASOR can work on longer chain aldehydes with considerably higher turnover numbers. Domain 1 of ASOR also contains an alpha helix (residues 143-166) that extends out 3

turns further than the equivalent helix in FOR or AOR. This extension forms a majority of the interface between ASOR and its polyferredoxin-like redox partner (Figure S2).

ASOR and AOR share 58% sequence similarity within Domain 1 (Residues 1-210) 50% similarity in Domain 2 (Residues 211-417) and 52% similarity in Domain 3 (Residues 418-605). Domain 1 in ASOR, forming the characteristic “saddle” base for the tungsto-bispyranopterin, retains most of the same structural features seen in AOR.{Chan, 1995 #3540} The internal hydrogen bonding network of the tungsto-bispyranopterin contains two ordered water molecules, with slight asymmetry attributed to K77 (an arginine residue in AOR) hydrogen bonding to a phosphate oxygen. Similar to FOR, Domains 2 and 3 of ASOR lack the mononuclear iron binding site observed in AOR. Domains 2 and 3 are involved in substrate binding and catalysis, although there are no direct protein ligands to the tungsten ion. However, there are only three amino acids in the active site that are conserved across all five WOR-type enzymes in *P. furiosus* (Figure S2) These are Y327, E328, and H469 (ASOR numbering). Two of these amino acids, E328 and H469 have been proposed to be involved in proton-transfer reactions. The ASOR electron density indicates that the side chain of E328 would be within hydrogen-bonding distance of a sulfonate oxygen at ~2.5 Å. The H469 N-ε nitrogen is also near another sulfonate oxygen at 2.8 Å (Figure 7). However, in addition to these conserved active site residues, ASOR contains another group of polar residues that are not found in the other AOR-type enzymes. These residues form a hydrogen bonding network that is not observed in the AOR or FOR structures (Figure 7). In the taurine-soaked crystals, the N-ε nitrogen of histidine 446 lies close to a substrate sulfonate oxygen, and the H446 N-δ nitrogen is within hydrogen-bonding distance of a carboxylate oxygen from D453. Tyrosine 199 is

within hydrogen bonding distance of the N-δ nitrogen of H469. The additional hydrogen bonding network in ASOR, may explain the novel functionality.

Other than ASOR, the only other ligand-bound structure available for an WOR-family enzyme in *P. furiosus* is the glutarate-bound structure of FOR (PDB ID: 1B4N). The carboxylate oxygens of glutarate in the FOR structure are 3.4 and 5.2 Å away. In our models, the proximity of the sulfonate oxygens to the tungsten site may suggest bidentate coordination, which could explain the higher affinity for taurine compared to aldehyde substrates (Table 2; the K_m value is 0.1 mM for taurine compared to 2.0 mM for propanal). However, given the ambiguous nature of the electron density it would be premature to make any specific assignments. Spectroscopic investigations are underway to further elucidate how sulfonated substrates may coordinate or interact with the tungsten metal center as well as the ASOR mechanism and the relevant oxidation states of the tungsten atom. Finally, it should be emphasized that the [4Fe-4S] cluster, adjacent to the tungsto-bispyranopterin cofactor, in the large subunit of ASOR is significantly different in that an aspartic acid is a ligand for one of the iron atoms. This will certainly influence the reduction potential of the [4Fe-4S] cluster and may have implications for the unique chemistry being catalyzed by ASOR.

The proposed mechanism for oxidative desulfonation by ASOR. Undoubtedly, the novel activity we observe for ASOR must be due to differences in the active site structure of this enzyme when compared to the structures and aldehyde oxidation reported for AOR and FOR. Based on all the available structural information as well as the biochemical and biophysical data discussed above, we propose the mechanism for ASOR shown in Figure 8. The reaction that ASOR catalyzes consists of two sequential

oxidation reactions. This consists of the oxidative desulfonation of the aliphatic sulfonate, followed by the oxidation of the resulting aldehyde to a carboxylic acid (Figure 8). The reduction potentials of these two reactions are approximately -700 mV and -510 mV,[182,202] respectively, more than sufficient to reduce *P. furiosus* ferredoxin (- 385 mV).[203] That ASOR catalyzes two electron transfer reactions each involving two electrons is consistent with the presence of the second small (S) subunit containing four [4Fe-4S] clusters. Hence, independent of the tungsten site, oxidized ASOR can accept up to five electrons per molecule in [4Fe-4S clusters. In contrast, oxidized AOR and GAPOR and presumably FOR and WOR4, which each catalyze a single two-electron reaction and lack the second polyferredoxin-like subunit of ASOR, can only accept a single electron in the single [4Fe-4S] cluster contained in the catalytic WOR subunit. Admittedly, the number of metal sites in a metalloprotein is not necessarily proportional to the number of electrons it will accept, but in the case of ASOR, the additional clusters may simply accommodate the electron transfer events associated with two rather than one oxidiation reaction associated with overall catalysis.

In trying to explain the mechanism of ASOR, a rational conclusion is that breaking the C-S bond must involve additional deprotonation and protonation steps compared to what is required for oxidation of the aldehyde to a carboxylic acid. This is supported by the presence of an additional Asp-His pair in the active site of ASOR (D453 & H446, Figure 7) but not in the active sites of AOR or FOR. Moreover, D453 in ASOR is partially buried and also interacting with R264, therefore, this side chain is likely negatively charged. E328 and H469 are structurally conserved in all three of these WOR enzymes (AOR, FOR and ASOR) and are therefore most likely involved in the oxidation of water

for subsequent conversion of the aldehyde to the corresponding acid. However, there is one notable difference. In ASOR, H469 is hydrogen bonded to Y199, potentially modulating the microscopic pKa for the H469 side chain lower. We ran the free software PROPKA and found the general trend of the predicted pKa values, based on the protein environment, to be consistent with these predictions.

Considering these factors, as well as what has been proposed previously for the mechanism of aldehyde oxidation at the tungsto-bispyranopterin site,[204] our mechanism begins with the aliphate sulfonate binding via the sulfonate near the W=O center (Figure 8). The oxidative reactions are facilitated by an additional proton transfer network in ASOR that is not present in AOR or FOR, specifically D453 and H446 (Figure 7). Upon substrate binding, the tungsten-bound oxygen acts as a nucleophile and attacks the sulfur atom of the sulfonate, forming a single bond with the sulfur atom (Figure 8, top left). The intermediate is further stabilized by the protonated form of H469. H446 acts as a general base to help facilitate breaking the S-C bond and formation of the C-O bond (Figure 8, top middle). Loss of sulfate is also made more favorable through protonation (Figure 8, top right). E328 is conserved in all enzymes and has been proposed to facilitate the oxidation/activation of water to yield the W=O state and we propose that this is also the case for WOR5 (Figure 8, bottom right). H469 is also a conserved amino acid and has been proposed to facilitate deprotonation as the tungsten-bound oxygen attacks the carbonyl carbon of the aldehyde (Figure 8, bottom middle). Protonation of the carboxylic acid, which is glycine in the case of taurine, facilitates the release of product from the tungsten center. Oxidation of another water molecule, again facilitated by the strictly conserved residue E328, returns the active site to the resting state. Future work will

address substrate diversity to include phosphonated compounds and probe the proposed reaction mechanism through spectroscopy and site specific mutagenesis.

Conclusions. In this work we report the structure of WOR5, now termed ASOR, as well as an unprecedented enzymatic activity. While the physiological activity and implications will require significantly more interrogation, our investigation demonstrates an exciting new structure and function for a tungsto-bispyranopterin enzyme that is consistent with the marine environment inhabited by *P. furiosus*. Admittedly, crystal screening of concentrated crude extract is, in fact, an uncontrolled experiment. However, given that the initial experiment was performed with cytoplasmic extract obtained from cells that were cold-shocked, as previously described,[186] the density we have observed may have physiological relevance. Regardless, these data led us to identify a new substrate representing aliphatic sulphonates, which are abundant in the marine environment. SDS-PAGE of the crude extract from the overexpression strain does not provide any additional insight as to why ASOR crystallized as there are clearly numerous other proteins present (Supplemental Figure S5). However, the time to obtain crystals was greatly reduced using this crude extract, consistent with more AOSR being present. An interesting idea, that was raised during the review of this work, is that overexpression of other difficult-to-crystallize enzymes may benefit from this approach. Specifically, that unknown metabolites or stabilizing factors, present in the crude extract, may facilitate crystallization.

EXPERIMENTAL PROCEDURES

Preparation of a P. furiosus mutant overexpressing genes pf1479 and pf1480. The genetically-tractable *P. furiosus* strain COM1 was used for the overexpression of WOR5.[205] An insertion cassette was assembled using overlapping PCR.[206] The upstream flanking region (UFR), downstream flanking region (DFR), and PF1479-PF1480 were amplified from COM1 genomic DNA, with primers designed to insert an N-terminal 9x-histidine-tag on PF1480. The selection marker (*pyrF-*P_{gdh}*-*P_{slp}) was amplified using pGLW021 as the template.[205] The genomic DNA was prepared using the ZymoBead Genomic DNA Kit (Zymo Research). *P. furiosus* COM1 transformants were grown as previously described.[205] Genomic DNA was used for PCR screening, which was carried out by using GXL polymerase (Takara, ClonTech). The PCR screening was performed using a pair of primers outside the intergenic GR1 locus to confirm that the transformation cassette recombined into the correct locus. Once a colony was positively identified, the genomic DNA was further sequenced using Genewiz Sanger Sequencing service (South Plainfield, NJ).

Growth of the parent P. furiosus strain and a strain overexpressing pf1479 and pf1480. Growth of the wild-type *P. furiosus* strain and cold-shock induction of WOR5 was performed as previously described.[191,207] Briefly, to construct the overexpression strain, the genetic system took advantage of the highly-expressed *P. furiosus* promoter (P_{slp}) for the gene encoding the S-layer protein. A 9x-Histidine tag was also introduced at the N-terminus of PF1480 in order to facilitate purification. The tag location was chosen to avoid the interface between genes encoding WOR5 and its potential polyferredoxin subunit. Previous work has shown that P_{slp} can lead to up-regulation of expression in

some cases by greater than an order of magnitude.[208] Large scale growth of the WOR5 expression strain was carried out in a 28-liter fermentor using maltose as the carbon source[209] at 90 °C for 14 hrs with constant flushing of N_2/CO_2. Cells (~15 g) were flash frozen in liquid nitrogen and stored at -80 °C.

WOR5 purification from overexpression strain. WOR5 was purified anaerobically from 40 g cell paste at 25° C. Cells were resuspended in 100mM sodium phosphate, pH 8.0, containing 150 mM KCl and 50 µg/ml DNase I and were lysed by osmotic shock. Following a 1-hour incubation in an anaerobic chamber, cells were centrifuged at 30,000 x g for 1 hour. The supernatant was loaded on an Amintra-CoHis column (Expedeon) pre-equilibrated with the same buffer but without DNase. Following a two-column volume buffer wash, the proteins were eluted using a stepwise gradient from 10 mM imidazole to 250 mM imidazole. Fractions containing WOR5 as determined by activity and SDS-PAGE were pooled and diluted twenty-fold in 100 mM sodium phosphate, pH 8.0 before being loaded onto an anaerobic QHP column. Buffer A contained 100mM sodium phosphate pH 8.0, and 1 mM cysteine, while Buffer B contained 100 mM sodium phosphate, pH 8.0, 1M KCl and 1 mM cysteine. Following a three-column volume buffer wash, proteins were eluted using a linear gradient from 0 to 100% Buffer B. Following SDS-PAGE analysis, fractions containing WOR5 were again pooled, concentrated, and the protein concentration was measured using the Biuret assay.

Preparation of cytoplasmic extract for crystallization. Frozen cell paste (50 g) of the WOR5 overexpression strain was thawed in 150 mL of 50 mM Tris/HCl, pH 8.0, on a vacuum manifold while the gas phase was continuously exchanged under vacuum with

oxygen-free argon. Cells were lysed using an anaerobic French Press system maintained under a slight argon pressure. The cell-free extract was centrifuged at 100,000 x g for one hour to remove insoluble material and the soluble fraction was concentrated using a gas concentrator and a 100 kDa cut-off membrane. The final protein concentration of the cytoplasmic extract was approximately 100 mg/mL, and this was again centrifuged at 100,000 x g for one hour to remove any insoluble material.

Crystallization of WOR5. Concentrated cytoplasmic extract (~100 mg/mL) was screened anaerobically in a soft-sided Coy™ glove box containing an atmosphere of 95% nitrogen and 5% hydrogen. The oxygen concentration was maintained below 1 ppm using a palladium catalyst that was regenerated on a bi-weekly basis. Crystal screening was carried out in 75 µL melting point capillaries by layering 20 µL of the concentrated crude extract on top of 30 µL of the crystallization condition. 480 unique conditions, from five sparse matrix crystallization kits, were screened. All crystallization experiments were carried out in an anaerobic chamber at room temperature (approximately 22-27 °C). Identification of crystalline material was facilitated by use of a polarizer. The identity of WOR5 crystals, when crystallized from concentrated crude extract, was confirmed by mass spectroscopy of crystals than had been resolubilized in 0.1 M HEPES pH 7.5. Optimization of the initial conditions resulted in a final crystallization solution consisting of 0.1 M HEPES pH 7.5, 2% (v/v) polyethylene glycol (PEG) 400, and 2.0 M Ammonium sulfate. Cryo protection of the crystals was achieved by incrementally (2.5 %, w/v) increasing the concentration of PEG 400, along with and equal percentage (v/v) of glycerol, DMSO and polyethylene glycol to 10%. Although cumbersome, there is a significant advantage of the anaerobic capillary batch method for oxygen sensitive

enzymes. Specifically, crystals are already in a sealed quartz capillary and can be safely removed from the chamber and subjected to a quick test for diffraction before being return to the anaerobic chamber.

Data collection, phasing, and refinement. Data was collected at 100 K on beamline 22ID, SER-CAT, Advanced Photon Source, Argonne National Laboratory using a 50-micron beam and an Eiger 16M Detector. Phases were obtained by collecting data at two wavelengths, 12,782 eV and 7,112 eV (the iron edge). The anomalous signal for tungsten at 12,651 eV is greater than ten electrons allowing two tungsten sites in the asymmetric unit to be readily identified. These positions were utilized by PHASER to further refine and search for the iron positions at 7,112 eV and led to interpretable electron density maps. Subsequent rounds of model building and refinement were accomplished using COOT[210,211] and PHENIX.[212]

Biochemical assays of WOR5, AOR and FOR. AOR and FOR were purified from wild-type *P. furiosus* cells as previously described[181,182] and their published enzymatic activities verified using in vitro assays and the artificial electron acceptor benzyl viologen (BV). Unlike WOR5, neither AOR nor FOR showed any BV reduction in the presence of taurine. All assays were conducted anaerobically using 100 mM sodium phosphate, pH 8.0, 150 mM KCl, 100 nM enzyme, and 1 mM BV at 80° C. Varying concentrations of substrate were injected using a gastight syringe to initiate the reaction. Specific activity was determined using a molar extinction coefficient for reduced BV at 600 nm of 7,400 $M^{-1} \cdot cm^{-1}$.[25]

NMR Analysis of WOR5 products. A 2.5-mL reaction mixture was flash frozen with liquid nitrogen and freeze-dried with the aid of a SpeedVac concentrator (Thermo

SAVANT, SPD111V) overnight. The dry powder was dissolved in 300 µL of D_2O (99.8%) containing 0.01% (w/v) 3-(trimethylsilyl) propane-1-sulfonate, sodium salt (DSS) for chemical shift referencing. The resultant solutions were centrifuged and then transferred to 4 mm NMR tubes (Norell). NMR spectra were acquired at 298 K on a Bruker AVANCE Neo 700 MHz spectrometer equipped with an HCN-Cryo-probe. One-dimensional ^{1}H NMR spectra were acquired (64 scans) using the 1D-excitation sculpting for pre-saturation of the water peak, with a spectral width of 16 ppm, 32 K data points, 1.4 s acquisition time and 2.0 s relaxation delay. ^{1}H-^{13}C HSQC (heteronuclear single quantum correlation) spectra were acquired with a spectral width of 13 ppm, 2048 data points and 1.5 s relaxation delay in the direct-detected dimension (32 scans), and 256 data points over a spectral width of 165 ppm in the indirect-detected dimension. ^{1}H-^{13}C HMBC (heteronuclear multiple bond correlation) spectra were acquired with a spectral width of 13 ppm, 4096 data points and 1.0 s relaxation delay in the direct-detected dimension (32 scans), and 256 data points over a spectral width of 220 ppm in the indirect-detected dimension (32 scans). Adjustments to the baseline, peak phasing and chemical shift referencing were made using Bruker Topspin 3.6.2. To confirm product identity, the chemical shifts in the NMR spectra were compared to in-house standards and the Biological Magnetic Resonance Database for positive matches.

Negative Ion Mass Spectrometry of Samples

Samples were analyzed on an Agilent 6230B time-of-flight mass spectrometer operating in negative ion mode. Figure 6, contains the mass spectra of the samples taken before (T_0) and after (T_f) the enzymatic reaction. In Figure 6, Panel A, the

presence of taurine is indicated by the 124 m/z peak. In Figure 6, Panel B, the 124 m/z is not detectable; however, the emergence of glycine (74 m/z) is observed.

Turbidimetric determination of sulfate

30 µL of 4.2 M NaCl (10% v/v HCl) was added to the 300 µL T_0 and T_f samples and vortexed for 1 min. After, 7 µL of 0.1 M $Ba(NO_3)_2$ was added to the mixtures, vortexed for 1 min, and settled for 5 min to observed the formation of precipitate (Supporting Information, Figure S4).

Table A1. Data collection and refinement statistics.

Sample	Wor5 crystallized from crude extract Taurine soak	
Data Collection		
Beamline	APS 22-ID	APS 22-ID
Space Group	$P2_12_12$	$P2_12_12$
Wavelength(s) (Å)	0.98	0.98
Resolution Range (Å)	50.0-2.10	50.0-1.97
Outer Shell (Å)	2.18-2.10	2.04-1.97
Unique Observations	130,184	157,481
Completeness (%)	99.3(97.4)[b]	87.3(74.2)
R_{sym} (%)[c]	5.5(29.8)	4.2(22.2)
CC ½	99.4(89.8)	99.6(91.5)
Redundancy	6.3(5.5)	5.8(5.4)
I/s	15.5(1.7)	15.2(2.0)
Phasing (Fe anomalous)[b]		
Sites	18(initial sites)	
BAYES-CC	49.4 +/- 15.3	
Figure of Merit	0.49	
Refinement		
Unit Cell (*a, b, c*) in Å	123.0, 126.8, 141.2	125.2, 127.5, 140.7

Protein Atoms	12,479			
12,520				
Solvent Atoms	214		793	
Resolution Limits (Å)	47.1-2.1		38.1-1.97	
R_{cryst} (%)	17.9		17.2	
R_{free} (%)	21.4		20.3	
rmsd bonds (Å)	0.012		0.013	
rmsd angles (°)	1.64		1.84	
average B factor (Å^2)	32.5		22.0	

[a]Numbers in parentheses denote values for the outermost resolution shell. [c]R_{sym} = $\sum_{hkl}[\sum_{I}(|I_{hkl,I} - \langle I_{hkl}\rangle|)]/\sum_{hkl,I}\langle I_{hkl}\rangle$, where I_{hkl} is the intensity of an individual measurement of the reflection with indices hkl and $\langle I_{hkl}\rangle$ is the mean intensity of that reflection.

[b]Phases were obtained from anomalous scattering of the iron and tungsten ions from data collected at 1.74 Å energy. The asymmetric unit contains two tungsten ions and forty iron atoms.

Table A2. Kinetic constants for WOR5 activities.

Substrate	K_{cat} (s^{-1})	K_m (μM)	K_{cat}/K_m ($mM^{-1} \cdot s^{-1}$)
Hexanal	63.5 ± 6.7	230 ± 9	276 ± 27
Taurine	4.5 ± 0.3	112 ± 4	40 ± 4.6
Propionaldehyde	166.6 ± 12.7	2047 ± 67	81 ± 5.2

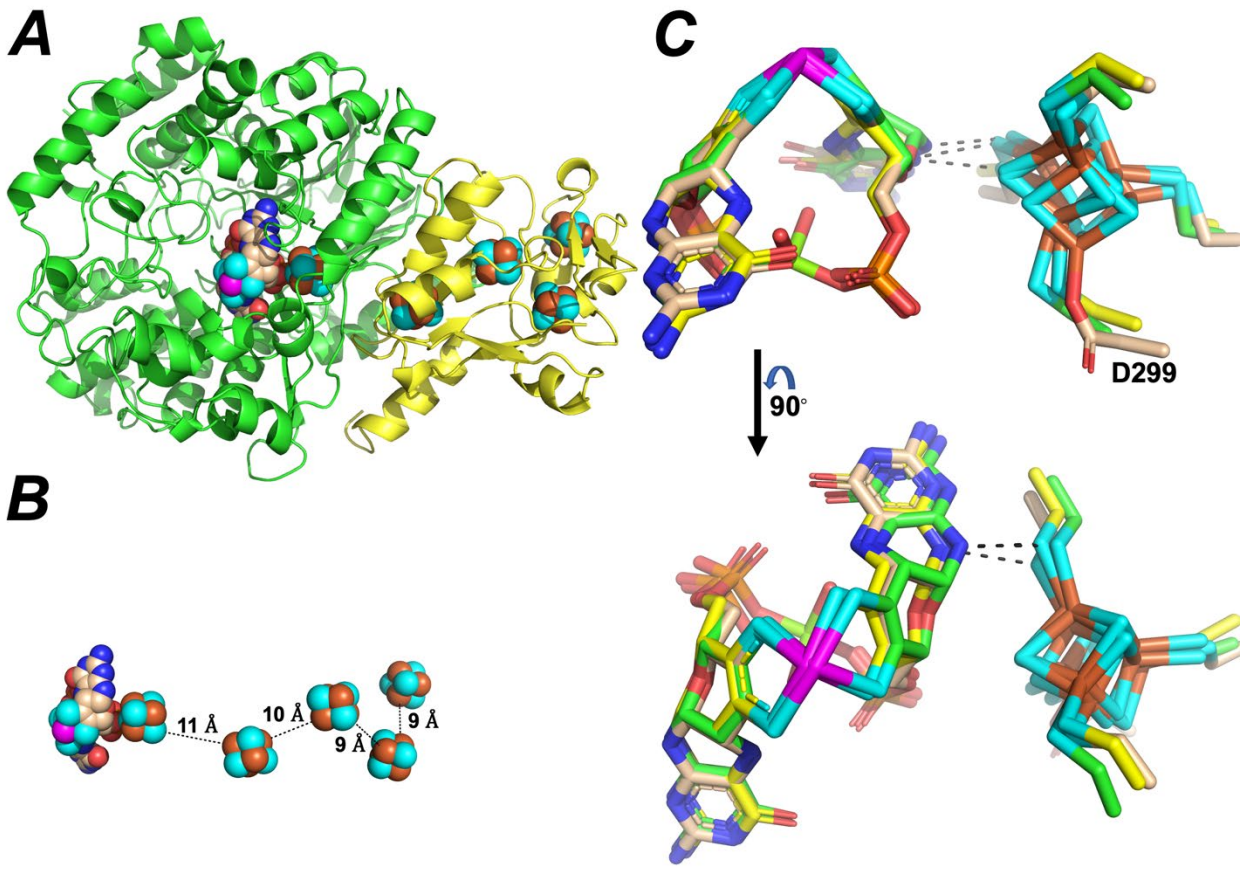

Figure A1. Cartoon representation showing the heterodimeric structure (*Panel A*) of WOR5, the relative spatial orientation of the cofactors (*Panel B*) shown as space filling spheres, and a stick representation showing a structural overlay (*Panel C*) of the tungsto-bispyranopterin and [4Fe-4S] cluster in the catalytic subunit of WOR5 (tan carbon atoms), AOR (yellow carbon atoms), and FOR (green carbon atoms). The buried surface area for the dimer interface between the large subunit (green cartoon) and the polyferredoxin subunit (yellow cartoon) is 2,073 Å^2. Nitrogen, oxygen, sulfur, phosphorous, magnesium, and tungsten are colored, blue, red, cyan, orange, lime green, and magenta, respectively. The aspartic acid (E299) ligand to [4Fe-4S] is

identified and the dashed lines represent the closest contact distance (less then 3.3 Å) between the [4Fe-4S] cluster and the tungsto-bispyranopterin cofactor in all models.

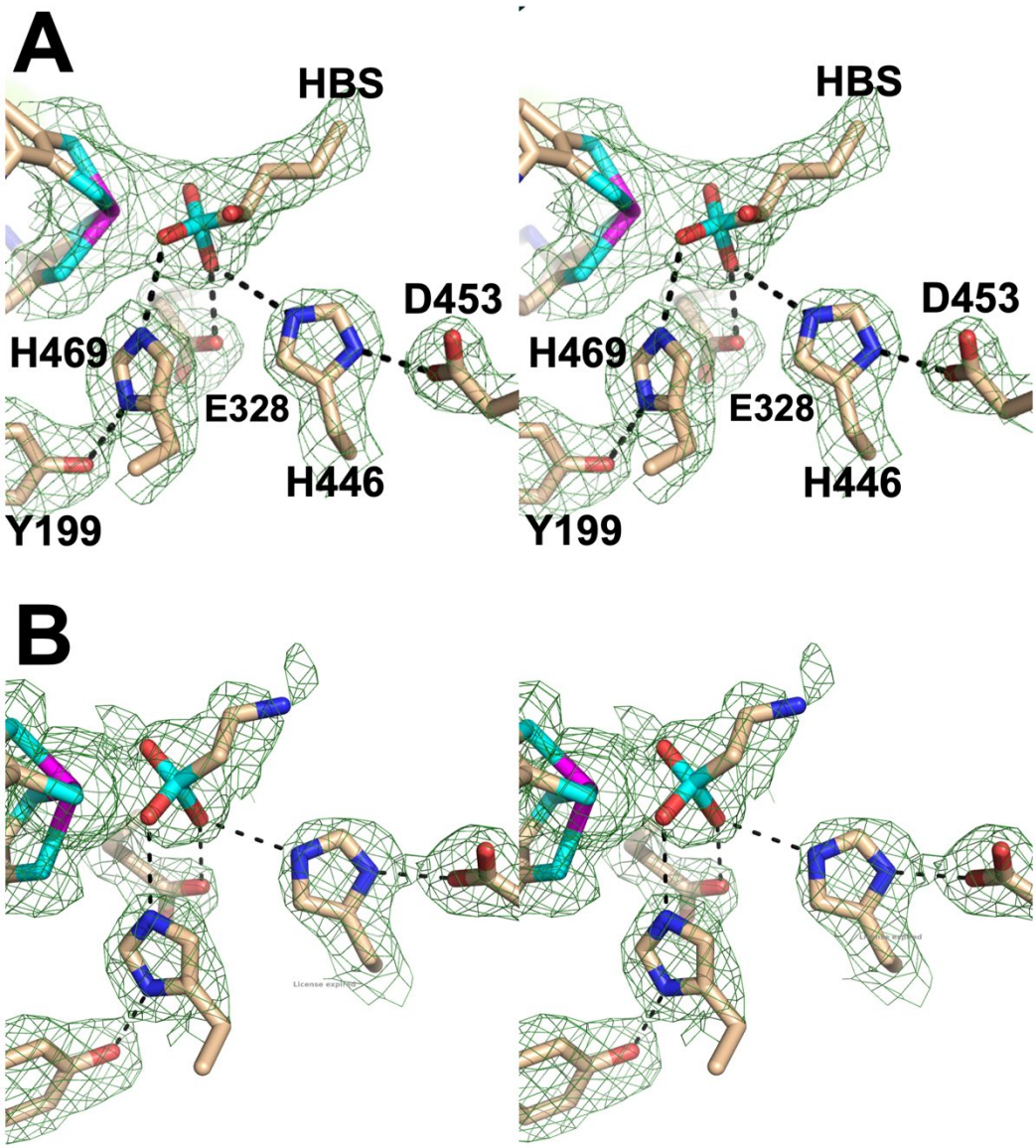

Figure A2. Wall-eyed stereo view showing the models (stick format) and F_o-F_c composite omit density (green cage) for WOR5 crystals obtained crude extract (Panel A) and following treatment with 5 mM taurine (Panel B). The composite omit maps are contoured at 3 s and were generated using the simulated annealing protocol. Carbon, nitrogen, oxygen, sulfur and tungsten atoms are colored tan, blue, red, cyan, and magenta, respectively. Dashed lines represent distances shorter than 3.3 Å.

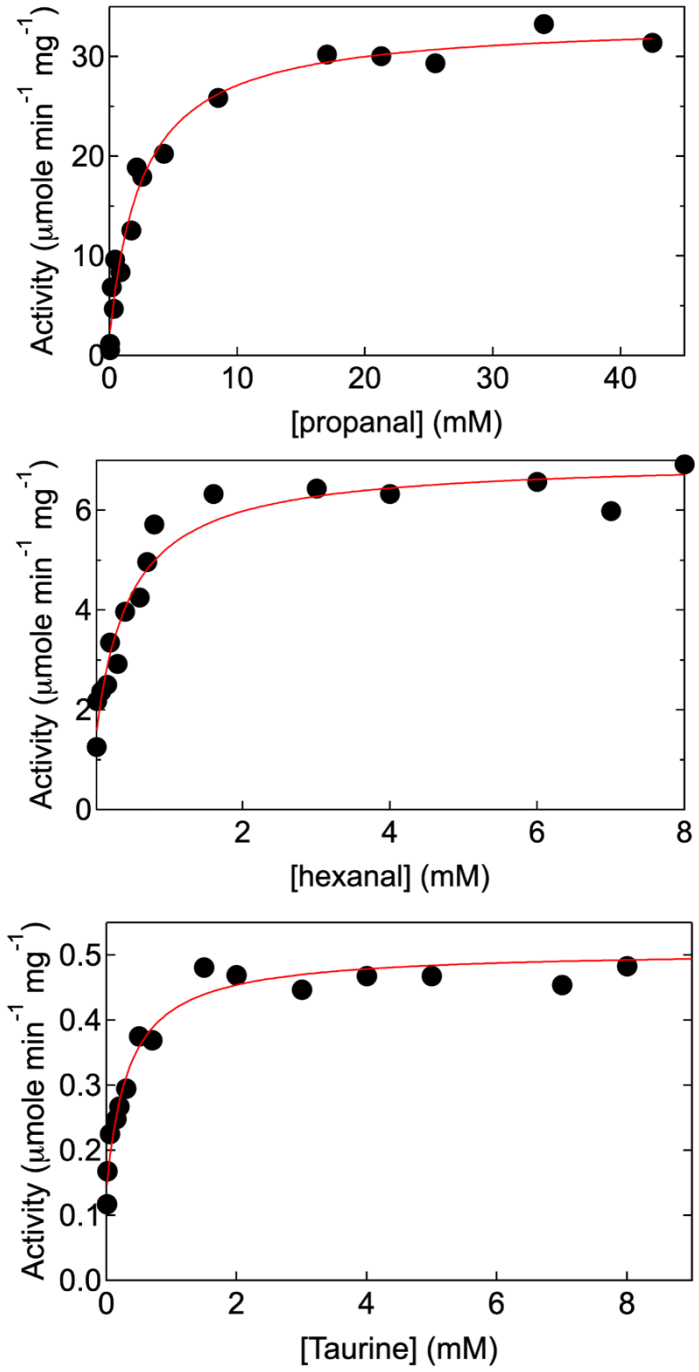

Figure A3. Saturation curves observed for WOR5 with the substrate butanal (Panel A), propanal (Panel B) or taurine (Panel C) as substrates. Oxidation of the substrates by WOR5 measured using the benzyl viologen as the electron carrier.

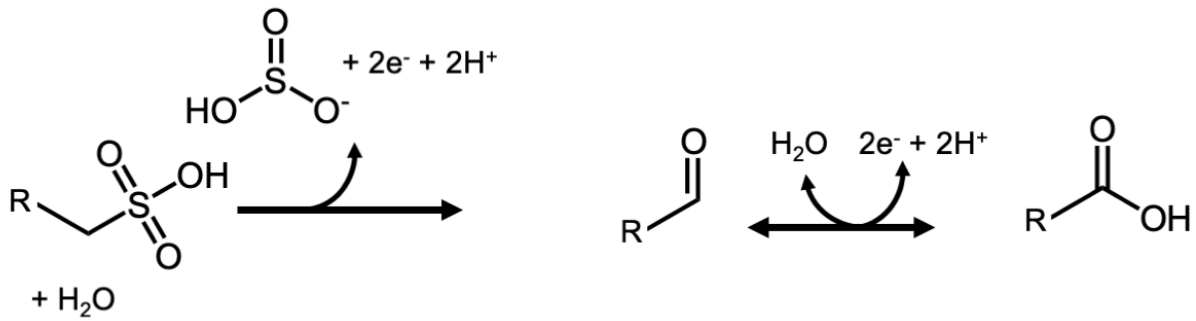

Figure A4. Proposed reaction catalyzed by ASOR. R- represents an aliphatic side-chain. See text for details.

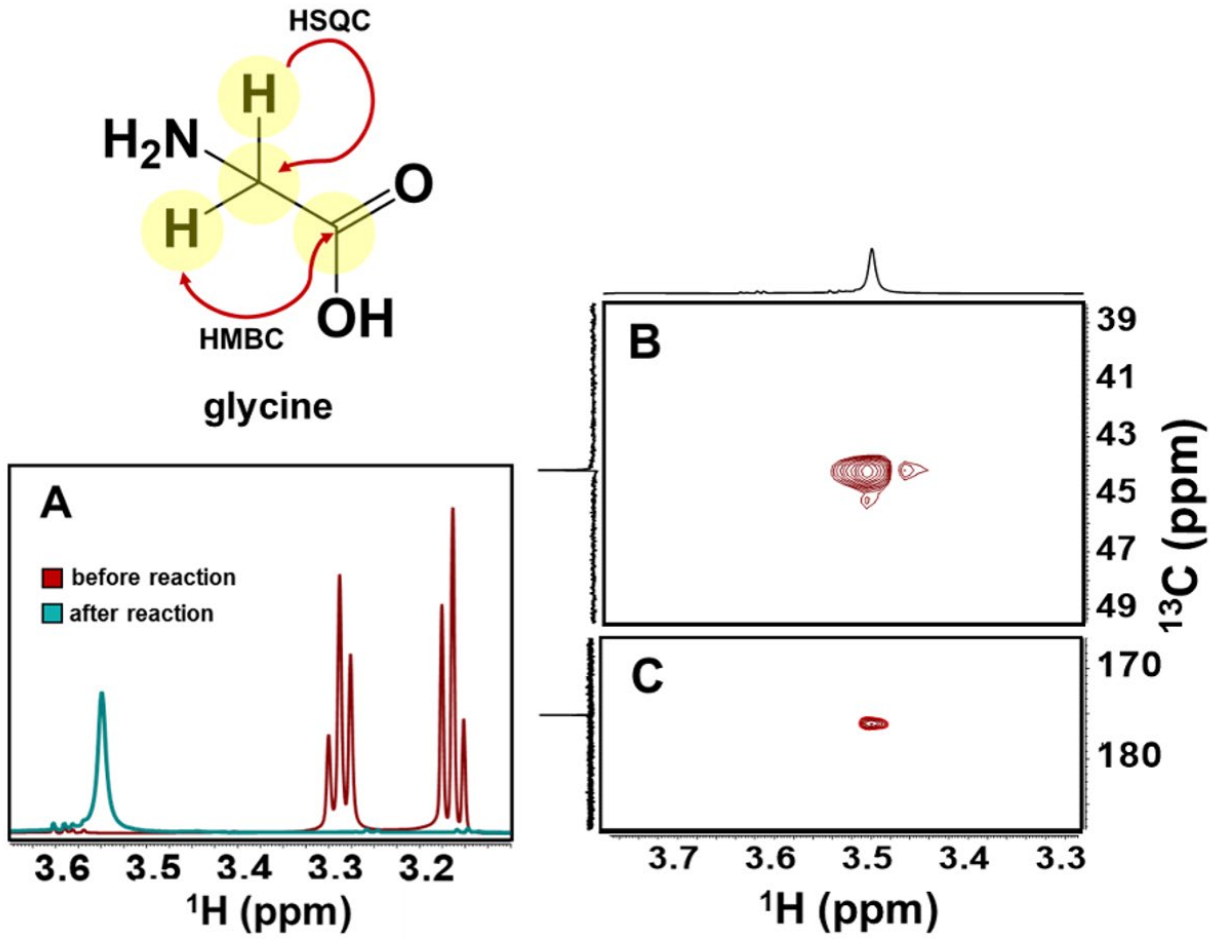

Figure A5. NMR Spectra monitoring the conversion of taurine to glycine. ^{1}H NMR spectra (Panel A) were recorded of samples taken before and after the enzymatic reaction. In addition, ^{1}H-^{13}C HSQC (Panel B) and ^{1}H-^{13}C HMBC spectra of the post-turnover samples were also recorded.

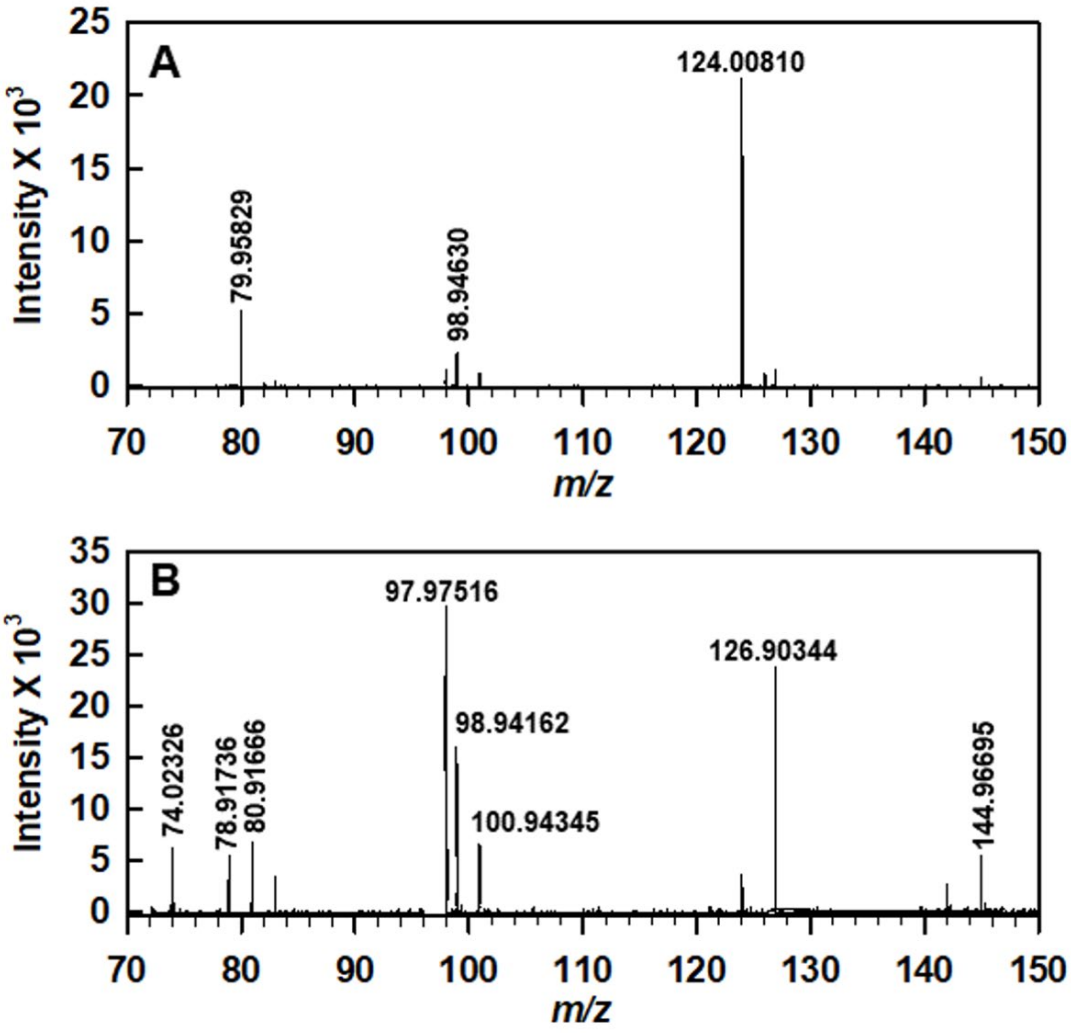

Figure A6. Negative-ion mode mass spectra of sample taken (A) before and (B) after enzymatic reaction. The *m/z* 124 corresponds to taurine pre-turnover (Panel A). Following turnover, glycine is observed (*m/z* 74, Panel B). Sample preparation and experimental parameters are described in the Experimental Procedures.

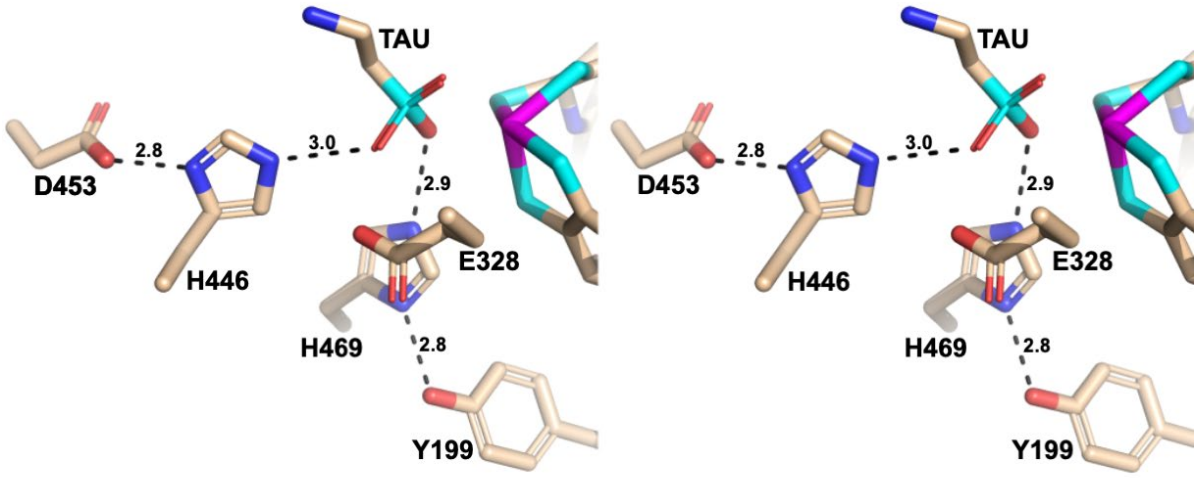

Figure A7. Wall-eyed stereo view highlighting proton transfer networks that are unique to ASOR in the model for the taurine-soaked crystals. See text for details.

Figure 8, Mathew et al.

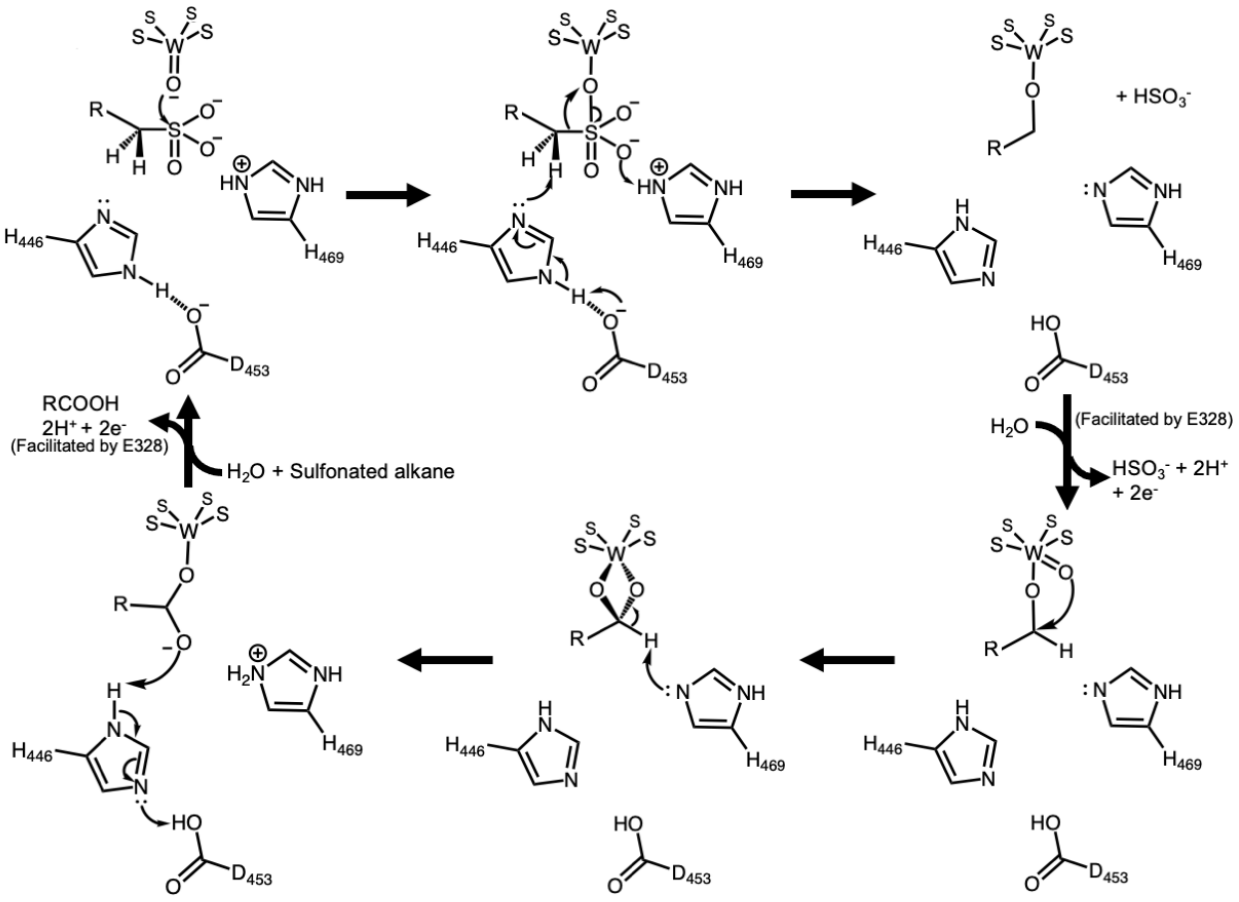

Figure A8. Proposed mechanism for the oxidation of aliphatic sulfonates by ASOR incorporating the roles of its unique active site residues. R- represents an aliphatic side-chain. The four sulfur atoms surrounding the W atom are provided by the dithioline groups of two pyranopterin molecules. See text for details.

REFERENCES

(1) Schicho, R. N.; Snowden, L. J.; Mukund, S.; Park, J.-B.; Adams, M. W. W.; Kelly, R. M. Influence of Tungsten on Metabolic Patterns in Pyrococcus Furiosus, a Hyperthermophilic Archaeon. *Arch. Microbiol.* **1993**, *159* (4), 380–385. https://doi.org/10.1007/bf00290921.

(2) Schut, G. J.; Thorgersen, M. P.; Poole, F. L.; Haja, D. K.; Putumbaka, S.; Adams, M. W. W. Tungsten Enzymes Play a Role in Detoxifying Food and Antimicrobial Aldehydes in the Human Gut Microbiome. *Proc. Natl. Acad. Sci.* **2021**, *118* (43). https://doi.org/10.1073/pnas.2109008118.

(3) Mukund, S.; Adams, M. W. W. Glyceraldehyde-3-Phosphate Ferredoxin Oxidoreductase, a Novel Tungsten-Containing Enzyme with a Potential Glycolytic Role in the Hyperthermophilic Archaeon Pyrococcus Furiosus. *J. Biol. Chem.* **1995**, *270* (15), 8389–8392. https://doi.org/10.1074/jbc.270.15.8389.

(4) Nguyen, D. M. N.; Schut, G. J.; Zadvornyy, O. A.; Tokmina-Lukaszewska, M.; Poudel, S.; Lipscomb, G. L.; Adams, L. A.; Dinsmore, J. T.; Nixon, W. J.; Boyd, E. S.; et al. Two Functionally

Distinct NADP-Dependent Ferredoxin Oxidoreductases Maintain the Primary Redox Balance of Pyrococcus Furiosus. *J. Biol. Chem.* **2017**, *292* (35), 14603–14616. https://doi.org/10.1074/jbc.m117.794172.

(5) Mukund, S.; Adams, M. W. The Novel Tungsten-Iron-Sulfur Protein of the Hyperthermophilic Archaebacterium, Pyrococcus Furiosus, Is an Aldehyde Ferredoxin Oxidoreductase. Evidence for Its Participation in a Unique Glycolytic Pathway. *J. Biol. Chem.* **1991**, *266* (22), 14208–14216. https://doi.org/10.1016/s0021-9258(18)98669-2.

(6) Roy, R.; Mukund, S.; Schut, G. J.; Dunn, D. M.; Weiss, R.; Adams, M. W. W. Purification and Molecular Characterization of the Tungsten-Containing Formaldehyde Ferredoxin Oxidoreductase from the Hyperthermophilic Archaeon $\less$i$\greater$Pyrococcus Furiosus$\less$/I$\greater$: The Third of a Putative Five-Member Tungstoenzyme . *J. Bacteriol.* **1999**, *181* (4), 1171–1180. https://doi.org/10.1128/jb.181.4.1171-1180.1999.

(7) Roy, R.; Adams, M. W. W. Characterization of a Fourth Tungsten-Containing Enzyme from the Hyperthermophilic Archaeon Pyrococcus Furiosus. *J. Bacteriol.* **2002**, *184* (24), 6952–6956. https://doi.org/10.1128/jb.184.24.6952-6956.2002.

(8) Chan, M. K.; Mukund, S.; Kletzin, A.; Adams, M. W. W.; Rees, D. C.

STRUCTURE OF A HYPERTHERMOPHILIC TUNGSTOPTERIN ENZYME, ALDEHYDE FERREDOXIN OXIDOREDUCTASE. Worldwide Protein Data Bank April 1995. https://doi.org/10.2210/pdb1aor/pdb.

(9) Hu, Y.; Faham, S.; Roy, R.; Adams, M. W. W.; Rees, D. C. Formaldehyde Ferredoxin Oxidoreductase from Pyrococcus Furiosus: The 1.85 A Resolution Crystal Structure and Its Mechanistic Implications 1 1Edited by I. A. Wilson. *J. Mol. Biol.* **1999**, *286* (3), 899–914. https://doi.org/10.1006/jmbi.1998.2488.

(10) Weinberg, M. V; Schut, G. J.; Brehm, S.; Datta, S.; Adams, M. W. W. Cold Shock of a Hyperthermophilic Archaeon: Pyrococcus Furiosus Exhibits Multiple Responses to a Suboptimal Growth Temperature with a Key Role for Membrane-Bound Glycoproteins. *J. Bacteriol.* **2005**, *187* (1), 336–348. https://doi.org/10.1128/jb.187.1.336-348.2005.

(11) Bevers, L. E.; Bol, E.; Hagedoorn, P. L.; Hagen, W. R. WOR5, a Novel Tungsten-Containing Aldehyde Oxidoreductase from Pyrococcus Furiosus with a Broad Substrate Specificity. *J. Bacteriol.* **2005**, *187* (20), 7056–7061. https://doi.org/10.1128/JB.187.20.7056-7061.2005.

(12) Berks, B. C.; Page, M. D.; Richardson, D. J.; Reilly, A.; Cavill, A.;

Outen, F.; Ferguson, S. J. Sequence Analysis of Subunits of the Membrane-Bound Nitrate Reductase from a Denitrifying Bacterium: The Integral Membrane Subunit Provides a Prototype for the Dihaem Electron-Carrying Arm of a Redox Loop. *Mol. Microbiol.* **1995**, *15* (2), 319–331. https://doi.org/10.1111/j.1365-2958.1995.tb02246.x.

(13) Jormakka, M.; Yokoyama, K.; Yano, T.; Tamakoshi, M.; Akimoto, S.; Shimamura, T.; Curmi, P.; Iwata, S. Molecular Mechanism of Energy Conservation in Polysulfide Respiration. *Nat. Struct. {\&}amp$\mathsemicolon$ Mol. Biol.* **2008**, *15* (7), 730–737. https://doi.org/10.1038/nsmb.1434.

(14) Scott, I. M.; Rubinstein, G. M.; Poole, F. L.; Lipscomb, G. L.; Schut, G. J.; Williams-Rhaesa, A. M.; Stevenson, D. M.; Amador-Noguez, D.; Kelly, R. M.; Adams, M. W. W. The Thermophilic Biomass-Degrading Bacterium Caldicellulosiruptor Bescii Utilizes Two Enzymes to Oxidize Glyceraldehyde 3-Phosphate during Glycolysis. *J. Biol. Chem.* **2019**, *294* (25), 9995–10005. https://doi.org/10.1074/jbc.ra118.007120.

(15) Chandrayan, S. K.; McTernan, P. M.; Hopkins, R. C.; Sun, J.; Jenney, F. E.; Adams, M. W. W. Engineering Hyperthermophilic Archaeon Pyrococcus Furiosus to Overproduce Its Cytoplasmic [NiFe]-Hydrogenase. *J. Biol. Chem.* **2012**, *287* (5), 3257–3264.

https://doi.org/10.1074/jbc.m111.290916.

(16) Gray, H. B.; Winkler, J. R. Electron Flow through Metalloproteins. *Biochim. Biophys. Acta - Bioenerg.* **2010**, *1797* (9), 1563–1572. https://doi.org/10.1016/j.bbabio.2010.05.001.

(17) Winkler, J. R.; Gray, H. B. Electron Flow through Metalloproteins. *Chem. Rev.* **2013**, *114* (7), 3369–3380. https://doi.org/10.1021/cr4004715.

(18) Schindelin, H.; Kisker, C.; Rees, D. C. The Molybdenum-Cofactor: A Crystallographic Perspective. *{JBIC} J. Biol. Inorg. Chem.* **1997**, *2* (6), 773–781. https://doi.org/10.1007/s007750050194.

(19) Clifford, E. L.; Hansell, D. A.; Varela, M. M.; Nieto-Cid, M.; Herndl, G. J.; Sintes, E. Crustacean Zooplankton Release Copious Amounts of Dissolved Organic Matter as Taurine in the Ocean. *Limnol. Oceanogr.* **2017**, *62* (6), 2745–2758. https://doi.org/10.1002/lno.10603.

(20) Esteves, A. M.; Chandrayan, S. K.; McTernan, P. M.; Borges, N.; Adams, M. W. W.; Santos, H. Mannosylglycerate and Dimyo-Inositol Phosphate Have Interchangeable Roles during Adaptation of Pyrococcus Furiosus to Heat Stress. *Appl. Environ. Microbiol.* **2014**, *80* (14), 4226–4233. https://doi.org/10.1128/aem.00559-14.

(21) Lambert, I. H. Regulation of the Cellular Content of the Organic

Osmolyte Taurine in Mammalian Cells. *Neurochem. Res.* **2004**, *29* (1), 27–63. https://doi.org/10.1023/b:nere.0000010433.08577.96.

(22) Peck, S. C.; Denger, K.; Burrichter, A.; Irwin, S. M.; Balskus, E. P.; Schleheck, D. A Glycyl Radical Enzyme Enables Hydrogen Sulfide Production by the Human Intestinal Bacterium Bilophila Wadsworthia. *Proc. Natl. Acad. Sci.* **2019**, *116* (8), 3171–3176. https://doi.org/10.1073/pnas.1815661116.

(23) Dawson, C. D.; Irwin, S. M.; Backman, L. R. F.; Le, C.; Wang, J. X.; Vennelakanti, V.; Yang, Z.; Kulik, H. J.; Drennan, C. L.; Balskus, E. P. Molecular Basis of C-S Bond Cleavage in the Glycyl Radical Enzyme Isethionate Sulfite-Lyase. *Cell Chem. Biol.* **2021**, *28* (9), 1333--1346.e7. https://doi.org/10.1016/j.chembiol.2021.03.001.

(24) van Severen, M.-C.; Andrejić, M.; Li, J.; Starke, K.; Mata, R. A.; Nordlander, E.; Ryde, U. A Quantum-Mechanical Study of the Reaction Mechanism of Sulfite Oxidase. *{JBIC} J. Biol. Inorg. Chem.* **2014**, *19* (7), 1165–1179. https://doi.org/10.1007/s00775-014-1172-z.

(25) Caldararu, O.; Feldt, M.; Cioloboc, D.; van Severen, M.-C.; Starke, K.; Mata, R. A.; Nordlander, E.; Ryde, U. QM/MM Study of the Reaction Mechanism of Sulfite Oxidase. *Sci. Rep.* **2018**, *8* (1). https://doi.org/10.1038/s41598-018-22751-6.

(26) Arendsen, A. F.; de Vocht, M.; Bulsink, Y. B. M.; Hagen, W. R. Redox Chemistry of Biological Tungsten: An EPR Study of the Aldehyde Oxidoreductase from Pyrococcus Furiosus. *JBIC J. Biol. Inorg. Chem.* **1996**, *1* (4), 292–296. https://doi.org/10.1007/s007750050056.

(27) Brereton, P. S.; Duderstadt, R. E.; Staples, C. R.; Johnson, M. K.; Adams, M. W. W. Effect of Serinate Ligation at Each of the Iron Sites of the [Fe4S4] Cluster of Pyrococcus Furiosus Ferredoxin on the Redox, Spectroscopic, and Biological Properties. *Biochemistry* **1999**, *38* (32), 10594–10605. https://doi.org/10.1021/bi990671d.

(28) Tong, I. T.; Liao, H. H.; Cameron, D. C. 1,3-Propanediol Production by Escherichia Coli Expressing Genes from the Klebsiella Pneumoniae Dha Regulon. *Appl. Environ. Microbiol.* **1991**, *57* (12), 3541–3546. https://doi.org/10.1128/aem.57.12.3541-3546.1991.

(29) Lipscomb, G. L.; Stirrett, K.; Schut, G. J.; Yang, F.; Jenney, F. E.; Scott, R. A.; Adams, M. W. W.; Westpheling, J. Natural Competence in the Hyperthermophilic Archaeon Pyrococcus Furiosus Facilitates Genetic Manipulation: Construction of Markerless Deletions of Genes Encoding the Two Cytoplasmic Hydrogenases. *Appl. Environ. Microbiol.* **2011**, *77* (7), 2232–2238. https://doi.org/10.1128/aem.02624-10.

(30) Bryksin, A. V; Matsumura, I. Overlap Extension PCR Cloning: A Simple and Reliable Way to Create Recombinant Plasmids. *Biotechniques* **2010**, *48* (6), 463–465. https://doi.org/10.2144/000113418.

(31) Wu, C.-H.; Ponir, C. A.; Haja, D. K.; Adams, M. W. W. Improved Production of the NiFe-Hydrogenase from Pyrococcus Furiosus by Increased Expression of Maturation Genes. *Protein Eng. Des. Sel.* **2018**, *31* (9), 337–344. https://doi.org/10.1093/protein/gzy025.

(32) Chandrayan, S. K.; Wu, C.-H.; McTernan, P. M.; Adams, M. W. W. High Yield Purification of a Tagged Cytoplasmic [NiFe]-Hydrogenase and a Catalytically-Active Nickel-Free Intermediate Form. *Protein Expr. Purif.* **2015**, *107*, 90–94. https://doi.org/10.1016/j.pep.2014.10.018.

(33) Verhagen, M. F. J. M.; Menon, A. L.; Schut, G. J.; Adams, M. W. W. Pyrococcus Furiosus: Large-Scale Cultivation and Enzyme Purification. In *Methods in Enzymology*; Elsevier, 2001; pp 25–30. https://doi.org/10.1016/s0076-6879(01)30368-3.

(34) Emsley, P.; Cowtan, K. Coot: Model-Building Tools for Molecular Graphics. *Acta Crystallogr. Sect. D Biol. Crystallogr.* **2004**, *60* (12), 2126–2132. https://doi.org/10.1107/s0907444904019158.

(35) Emsley, P.; Debreczeni, J. É. The Use of Molecular Graphics in Structure-Based Drug Design. In *Methods in Molecular Biology*; Humana Press, 2011; pp 143–159. https://doi.org/10.1007/978-1-61779-520-6_6.

(36) Adams, P. D.; Afonine, P. V; Bunkóczi, G.; Chen, V. B.; Davis, I. W.; Echols, N.; Headd, J. J.; Hung, L.-W.; Kapral, G. J.; Grosse-Kunstleve, R. W.; et al. PHENIX: A Comprehensive Python-Based System for Macromolecular Structure Solution. *Acta Crystallogr. Sect. D Biol. Crystallogr.* **2010**, *66* (2), 213–221. https://doi.org/10.1107/s0907444909052925.